ULTRASONIC ABSORPTION ALONG THE PRINCIPAL AXES OF SINGLE CRYSTALLINE BENZINE.

Alfred Erwin Victor

Abstract of

Ultrasonic Absorption Along the Principal Axes of

Single Crystalline Benzene

by

Alfred Erwin Victor

Ph.D., Brown University, June, 1972

Ultrasonic absorption measurements were performed as a function of temperature and frequency along the principal axes of single crystalline benzene. Measurements were made with longitudinal sound waves between 6 and 26 MHz on all three axes and up to 34 MHz and 38 MHz on the a and c axes, respectively. The temperature range of the experiment extended from 170°K to 250°K; the range was limited by the characteristics of the transducer bond.

The values of sound absorption (α) obtained ($\sim$ 0.1 cm^{-1} to 0.9 cm^{-1}) are much higher than normally observed in solids ($\sim 10^4$ higher than quartz). The magnitude of α corresponds to that obtained in previous experimental investigations of organic solids; however, the frequency and temperature dependence of α depart significantly from that which has been previously observed and from that predicted by theory. Present theories predict α to be proportional to the square of the frequency (ν) in the temperature and frequency range of this experiment; however, α was observed to depart from the ν^2 dependence as the temperature was low-

ered, the change being different for each axis. Relaxation effects were observed for each axis and indicate relaxation times of approximately 10^{-9} sec; this is much slower than theoretically predicted ($\sim 10^{-11}$ sec). Specifically, for the a-axis the relaxation peak is centered at 17 MHz at 240°K and shifts to 12 MHz at 170°K. For the b-axis, the relaxation peak occurs at 26 MHz at 240°K and shifts to 20 MHz at 170°K. The c-axis data indicates the presence of multiple relaxation effects. It appears that one relaxation mechanism is occuring in the vicinity of 14 MHz and another around 120 MHz.

By comparing the change in the observed relaxation strengths as a function of temperature it was qualitatively determined that the sound absorption results from an exchange of energy between the lattice vibrations and the low frequency molecular oscillations. This was done by calculating the specific heat contributions to the relaxation strength for each internal mode for the upper and lower temperatures of the experiment and comparing the change with the observed values. Examination of the molecular arrangement within the unit cell of benzene indicates that one should expect sound energy, which is propagated along each principal axis, to interact with the inter- and intramolecular vibrations in a different manner.

ULTRASONIC ABSORPTION ALONG THE PRINCIPAL AXES OF SINGLE CRYSTALLINE BENZENE

by

Alfred Erwin Victor

Sc.B., United States Naval Academy, 1958
Sc.M., Brown University, 1967

Thesis

submitted in partial fulfillment of the requirements for the Degree of Doctor of Philosophy in the Department of Physics at Brown University

June, 1972

This thesis by Alfred Erwin Victor

is accepted in its present form by the Department of Physics as satisfying the thesis requirements for the degree of Doctor of Philosophy

Date ....

Recommended to the Graduate Council

Date ....

....

Date ....

....

Approved by the Graduate Council

Date ....

VITA

Alfred Erwin Victor was born in New York City on October 2, 1936. He graduated from Clifford J. Scott High School in East Orange, New Jersey in 1954 and entered the U. S. Naval Academy in June of that year. Upon graduating from the Naval Academy in June 1958, he entered the U. S. Navy's flight training program and was designated a Naval Aviator in December 1959.

After three and one-half years of operational duty with the Navy, he was selected to attend the U. S. Naval Postgraduate School in Monterey, California, and after one year at that institution, he was enrolled in the Advanced Science Program (Physics), which is sponsored by the Office of Naval Research, to study towards an advanced degree in Physics.

In September 1964 the author enrolled in the Graduate School at Brown University. He completed the requirements for the Sc.M. Degree in Physics in February 1967 and returned to operational duty with the Navy at that time. In August 1969 he returned to Brown University to continue study and research towards a doctoral degree in Physics.

In June 1958 the author married Miss Jacquelyn Appell. They are the parents of three children: Susan Jacquelyn, born in October 1959, Andrea Eve, born in March 1961, and Wayne Alfred, born in March 1968.

The author has been elected to membership in Sigma Xi and is a member of the Acoustical Society of America and of the Institute of Electrical and Electronics Engineers. The results of his research for the Sc.M. Degree (Title: Ultrasonic Absorption in Liquid Oxygen) were published in the Journal of Chemical Physics in February 1970 (J. Chem. Phys., 52, 1573 [1970]).

TABLE OF CONTENTS

ACKNOWLEDGMENTS

The author would like to express his deepest appreciation to his research advisor, Professor R. T. Beyer, for his encouragement, advice, and patience during the course of this work. Also, he would like to thank Professor A. O. Williams, Jr. for his many helpful suggestions and discussions and for substituting as his research advisor during Professor Beyer's sabbatical leave.

The author would like to thank his colleagues, Dr. Joseph Blinick, Dr. Mark Moffett, Mr. Eugene Ring, and Mr. Harry Altman for their invaluable assistance and constructive criticisms; their aid and friendship were a major factor in the successful completion of this work. He would like to thank Mr. Charles Forrest for his help in the design and construction of the experimental apparatus.

The author would like to express his gratitude to the following people for their assistance in the preparation of the thesis: Mrs. Susan Whitney, Miss Sharon Perlow, and Miss Susan Desilets for typing the manuscript, Mr. James Smith for his help in preparing the drawings, and Mr. James Barber for taking the photographs.

He would like to thank the Division of Engineering for the extended use of their temperature control equipment and the Department of Geological Sciences for the loan of their Leitz Universal Stage.

He would like to thank the Department of the Navy for providing him with the opportunity to pursue an advanced education and, in particular, gratefully acknowledges the sponsorship and support of the Office of Naval Research throughout the period of his graduate school study.

Finally, he would like to thank his wife for her patience and understanding during the years of study and research.

1. INTRODUCTION

The inherent complexity of molecular substances has been the stimulus for a large number of theoretical and experimental investigations. In many cases molecular structure has been precisely determined through the use of X-rays, neutron scattering, and Raman and infrared spectroscopy. The spectroscopic experiments together with the predictions of group theory have led to the determination of the vibrational spectrum of molecules, which, in turn, has been used to determine the force constants between neighboring atom-atom bonds. As the phase of a molecular substance changes, the structure of the molecule itself essentially remains intact. This has been borne out by Raman and infrared spectra experiments where the width of the lines may be altered but the fundamental intramolecular vibration frequencies remain about the same.[1] Additional low-frequency vibrations appear in the solid state which originate from the vibrations between the molecules in the lattice, i.e., the intermolecular vibrations. Since the intermolecular vibration frequencies are low, the coupling between the molecules in the lattice must be much weaker than the intramolecular couplings. For example, in solid benzene at 0°C the highest lattice vibrational frequency is 3.15×10^{12} Hz [2] whereas the lowest intramolecular frequency is 1.215×10^{13} Hz.[3] In the harmonic approximation of lattice vibration theory the two types of vibrations are assumed to be independent of each other; however, when one takes into account the third and higher order terms of the intermolecular potential energy expansion, interactions between the two types of vibrations can take place. Raman and infrared spectra give experimental proof that such interactions do occur and are manifested in

combination frequencies which are observed but not predicted by the selection rules based on the harmonic approximation.[4]

The possibility that the interaction between the intra- and intermolecular vibrations could cause a large absorption of sound energy was first proposed by Liebermann.[5] He hypothesized that the absorption would be a result of the slow exchange of energy between the two modes if their energy difference was not too great. Using a theory which is based on a model of the molecular interaction in the gaseous state in combination with the Debye lattice continuum theory, he shows that (1) the resonance absorption is very large compared to other absorption mechanisms in solids, (2) that it is proportional to the square of the frequency, and (3) it is almost independent of explicit temperature variations. Later Liebermann[6] substantiated his theoretical prediction with absorption measurements on single crystalline benzene. The absorption values obtained were anomalously high (10^4 higher than crystalline quartz) and could not be attributed to the classical absorption mechanisms in solids; however, the values were of the same order of magnitude as predicted by the resonance absorption theory. Rasmussen[7,8] elaborated on Liebermann's theory and made measurements on single crystalline cyclohexane and carbon tetrachloride. His theory and experiments qualitatively corroborated Liebermann's results. The details of Liebermann's theory and Rasmussen's modifications of it will be discussed in Section 2.1.

Further experimentation in the field was performed by Yun and Beyer[9,10] on single crystals of naphthalene and p-dichlorobenzene. The absorption values for both substances exhibited a frequency-squared dependence and little variation with temperature as ostensibly predicted by Liebermann's theory. Although the absorption values were relatively high for the frequency range investigated (5-95 MHz), they were about one order of magnitude

lower than those for benzene and cyclohexane. As a result, Yun and Beyer examined the contributions of the thermoelastic effect and dislocation damping more closely. It was found that the former mechanism was two orders of magnitude smaller than the observed absorption values. To determine the contribution due to dislocation damping, a uniaxial pressure was applied to the crystals in small increments in a direction perpendicular to the direction of sound propagation. Although such treatment should increase the number of dislocations, no apparent change in absorption was detected.

Wilson and Yun[11] extended the measurements in naphthalene down to liquid nitrogen temperatures. (Previous measurements in naphthalene were made between 200°K and 300°K.) At approximately 170°K a relaxation effect begins to appear. The absorption increases as the temperature is decreased below 170°K and peaks at a lower temperature; the position of the peak depends on the frequency. As the temperature is further decreased to the lower experimental limit (77°K), the absorption begins to decrease once again. Wilson and Yun interpret their results in terms of Liebermann's theory which does predict a relaxation effect at lower temperatures. However, the predicted relaxation depends very strongly on the thermodynamic properties of the substance under consideration; consequently, the quantitative agreement between experiment and theory in this case may be fortuitous. The same calculation for benzene does not predict as strong a relaxation effect although this work does indicate the existence of relaxation effects in benzene as well.

Danielmeyer[12,13] extended the frequency range of the absorption measurements up to the 100-MHz region. He made measurements in liquid and

solid bromine, benzene, and cyclohexane; however, his work had two shortcomings. First, the thermal contraction of the experimental apparatus limited the temperature to -20°C; and second, the measurements on solids used polycrystalline samples, which made it difficult to correlate with previous single crystalline data. Danielmeyer did attempt to relate his measurements to previous investigations by proposing a theory which departs significantly from Liebermann's. The theory is based on a multiphonon interaction process and will be discussed in Section 2.2.

All the absorption measurements discussed above were made on specimens whose crystalline orientations were unknown; consequently, the effects of mode conversion between the longitudinal and transverse waves which are present under such conditions practically rules out correlation with the actual structure of the substance under consideration. Heseltine, Elliot, and Wilson[14] performed the first ultrasonic measurements on an oriented molecular crystal when they measured the longitudinal and shear sound velocities of single crystalline benzene. Since benzene is the basic aromatic hydrocarbon, many other experimental investigations have been performed on this substance; consequently, most of its structural and thermodynamic properties are known. It seemed appropriate, therefore, to carry out an experimental investigation on the ultrasonic absorption along the principal axes of crystalline benzene as a function of temperature. This is the subject of the present thesis.

2. THEORY

2.1 Liebermann's Theory

Liebermann[5,15] proposed that the chief cause of the large acoustic absorption in single crystals of organic materials is a relaxation process that converts, with a time delay, acoustic vibrations of the lattice into oscillations involving the internal degrees of freedom. That is, the transfer of energy from acoustic branches of the lattice spectrum into the optical branches is contemplated. He assumed that the absorption α could be expressed in terms of the standard equation for a relaxation process in a gas[16]

$$\alpha = \frac{1}{2s} \frac{(C_p - C_v)}{C_p} \frac{C_i}{(C_p - C_i)} \frac{\omega^2 \tau}{1 + \omega^2 \tau^2} \tag{2.1}$$

where s is the sound velocity, C_i the internal specific heat per mole associated with the internal degrees of freedom, C_p and C_v are the specific heats per mole at constant pressure and constant volume, respectively. τ is the relaxation time of the relaxation; its reciprocal τ^{-1} is an approximation to the initial time rate of energy transfer between the external and internal degrees of freedom. Hence, a theoretical calculation of τ yields $\alpha(\omega)$ if the other parameters in Eq. 2.1 are known.

Van der Waals forces are the main binding forces in a molecular crystal.[17] They can be represented in various ways; the Lennard-Jones potential is convenient:

$$U(r) = -4\varepsilon \left[\left(\frac{r_o}{r} \right)^6 - \left(\frac{r_o}{r} \right)^{12} \right] \tag{2.2}$$

where ε and r_o are the Lennard-Jones parameters for, respectively, the depth of the potential well and the lattice distance from the reference

molecule, where $U(r)$ is zero. Liebermann applied Eq. 2.2 to nearest neighbor pairs of rigid or almost rigid molecules. Close to its minimum value, $U(r)$ is nearly parabolic and therefore to first approximation it implies simple-harmonic oscillations, whether classical or quantum in detailed description. Deviations of $U(r)$ from a parabolic form can be treated as quantum mechanical perturbations that distort the zero-th order quantum mechanical wave functions. In particular, an acoustic signal applied at $t = 0$ can excite the lowest linear oscillator state of the lattice. Then, conventional use of first-order time-dependent perturbation theory will predict the time rate at which higher quantum states of lattice oscillations are excited.

The Lennard-Jones potential deviates in a skewed fashion from parabolic form. Therefore, to a good approximation, only excited states of odd parity (in zero-th order) will be excited from the ground state, which is of even parity. When Liebermann applied first-order perturbation theory to calculate the transition rate for benzene, the third excited state was the highest energy eigenvalue contained in the resulting expression. He chose this state to be approximately equal to the lowest energy state of the optical branch. (Spectroscopic data[2,18] available at the time would have shown this assumption to be invalid.) The calculation of the acoustic absorption coefficient is ostensibly completed by use of Eq. 2.1 under the assumption that the relaxation is from the third excited state of a longitudinal acoustic branch to the ground state of the lowest optical branch. When Liebermann calculated the value of α for benzene he used values of C_i given by Lord, Ahlberg and Andrews.[19] For substances for which the value of C_i are not available in the literature, the Einstein model

has been used to obtain the specific heat[20]

$$C_i = Rx^2e^x(e^x - 1)^{-2} \qquad (2.3)$$

R is the molar gas constant and $x = h\nu/k_BT$ where h is Planck's constant, ν the frequency of the optical branch in question, k_B the Boltzmann constant, and T the absolute temperature. Rasmussen[7,8] and Yun and Beyer[9] employed Eq. 2.3 to calculate the values of C_i for substances used in their experiments.

There are several assumptions, implicit or explicit, within the analysis for benzene. (a) The energy eigenvalue of the third excited state in the acoustical branch and an energy eigenvalue of an optical branch are essentially equal. (b) The center of mass of each molecule executes simple harmonic motion about its equilibrium position. The amplitude X_o of the associated lattice vibration of the acoustical branch caused by an applied acoustical signal is given by the classical equipartition of energy

$$MX_o^2\omega^2 = k_BT \qquad (2.4)$$

where M is the molecular mass and ω is the angular frequency of the lattice vibrations; i.e., the energy of the applied acoustic wave is already in thermal equilibrium with the lattice vibrations. (c) The time rate of transition in the relaxation process (τ^{-1} in Eq. 2.1) equals the time rate for excitation of the third excited state in the acoustical branch. (d) The density of states in the acoustical branch is given by the Debye theory of specific heats of solids.

Liebermann's final prediction for τ^{-1} is

$$\tau^{-1} = \frac{9A^2 N_o{}^4 (k_B T)^3}{16h(4\pi^2 M)^3 m_{01} \nu_{01} \nu_D{}^7} \qquad (2.5)$$

where N_o is Avogadro's number, m_{01} is the apparent internal vibrating mass, ν_{01} is the atomic vibrational frequency associated with the transition of an optical branch from its ground state to its first excited state, ν_D is the Debye frequency, and A is the coupling parameter which is derived from the first anharmonic term in the Lennard-Jones potential.

Liebermann[6] made measurements in single crystalline benzene at 6.4 MHz and 10.7 MHz at a temperature of 273°K. He found α proportional to ω^2 for these two values and α nearly independent of temperature down to 215°K. Upon substituting his values of α in Eq. 2.1 along with his experimentally measured sound velocity and the known values for the specific heats,[19] Liebermann found $\tau \simeq 0.5 \times 10^{-9}$ sec. Substitution of known values for benzene in Eq. 2.5 yielded $\tau \simeq 1 \times 10^{-9}$ sec. This agreement tends to substantiate assumption (c) above. Also, either value of τ makes $\omega^2\tau^2 << 1$, in agreement with the ω^2-dependence of the measured absorption coefficients.

Treating acoustic absorption in single crystalline cyclohexane (which is face centered cubic, fcc), Rasmussen[7] followed Liebermann's approach but attempted to improve on the details in three main ways. First, he replaced Liebermann's Lennard-Jones potential between nearest neighbor molecules by a similar potential between pairs of atoms in the nearest neighbor molecules. In doing this he assumed that each atom site had the mass of one carbon and two hydrogen atoms and calculated effective Lennard-Jones parameters between the atom-atom pairs. Second, he assumed

no orientation effect, i.e., the plane of the molecule was considered to lie parallel to the x-y plane of the crystal unit cell. Third, he replaced the Debye lattice spectrum by that proper for an fcc crystal (Brillouin[21]). Fourth, he replaced the classical expression in Eq. 2.4 by the analogous quantum mechanical expression

$$\omega \coth\left(\frac{h\omega}{2k_B T}\right) \simeq \frac{2k_B T}{h}\left[1 + \frac{h^2\omega^2}{12k_B{}^2T^2} + \ldots\right] \tag{2.6}$$

With these changes Rasmussen's expression for the relaxation time is

$$\tau^{-1} = \frac{D^2 N_o^4 (k_B T)^3}{14 m_{01} h \nu_{01} \nu_m{}^7 (4\pi^2 M)^3}\left[1 + \frac{h^2}{12(k_B T)^2}\left(\nu_{01}{}^2 + \frac{3}{2}\nu_m{}^2 - 2\nu_{01}\nu_m\right)\right] \tag{2.7}$$

where D is the coupling parameter analogous to A in Eq. 2.5 and ν_m is the maximum allowable frequency in the first Brillouin zone. The first term in Eq. 2.7 is nearly identical to Eq. 2.5 except that ν_D has been replaced by ν_m and the numerical constants are different. The second term in the brackets in Eq. 2.7 turns out to contribute a small correction factor (approximately 5%) to the overall value of τ^{-1}; consequently, although the basic assumptions between Liebermann's and Rasmussen's theories are different, the functional forms of the final results are essentially the same. Rasmussen's predicted values of absorption for cyclohexane were about 50% higher than his observed values. His experimental measurements ranged from 3.8 to 8 MHz and showed frequency-squared dependence. Also, little change in absorption was observed with decreasing temperature down to 180°K.

Considering the number and the vagueness of Liebermann's approximations, the agreement between his theoretically predicted and experimentally observed absorption values is fairly good. However, as Liebermann himself

points out, to describe the absorption process more accurately a more realistic intermolecular potential must be used to calculate the relaxation time. Although the Lennard-Jones potential was probably the best approximation available at the time (1959), it has been mainly used to describe the gaseous and liquid states; therefore, the Lennard-Jones parameters do not account for the interaction of molecules within the rigid structure of a solid where the relative orientation and intermolecular distances of the molecules are fixed compared to those in the fluid states. Rasmussen attempted to correct for the latter discrepancy by treating the atom-atom interactions between neighboring molecules; however, he assumed that the adjusted Lennard-Jones parameters which he derived for the nearest neighbor intermolecular atom-atom pairs had the same value whether the two atoms were at adjacent ends of two molecules or at greater separations.

More recently D. E. Williams[22] has empirically derived an intermolecular potential for nine different molecular crystals (including benzene) which takes into account the actual atom-atom distances between neighboring molecules as determined from X-ray and neutron scattering experiments. Hence, the orientation of the molecules within the crystal structure is implicitly taken into account. The potential has the form

$$\begin{aligned} E = {} & A_{CC} \sum r_{CC}^{-6} + B_{CC} \sum \exp(-C_{CC} r_{CC}) \\ & + A_{CH} \sum r_{CH}^{-6} + B_{CH} \sum \exp(-C_{CH} r_{CH}) \\ & + A_{HH} \sum r_{HH}^{-6} + B_{HH} \sum \exp(-C_{HH} r_{HH}) \end{aligned} \qquad (2.8)$$

where r_{CC}, r_{CH} and r_{HH} represent the interatomic distances between the carbon-carbon, carbon-hydrogen, and hydrogen-hydrogen atom pairs of nearest neighbor molecules. The maximum distance used in the summation is 6A°. The A, B, and C's are adjustable constants which are determined for each

type of atom-atom interaction by correlating the potential energy with known values of the thermodynamic and structural properties for the substance under consideration. Bernstein[23] used Eq. 2.8 with Williams' values of the A, B, C constants to calculate the values of the acoustical and optical phonon frequencies for crystalline benzene. The agreement between the calculated and experimental values is good, which suggests that Eq. 2.8 would be useful in future theoretical investigations of acoustic absorption in molecular crystals, provided that the crystalline structure is known in detail.

Liebermann's calculation for the transition probability implicitly assumes that the number of transitions per unit time from the third excited state of the acoustical branch to the ground state of the lowest optical branch is equal to the number of transitions per unit time for the reverse process. Such a supposition is questionable from statistical mechanical considerations. The Bose-Einstein distribution predicts the occupation number of the lower energy state to be greater than that of the upper state which implies that the number of transitions per unit time should be unequal for the two processes.

Equation 2.5 indicates that τ^{-1} is proportional to $\nu_D^{-7}T^3$. If ν_D is considered to be a constant, then τ would decrease with increasing temperature. Also, the values of C_i are directly proportional to the temperature whereas the sound velocity is inversely proportional. Therefore, in the region where $\omega\tau << 1$, i.e., where α is proportional to ω^2, the temperature dependences of the parameters in Eq. 2.1 counteract each other. Thus, α is predicted to increase only slightly with increasing temperature. A. O. Williams[24] points out, however, that ν_D is directly

proportional to the sound velocity through the relation[25]

$$\nu_D = \left(\frac{9N}{4\pi V}\right)^{1/3} s_{avg} \qquad (2.9)$$

(A similar expression exists for ν_m of the fcc structure[25].) Subsequent to Liebermann's theoretical formulation, velocity measurements as a function of temperature have been made in cyclohexane,[7] carbon tetrachloride,[8] naphthalene[9] p-dichlorobenzene,[9] and benzene,[13] and in all cases the sound velocity exhibits a strong linear dependence on T; s decreases as T increases. (In benzene the velocity changes by 14% between 170°K and 250°K.) Erickson[26] showed that when the experimental velocity values are used to obtain τ^{-1} from Eq. 2.5, α is predicted to fall very fast with increasing temperature in the temperature range of the experimental investigations (180°K-310°K). This is inherently implausible and in strong disagreement with the approximate independence of α on T from the measurements of Liebermann,[6] Rasmussen[7,8] and Yun and Beyer.[9,10]

Finally, reference to experimental spectroscopic data on crystalline benzene upsets the energy eigenvalues used by Liebermann [assumption (a) above]. At 273°K the highest energy level in the acoustic branch is found to correspond to 105 cm^{-1} (Θ = 150°K)[2] and the lowest in the optical branch to 406 cm^{-1} (Θ = 582°K)[18], a ratio considerably exceeding three. Consequently, higher energy states of the acoustical branch must be considered in order to conserve energy between the two levels. This approach will be considered in the next section.

2.2 Danielmeyer's Theory

Danielmeyer[12,13] proposed a theory which would be applicable to the acoustic absorption in any molecular crystal, providing the Raman and infrared spectra, the specific heats, and the elastic constants of the substance are known. He postulates that the sound absorption is primarily a result of multi-phonon processes between the acoustical and optical energy levels, and for some substances between different levels of optical branches. In using the multi-phonon concept, the transition probability is calculated between the different energy levels involved which results in a relaxation time for the process. The relaxation time is related to the acoustic absorption by deriving an expression for the complex sound velocity by combining (1) the equation of motion for a solid, (2) the equations of state for a solid as described by Liebfried and Ludwig,[27] and (3) the reaction rate equation of Herzfeld and Rice.[28] The resulting equation for the complex sound velocity is then separated into its real and imaginary parts which, in turn, yield expressions for the velocity dispersion and sound absorption, respectively. Both quantities are described in terms of a relaxation strength relating the structural and thermodynamic properties of a substance and the relaxation time, which combines the transition probability between energy levels with the anharmonic properties of the intermolecular potential. To derive the above expressions, Danielmeyer assumes the Debye-Einstein model for the molecular solid which stipulates that the frequency of each optical branch is constant throughout the first Brillouin zone and that the frequency of each acoustical branch is linearly proportional to the appropriate sound velocity (longitudinal or transverse)

throughout the first Brillouin zone, with a maximum frequency of ν_D at the outer edge of the zone. Furthermore, only transitions between the longitudinal acoustic branches and the optical branches are considered because in most solids the longitudinal acoustic energy levels lie closer to the optical levels; hence, a greater transition probability would be expected.

To conserve energy in a phonon-phonon interaction, the sum of the energies of the phonons which are destroyed must equal the energy of the phonon which is created. Since the optical levels are usually much higher than the acoustical levels, Umklapp processes (U-processes) play an important role in such a transition. Using the Debye-Einstein model, Ziman shows that the fraction of U-processes involved in a three-phonon interaction is[29]

$$\frac{\nu_o^2 - \nu_D^2}{2qs(\nu_o - qs)} \tag{2.10}$$

where ν_o is the frequency of the optical branch, ν_D is the Debye frequency, q is the magnitude of an arbitrary acoustic wave vector, and s is the sound velocity. Equation 2.10 shows that the number of U-processes increases as the difference between ν_o and ν_D increases. ν_o and ν_D are proportional to the Einstein temperature Θ_E and the Debye temperature Θ_D, respectively. Hence, Eq. 2.10 implies that the ratio of U-processes increases up to the limit where $\Theta_E/\Theta_D = 2$, at which point no two acoustic wave vectors would be large enough to satisfy the energy condition and still be less in magnitude than the maximum allowable wave vector in the first Brillouin zone, q_D. In general the ratio Θ_E/Θ_D is greater than two for most organic solids; consequently, it is necessary to consider higher-order phonon processes in the calculation of the transition probability. In benzene, for example, $\Theta_E/\Theta_D = 3.85$; therefore, at least four acoustic phonons must combine

to produce one optical phonon; hence, a five-quantum process is required.

To calculate rigorously the transition probability of multi-phonon processes (m-quantum processes) one must use the higher order, anharmonic terms in the potential energy. Each anharmonic term used yields an additional contribution to the transition probability. However, a generalized intermolecular potential for organic solids was not known at the time; consequently, Danielmeyer proposed that the m-quantum process could be constructed from a series of three-quantum processes. The transition probability for each three-quantum process is calculated using first-order time-dependent perturbation theory and the first anharmonic term in the potential energy expansion for an isotropic solid. The energy levels between the initial and final states are considered to be virtual energy states which are short lived, and consequently not well defined as a result of the uncertainty principle. Danielmeyer shows that for a given m-quantum process there will be (m-2) three-phonon processes involved.

To determine the order of the phonon process involved for a particular substance one must know the energy relationships between the various acoustical and optical levels. This information can be readily obtained from Raman and infrared spectroscopy data. In some cases the separation between energy levels in the optical spectrum is large enough to consider two or more separate optical groups. This occurs in cyclohexane, for example, where the spectroscopic data show one group of optical levels falling in the range θ_E = 333°K to 751°K and a second group between θ_E = 1154°K to 2094°K. The difference between the closest energy levels of the two groups is 402°K whereas the difference between the highest acoustical energy level

(characterized by Θ_D, which is 130°K for this case) and the lowest optical level is 203°K. Therefore, two relaxation processes are possible. The acoustic-optic process with $\Theta_E/\Theta_D = 2.55$ requires the annihilation of three acoustic phonons to create one optical phonon, a four-phonon process. The optic-optic transition with $\Theta_E/\Theta_D = 3.1$ requires four acoustical phonons plus one optical phonon from the lower optical group to be annihilated to create one optical phonon in the upper optical group, a six-phonon process. In general, the optic-optic transition will influence the sound absorption only when it is of a higher order than that of the acoustic-optic transition because a larger value of τ is predicted for the higher order process and, as will be shown later, in the region where $\omega\tau << 1$, α is proportional to $\omega^2\tau$. Hence, the optic-optic transition will be taken into consideration only when the process is at least one order higher than the acoustic-optic process for the same material.

The levels within an optical group are spaced so close together in comparison to the energy spacing between groups that, once energy is coupled into the group, the excess energy is rapidly distributed among the levels within the group. In many cases where a vibrational relaxation has been observed in a molecular gas or liquid, it has been found that the total vibrational specific heat can be associated with a single relaxation time; consequently, the entire optical group can be represented by a single characteristic internal temperature, T_i.[30] Danielmeyer assumes that this generalization holds true in the molecular solid and uses it in deriving an expression for the acoustic absorption (the derivation will be discussed below).

Danielmeyer examined the spectroscopic data of all the materials on

which acoustic absorption measurements had been made, i.e., benzene,[6] cyclohexane,[7] naphthalene,[9] p-dichlorobenzene[9] and bromine,[13] and found the p-dichlorobenzene was the only other substance besides cyclohexane for which the optic-optic transition was important. (Note: All equations which are not directly referenced below have been taken from Danielmeyer's original work[13].) To treat the spectroscopic data in a general manner, the ratio Θ_E/Θ_D is defined in terms of a transition parameter

$$\lambda \equiv \frac{\Theta_j - \Theta_{j'}}{\Theta_D} \equiv \frac{\Theta}{\Theta_D} = \frac{\nu_j - \nu_{j'}}{\nu_D} \tag{2.11}$$

where $j = j' + 1$ and the notation Θ_E is replaced by Θ_j. The index j denotes the optical level under consideration and is equal to 1, 2, or 3 corresponding to the bottom of the first optical group, the top of the first optical group, and the bottom of the second optical group, respectively. The transition parameter is greater than two for all the organic substances discussed; consequently, an m-quantum process must be considered for each case.

The quantitative calculation of the m-phonon transition probability incorporates a number of simplifying assumptions. (1) The m-phonon process can be described as the sum of a series of three-phonon processes. There are (m-2) three-phonon processes for a given m. (2) Each acoustical and optical energy level is considered to be a simple harmonic oscillator. The isothermal relaxation time between oscillator states $\langle f|$ and $|i\rangle$ is given by

$$\tau_T^{-1} = P_{if} - P_{fi} \tag{2.12}$$

where τ_T is the isothermal relaxation time. P_{if} is the probability that a particle in energy level $|i\rangle$ will make a transition to energy level

$< f|$. P_{fi} is the corresponding probability for the reverse reaction.

(3) The number of particles in an energy state j is given by the Bose-Einstein distribution

$$n_j = \frac{1}{e^{\Theta_j/T} - 1} \quad , \tag{2.13}$$

For acoustic phonons the high temperature approximation of Eq. 2.13 is assumed, i.e., $T >> \Theta_D$; hence, the occupation number becomes

$$n_{ai} \simeq \frac{k_B T}{h\nu_{ai}} \tag{2.14}$$

where the index ai refers to the ith acoustic phonon.

(4) The number of particles making transitions via a three-phonon process from state $|i>$ to $<f|$ is given by the product $n_i P_{if}$, which is related to the standard transition probability expression derived from first-order time-dependent perturbation theory by

$$n_i P_{if} = W_{if} = \frac{2}{\pi} \int |H_{fi}|^2 \rho(q) \delta[E_f - E_i] dE_q \quad . \tag{2.15}$$

Here H_{fi} is the matrix element $<f|H_3|i>$ and H_3 is the perturbation Hamiltonian obtained from the first anharmonic term in the intermolecular potential. The density of states is assumed to be given by the Debye approximation and is expressed in the form

$$\rho(q) dE_q = \frac{V}{2\pi^3} q_{ai}^2 \, dq_{ai} \tag{2.16}$$

where V is the volume and q_{ai} is the ith acoustic phonon wave vector. The delta function ensures energy conservation between the two states in question. By combining Eqs. 2.11 and 2.16 and using the properties of the delta function to integrate over the volume, Eq. 2.15 can be expressed in terms of the transition parameter λ:

$$n_i P_{if} = W_{if} = \frac{V}{h^2\pi}\frac{\lambda^2}{s_o} q_D^2 |H_{fi}|^2 \qquad (2.17)$$

where s_o is the sound velocity in the frequency range in which no dispersion exists.

(5) The perturbation Hamiltonian is obtained from the theory of vibrations in an elastic continuum. In the classical theory of elasticity it is assumed that the potential energy density at any point is a quadratic function of the local strain, i.e., Hooke's Law. The first anharmonic potential energy density term involves a cubic function of the local strain and is given by the expression[31]

$$H_3 = \frac{1}{3!}\int_V \sum_{ijk\ell mn} s_{i,j}\, s_{k,\ell}\, s_{m,n}\, A_{ijk\ell mn}\, dV \qquad (2.18)$$

where the $A_{ijk\ell mn}$ are rrelated to the third order elastic constants and the $s_{i,j}$ are the displacement gradients. Equation 2.18 is usually written in a more convenient form utilizing the creation and annihilation operators. After several substitutions involving the relationships between the displacement gradients, normal coordinates, and the creation and annihilation operators, Eq. 2.18 can be rewritten for the special case of a single three-phonon process as[32]

$$H_3 = i\left(\frac{h}{8V\rho^3}\right)^{3/2}\left(\frac{q_I q_{II} q_{III}}{s_o^3}\right)^{1/2} B\,(a^*_{q_I} a^*_{q_{II}} a_{q_{III}} - a_{q_I} a_{q_{II}} a^*_{q_{III}})\,\delta(\vec{q}_I+\vec{q}_{II}-\vec{q}_{III},\vec{g}) \qquad (2.19)$$

Here the $a^*_{q_i}$ and a_{q_i} are the creation and annihilation operators, respectively. The delta function ensures momentum conservation within the first Brillouin zone (Normal processes) and allows for the possibility of U-processes through the reciprocal lattice vector $\vec{g}$. B is defined as the

coupling parameter and is related to a summation of the $A_{ijk\ell mn}$.[33] For longitudinal sound waves propagating in an isotropic solid B can be expressed in terms of the Grüneisen constant,[34] γ:

$$\gamma = -\frac{1}{6}\frac{B}{c^s_{11}} \tag{2.20}$$

c^s_{11} is the second-order elastic constant associated with the longitudinal sound velocity. The Grüneisen constant, in turn, can be related to the macroscopic thermodynamic properties of a solid by[35]

$$\gamma = \frac{M\beta}{\rho C_v \chi^T} \tag{2.21}$$

where β is the volume expansion coefficient and χ^T is the isothermal compressibility. Thus, the coupling parameter can be related to the bulk properties of the solid. Substitution of Eq. 2.19 into Eq. 2.17 allows one to calculate W_{if} and W_{fi} for the process being considered, i.e., optic-optic or acoustic-optic. The transition between two optical levels involves one acoustical phonon ($\vec{q}_I = \vec{q}_{ai}$) and two optical phonons ($\vec{q}_{II} = \vec{q}_2$, $q_{III} = \vec{q}_3$). By use of Eqs. 2.13, 2.17, and 2.22, Eq. 2.12 becomes

$$\frac{1}{\tau_T} = P_{23}-P_{32} = 4\pi^2\nu_D\lambda^2\left(\frac{\pi k_B T \nu_D{}^3 B^2}{2\lambda^2\rho^3 s_o{}^9}\right)\left(e^{\Theta/T}-1\right)\lambda^2 \equiv 4\pi^2\nu_D\lambda^2 K\left(e^{\Theta/T}-1\right)J_1 \tag{2.23}$$

where the quantities K and J_1 are defined as indicated. (J_1 will be discussed below). The factor $(e^{\Theta/T}-1)$ arises from consideration of the occupation numbers of the phonons at equilibrium as given by the Bose-Einstein distribution. (Note that Liebermann neglected to take this into account, which was one of the basic criticisms of his theory).

The same equations are used to calculate the three-phonon acoustic-optic

process, with one exception. Because the process involves two acoustical phonons, the delta function in Eq. 2.22 can be satisfied by many values of $\vec{q}_{a1}$ and $\vec{q}_{a2}$; consequently, the integral over the density of states must be modified. Looking ahead to the m-quantum process in which Γ acoustic phonons are involved, Danielmeyer defines a density-of-state function J_Γ in terms of the transition parameter λ. He then calculates J_Γ for several values of Γ and from the set of values obtained he empirically derives a function J_λ. J_λ turns out to have the simple form

$$\begin{aligned} J_\lambda &= 10^{-3}\,\frac{(\lambda-1)}{2} \qquad \text{for} \quad \lambda > 1 \\ J_1 &= \lambda^2 \qquad\qquad\qquad\quad \text{for} \quad \lambda \leq 1 \end{aligned} \tag{2.24}$$

Γ and λ are related by the expression

$$\Gamma = \lambda + \frac{1}{4}\,[3 + \cos(2\pi[\lambda-0,1])] \tag{2.25}$$

where in the argument of the cosine function 0 and 1 are used for the acoustic-optic and optic-optic transitions, respectively. The transition parameter λ, then, is the fundamental quantity of the calculation.

For a three-phonon acoustic-optic process τ_T^{-1} becomes

$$\begin{aligned} \tau^{-1} &= P_{01} - P_{10} \\ \tau_T^{-1} &= \frac{4\pi^2 \nu_D \lambda^2 KT(e^{\Theta/T} - e^{-\Theta/T})J_2}{6\Theta_D} \end{aligned} \tag{2.26}$$

where the index 0 refers to the top of the acoustical band. Once again the exponential factors arise from consideration of the occupation numbers in the two states. Equation 2.26 does not fully agree with Eq. 2.23, but Danielmeyer[13] has attempted to keep their main structures alike.

Assumption (1) above states that for an m-quantum process there are (m-2) contributions to the total transition probability. Also, for a given

substance it was pointed out that the optic-optic transition would influence the absorption only if the process was at least one order higher than the acoustic-optic transition. With these criteria, Danielmeyer shows that the number of contributions to τ_T^{-1} is related to the number of acoustic phonons, Γ, involved in a given m-quantum process. For the optic-optic transition

$$(m-2) = \Gamma \tag{2.27a}$$

whereas for the acoustic-optic transition

$$(m-2) = \Gamma - 1 \tag{2.27b}$$

Equations 2.27 indicate that there are Γ-1 and Γ-2 intermediate virtual energy states for the respective transition types. To calculate τ_T^{-1} for the m-quantum process, the transition probability from the initial real energy state to the first virtual energy state must be calculated; then the transition probabilities between the successively higher virtual energy states are calculated and finally, the transition probability between the highest virtual state and the final real energy state is calculated. When this is done, the total transition probability for the optic-optic m-quantum process is

$$\tau_T^{-1} = \left(\frac{2\pi\lambda}{\Gamma}\right)^2 \nu_D K^\Gamma \Gamma(e^{\Theta/T}-1)J_\Gamma \tag{2.28}$$

and for the acoustic-optic case it is

$$\tau_T^{-1} = \left(\frac{2\pi\lambda}{\Gamma}\right)^2 \nu_D K^{\Gamma-1} \frac{\pi(\Gamma-1)T}{6\,\Theta_D} (e^{\Theta/T}-e^{-\Theta/T})J_\Gamma \tag{2.29}$$

Comparison of Eqs. 2.28 and 2.29, respectively, with Eqs. 2.23 and 2.26 show that they differ only via the factors of Γ involved. The factor K is raised to a power equal to the number of three-phonon processes that

contribute to the total relaxation time, i.e., Γ or Γ-1, and the entire equation is multiplied by the same factor. The density-of-states integral J_Γ is evaluated by using Eqs. 2.24 and 2.25.

To relate the relaxation times to the sound absorption, Danielmeyer derives an expression for the complex sound velocity in an isotropic molecular solid. The exchange of energy between the internal and lattice vibrational modes is described by the well known relaxation rate equation[28]

$$\frac{dT_i}{dt} = -\frac{1}{\tau_T}(T_i - T_a) \tag{2.30}$$

T_i, the characteristic temperature of the internal vibrations, is assumed to represent all the internal vibrations within the optical group under consideration (see discussion on page 16). T_a is the temperature that accompanies the sound wave due to the localized compressions and rarefactions; therefore, it is periodic in nature. In addition to the localized temperature variations, the sound wave will induce localized deformations in the solid which are described by the equation of motion[36]

$$\sigma_{ij,j} = \rho\ddot{s}_i \tag{2.31}$$

where $\sigma_{ij,j}$ is the derivative of the stress tensor σ_{ij} with respect to the jth coordinate; $\ddot{s}_i$ is the second time derivative of the particle displacement in the ith direction; ρ is the density. Under the assumption that the deformations are small enough to allow neglect of second-order effects, s_i is related to the strain tensor ε_{ij} by[37]

$$\varepsilon_{ij} = \frac{1}{2}(s_{i,j} + s_{j,i}) \tag{2.32}$$

The perturbation of the thermal and mechanical properties of a solid that is caused by the passage of a sound wave can be described in terms of the

thermal and caloric equations of state (Liebfreid and Ludwig[27]) which relate, respectively, the pairs of quantities T_a and ε_{ij} and σ_{ij} and ε_{ij} to variations of the Helmholtz free energy of the system, which, in turn, can be expressed in terms of macroscopic thermodynamic quantities. For an isotropic solid the thermal equation of state becomes

$$\sigma_{ii} = c_{11}^{T} \varepsilon_{ii} - \frac{\gamma C_v \rho (T_a - T)}{M} \tag{2.33}$$

where c_{11}^{T} is the isothermal elastic constant associated with any longitudinal sound velocity and γ is the Grüneisen constant which can be calculated from Eq. 2.21. The time derivative of the caloric equation of state is

$$C_v^{\,i} \frac{d}{dt}(T_i - T) + C_v^{\,a} \frac{d}{dt}(T_a - T) + T\gamma C_v \dot{\varepsilon}_{ii} = 0 \tag{2.34}$$

where $C_v^{\,i}$ and $C_v^{\,a}$ are the specific heats associated with the internal (optical) modes and acoustical modes, respectively. Assuming that the sound wave propagates as a plane wave described by $e^{i(\vec{k}\cdot\vec{r}-\omega t)}$ with amplitude small enough so that T_i and T_a can be represented by small departures from the equilibrium temperature, Danielmeyer combines Eqs. 2.30 through 2.34 to obtain an expression for the complex sound velocity

$$\frac{\omega^2}{k^2} = \frac{c_{11}^{T}}{\rho} + \frac{\gamma^2 T C_v^{\,2}/M}{C_v^{a} + C_v^{i}/(1+i\omega\tau_T)} \tag{2.35}$$

The real part of Eq. 2.35, which describes the velocity dispersion yields

$$\left(\frac{s}{s_o}\right)^2 = \frac{1 + (1-r)r^2\omega^2\tau_{ps}^2}{1 + (1-r)^2\omega^2\tau_{ps}^2} \tag{2.36}$$

The imaginary part, expressed in terms of absorption per wavelength, is

$$\mu \equiv \alpha\lambda = \frac{\pi r\omega\tau_{ps}}{1 + (1-r)\omega^2\tau_{ps}^2} \tag{2.37}$$

The quantity r is the relaxation strength, defined by

$$r = \frac{(C_p - C_v)\zeta_s C_v^i}{C_v(C_p - \zeta_s C_v^i) - C_p(1-\zeta_s)C_v^i} \tag{2.38}$$

ζ_s in Eq. 2.38 is related to the mechanical properties of the solid by

$$\zeta_s = 1 - \frac{4}{3}\frac{c_{44}^s}{c_{11}^s} \tag{2.39}$$

where c_{11}^s and c_{44}^s are the adiabatic elastic constants for an isotropic solid. The isothermal relaxation time τ_T has been replaced by τ_{ps}, the relaxation time at constant pressure and entropy. The two are related by the expression

$$\tau_{ps} = \frac{C_v^a/C_v}{1 - r}\tau_T \tag{2.40}$$

Danielmeyer uses τ_{ps} instead of τ_T so that the absorption values obtained in the solid can be compared with those of the gaseous and liquid state where τ_{ps} is the relaxation time customarily used to describe the relaxation process.[38]

Equations 2.35 and 2.36 are in the standard form of the relaxation theory for liquids and gases;[39] however, they have been obtained from a solid state viewpoint rather than from the fluid state approach used by Liebermann. The properties of the solid are explicitly contained in the relaxation strength, i.e. ζ_s, and the relaxation time, i.e., the coupling parameter B.

In the region where $\omega\tau_{ps} << 1$, Eq. 2.37 can be written in terms of α as

$$\alpha_{\ell} = \frac{2\pi^2 r\tau_{ps}\nu^2}{s_o} \tag{2.41}$$

For $\omega\tau_{ps} >> 1$

$$\alpha_h = \frac{r}{2(1-r)s\tau_{ps}} \tag{2.42}$$

Equation 2.41 indicates that the absorption coefficient is proportional to the square of the frequency as in Liebermann's case. Also, α_{ℓ} is directly dependent on r and τ_{ps}. τ_{ps} is inversely proportional to temperature, whereas r is directly proportional; therefore, the two temperature-dependent effects tend to counteract each other and result in a slight temperature dependence of α_{ℓ} , the absorption decreasing with decreasing temperature. Equation 2.42, however, indicates that α_h is independent of frequency. Also, since both $r(1-r)^{-1}$ and τ_{ps}^{-1} are directly proportional to the temperature, α_h is influenced by temperature changes a great deal more than α_{ℓ}.

Using values available at the time for parameters contained in the equations leading up to and including Eq. 2.41, Danielmeyer calculated the absorption coefficient for single crystalline benzene at 6 and 10 MHz at 270°K to be 0.099 cm^{-1} and 0.310 cm^{-1}, respectively. These values compared quite well with Liebermann's experimental values of 0.09 cm^{-1} and 0.24 cm^{-1} which were measured at 6.4 and 10.7 MHz, respectively, at 273°K. However, Danielmeyer's theory does not agree as well with other experimental results. A comparison will be made below.

From Eq. 2.37 , the frequency at which the sound absorption coefficient (per wavelength) reaches a maximum is

$$\omega_m = \frac{1}{\tau_{ps}\sqrt{1-r}} \tag{2.43}$$

Equation 2.43 predicts the maximum absorption per wavelength in solid benzene at 275°K to occur at 800 MHz. In liquid benzene the corresponding frequency has been theoretically predicted as approximately 600 MHz.[40] Experimental values of Heasell and Lamb[41] and Hunter and Dardy[42] qualitatively corroborate the predicted value although the measurements have been made only up to 510 MHz. Hence, Danielmeyer concludes that since no relaxation effects appear in the liquid state until the frequency reaches about 600 MHz, solid benzene will exhibit a similar behavior and relaxations will not appear until the frequency reaches the vicinity of his predicted 800 MHz. It will be shown in this work that although the frequency-squared dependence of the absorption in solid benzene is approximately true down to 250°K, the experimental absorption values exhibit relaxation effects at much lower frequencies than Danielmeyer predicts; the amount of departure from the ν^2 dependence is a function of crystal orientation.

As in Liebermann's case, Danielmeyer's relaxation times (Eqs. 2.28 and 2.29) are strongly dependent on the Debye frequency contained in the factors K^{Γ} and $K^{\Gamma-1}$ ($\Gamma = 4.52$ for benzene). All of Danielmeyer's predicted values assume ν_D independent of temperature. If τ_T is calculated for benzene, using Eq. 2.29 for the temperature range of 170-250°K with ν_D constant, τ_T increases with decreasing temperature and the absorption in the region where $\omega\tau << 1$ is predicted to be practically independent of temperature. Conversely, if ν_D is assumed to vary in accordance with Eq. 2.9 (using published velocities of benzene[14]), τ_T decreases by one order of magnitude in the same temperature range which, in turn, predicts a corresponding

decrease in α. Although this does not agree with published experimental results, the temperature dependence of the absorption values obtained in this work does show a decrease of absorption with decreasing temperature, at rates depending on the crystal orientation and the ultrasonic frequency. Therefore, in contrast to the effect of a temperature dependent ν_D on Liebermann's predicted relaxation times, Danielmeyer's equations still predict a plausible result. The exponential factors contained in Eqs. 2.28 and 2.29 and the velocity term, $(s_o^9)^{-1}$, in K offset the dependence of ν_D with temperature.

Table I shows a comparison of the experimental and theoretical relaxation times for both Liebermann's and Danielmeyer's theories. The experimental values were obtained by substituting the measured absorption values into Eq. 2.1 and 2.41, respectively. Equation 2.40 was used to convert the τ_{ps} obtained from Eq. 2.41 into τ_T. The theoretical values were calculated by the various investigators as indicated. When Danielmeyer calculated $(\tau_T)_{exp}$ for naphthalene and p-dichlorobenzene, he used the absorption values given in the original paper of Yun and Beyer;[9] however, they later published an Erratum[10] in which they noted that these experimental results as originally reported were in error due to a miscalculation. Danielmeyer apparently did not see the erratum; consequently, he was misled into believing that his theory predicted an order of magnitude agreement with experiment for these two substances. Danielmeyer's calculated values for $(\tau_T)_{exp}$ in Table I are shown in parentheses for naphthalene and p-dichlorobenzene. If these values were correct, Danielmeyer's theory would agree favorably with experimental results except for cyclohexane. The values of $(\tau_T)_{exp}$ calculated from the corrected

Table I

Comparison of Experimental and Theoretical Relaxation Time for Organic Single Crystals

Substance	Temp. (°K)	$(\alpha/\nu^2)_{exp}$ (cm^{-1} sec^2) $\times 10^{15}$	Liebermann's Theory τ_{theor} (sec) $\times 10^{10}$	Liebermann's Theory τ_{exp} (sec) $\times 10^{10}$	Danielmeyer's Theory τ^{e}_{theor} (sec) $\times 10^{10}$	Danielmeyer's Theory τ_{exp} (sec) $\times 10^{10}$
Benzene	275	2.4 [a]	10.0 [a]	5.0	3.4	3.7 [e]
Cyclohexane	272	3.7 [b]	19.0 [b]	13.0	(1) .045 [†] (2) 0.8 [††]	2.4 [e]
Naphthalene	294	0.32 [c]	1.4 [c]	2.4	0.038	0.52[*] (0.038) [e]
p-dichloro-benzene	294	1.3 [c]	0.29 [c]	3.0	(1) 0.003 [†] (2) 0.026 [††]	5.3[*] (0.026) [e]
Carbon tetrachloride	243	2.6 [d]	62 [d]	39	---	---

a. Reference 6
b. Reference 7
c. Reference 9,10
d. Reference 8
e. Reference 12
† Acoustic-Optic
†† Optic-Optic

[*]Recalculated values using corrections in reference 10.

absorption values are shown without parentheses. It can be seen that agreement is rather poor for all substances except benzene. Conversely, Liebermann's theory indicates an order-of-magnitude agreement with all the experimental results to date; however, as pointed out earlier some of the fundamental concepts of Liebermann's theory are questionable. Although Danielmeyer attempted to account for some of the weaknesses in Liebermann's theory, the experimental results do not corroborate his predictions.

Unquestionably, the theoretical analysis of acoustic absorption in molecular solids is an extremely complex problem. Danielmeyer and Liebermann attempted to simplify the problem to a point where a quantitative calculation could be made; however, the results of both theories indicate that further theoretical development of this subject is desirable.

2.3. Absorption Due to Thermal Conduction

The experimental absorption values are the sum of the vibrational absorption and the "classical" absorption due to thermal conduction. The latter quantity can be calculated from the theory of Woodruff and Ehrenreich.[43] In the region where $\omega\tau << 1$, the absorption due to thermal phonons is given by

$$\alpha = \frac{\gamma^2\omega^2 T\kappa}{\rho s^5} \qquad (2.44)$$

where κ is the thermal conductivity and γ is the Grüneisen constant. Instead of using experimental values of κ, Danielmeyer substitutes the expression[44]

$$\kappa = \frac{\rho s^3 d}{3\gamma^2 T} \tag{2.45}$$

in Eq. 2.44 where d is the lattice constant. Equation 2.44 becomes

$$\alpha_{c\ell} \simeq \frac{2\pi d\nu^2}{s^2} \tag{2.46}$$

By using Eq. 2.46 to calculate $\alpha_{c\ell}$, it can be shown that in none of the cases considered does $\alpha_{c\ell}$ exceed 1% of the experimental absorption values.

3. Experimental Apparatus and Procedures

3.1 Introduction

The properties of organic crystals differ considerably from those of ordinary "hard" solids; consequently, the handling of organic materials poses a number of onerous problems for the experimenter. Benzene freezes at 5.2°C and has a high vapor pressure of 36 mm Hg at that temperature which causes the solid to sublime very rapidly unless it is kept in a sealed container. To provide a work area that can be maintained below 5.2°C a refrigerated glove box which could be kept between -10°C and -15°C was constructed. Benzene crystals are relatively soft; therefore, special care had to be taken during cutting and facing operations, to avoid straining them. Benzene vapor is extremely toxic,[45] consequently, precautions had to be taken to exhaust the working area and to avoid breathing the fumes generated during preparation of the crystal for measurement. Hence, the glove box was located in a hood room and an organic vapor respirator was worn.

Since high values of acoustic attenuation were anticipated, double transducer operation would have been desirable; however, because of the rapid sublimation rate, a special transducer bonding technique had to be used which sealed the sample from the atmosphere while at the same time bonding the transducer onto the sample. Double transducer operation was incompatible with the bonding technique.

Prior to performing ultrasonic absorption measurements on oriented benzene samples a number of auxiliary experimental techniques had to be developed and/or applied. Liquid benzene was purified by vacuum sublimation. Large single crystals of benzene were grown from the melt. Orientation was accomplished by use of a polarizing microscope and a universal stage. Cutting

and polishing of the oriented sample was accomplished with a specially designed mechanical apparatus. Finally, the sample faces were sealed (the transducer bond provided the seal on one face) and ultrasonic measurements were made by the standard pulse-echo technique. Measurements were made from 6 to 26 MHz on all axes; additional measurements up to 38 MHz were made on the a and c axes. The characteristics of the bond restricted the temperature range between 170°K and 250°K. Since measurements were made as a function of temperature, only relative absorption values were obtained. Attempts were made to ascertain the attenuation due to the transducer bond; however, only an approximate estimate was obtained. Each step of the experimental procedure will be briefly described in the following sections; the specific details are given in the appendices.

3.2 Vacuum Sublimation Technique

The success of single crystal growth is largely dependent on the purity of the liquid when it is initially put into the crystal-growing apparatus. The benzene used in this experiment was purchased from the Fisher Scientific Company and was certified to be "99 Mol % Pure" and free of thiophene, the principal contaminant usually found in benzene. However, it was still necessary to degas the liquid benzene of dissolved air prior to crystal growth.

Among the many methods available for distillation, the vacuum sublimation technique[46] is particularly adaptable to materials that have a high vapor pressure in the solid state. Also, the procedure is carried out in a completely closed system; consequently, the problem of toxic vapors is eliminated. A vacuum sublimation system, constructed as an integral part of the crystal-growing apparatus, was designed to allow relatively large quantities

of benzene to be degassed fairly quickly.

The vacuum sublimation process is based on the fact that a substance maintained at a pressure or temperature below its triple point values cannot exist as a liquid. Phase transitions occur from the vapor to the solid, or vice versa, depending on whether heat is liberated or absorbed. On a phase diagram of pressure versus temperature (p-T diagram), the solid-vapor equilibrium curve (vapor-pressure curve) depicts the point at which a phase transition will take place for a given set of conditions. The substance will be a solid if both pressure and temperature are below the triple point; however, if the pressure is kept constant below the triple-point value and the temperature is raised, the substance will sublimate when the temperature reaches a value at which the solid and vapor are at equilibrium, i.e., when the temperature coordinate on the p-T diagram intersects the vapor pressure curve.

During a sublimation process, molecules leave the surface of the solid (the sublimand) and either remain in the vapor phase or recombine with the sublimand. Hence, the sublimation rate is directly proportional to the surface area of the sublimand and inversely proportional to the amount of recombination that takes place. The surface area is controlled by the physical dimensions of the vessel which contains the sublimand; therefore, the vessel is made as large as is practicable. Recombination can be prevented by providing an external means to carry off the molecules in the vapor before they can recombine. The external means in this case is a vacuum which is maintained throughout the system.

To dispose of impurities in it, the vapor must be recondensed to a solid at a temperature and pressure at which the impurity molecules remain in the vapor phase while the molecules of the substance to be purified are condensed.

If the pressure of the system is constant for both the sublimation and condensation processes, and is below the triple points of all the substances in the vapor, the condensation temperature must be above the triple point temperature of the impurities but below the triple point value of the substance to be purified.

The triple points of oxygen and nitrogen are approximately 2 mm Hg/54°K and 96 mm Hg/63°K, respectively.[47] The triple point of benzene is 36 mm Hg/278°K.[48] Therefore, if frozen benzene which contains dissolved air is sublimed at a pressure below 2mm Hg, the oxygen and nitrogen will pass off as gases. If the ensuing vapor is subsequently condensed at 77°K (at a pressure below 2mm Hg), the oxygen and nitrogen will remain in the vapor phase and continue to pass through the system, whereas the benzene will remain in the solid phase, freed of oxygen and nitrogen impurities.

In the construction of the vacuum sublimation system, it is necessary to insure that the components used in the system do not contaminate the substance which is being processed. Since benzene is a solvent for most greases, any stopcocks or glass joints which require vacuum grease as a lubricant cannot be used. Benzene also attacks most rubber materials used to make O-rings; however, viton is an exception and can be used safely. With these criteria, the system was fabricated from glass tubing of various diameters. Teflon stopcocks and glass-to-glass O-ring joints (with viton O-rings) were used where required.

A schematic drawing of the system is shown in Fig. 1. The teflon stopcocks are designated by T_i, the glass-to-glass O-ring joints by J_i, and the normal vacuum system valves are designated by V_i. The supply tube, the storage tube, and the large tube of the sublimate trap were made of glass

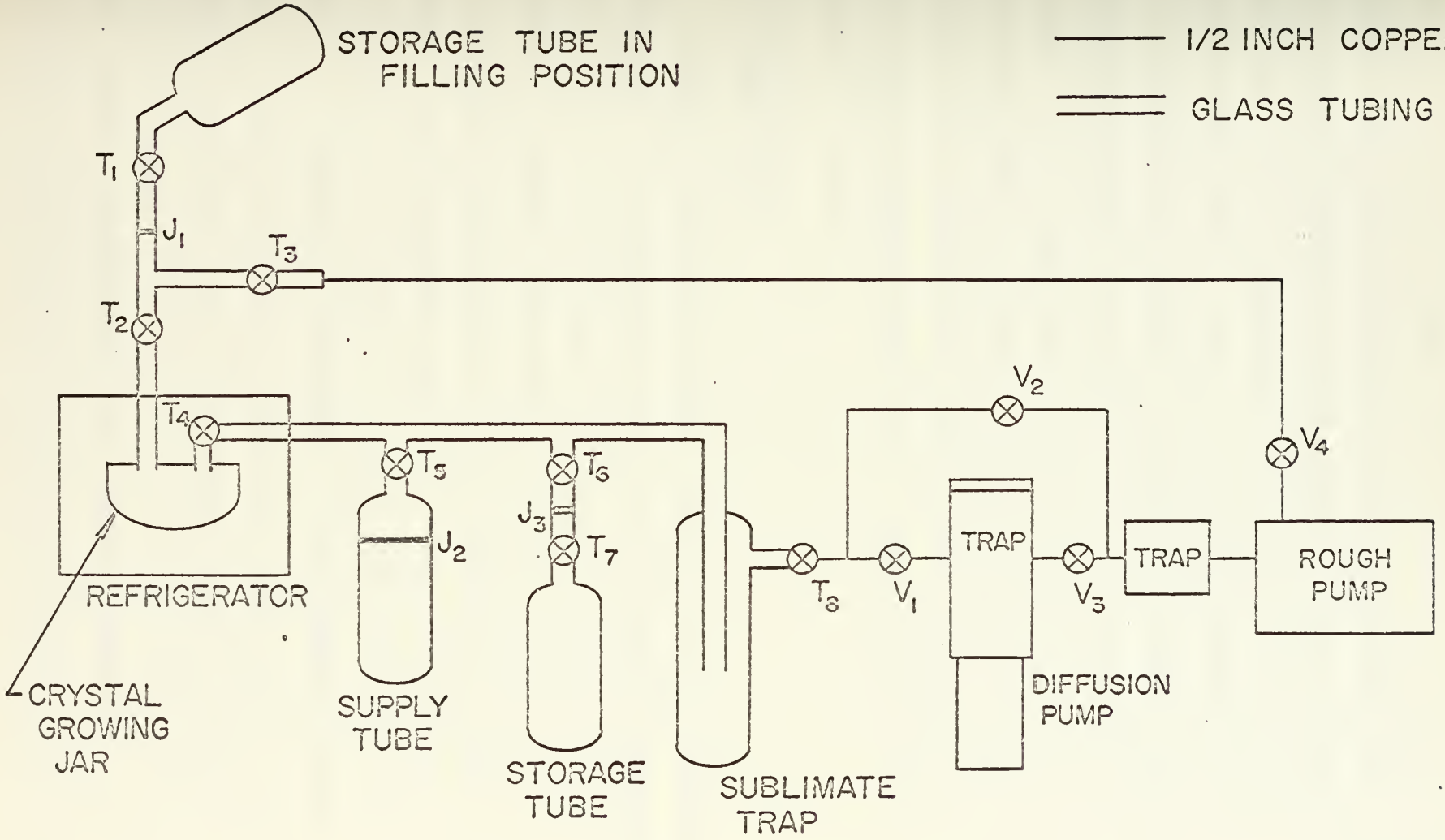

FIGURE 1 SCHEMATIC OF VACUUM SUBLIMATION AND CRYSTAL GROWING APPARATUS

tubing with an outside diameter (O.D.) of 52 mm. Since the sublimation rate depends a great deal on the surface area of the sublimand, these tubes were made as wide as possible yet narrow enough to fit into a standard one-liter dewar flask. The glass manifold and the inner tube of the sublimate trap were made from 10-mm O.D. tubing. The length and diameter of the inner tube in the sublimate trap determine the capacity of sublimate that can be deposited during the process. The wider the tube, the less likely it is to become clogged. The inner tube length is two-thirds that of the outer tube. Thus, approximately 100 ml of sublimate could be deposited at a time. The actual procedure used to sublimate the required amount of benzene and the method for putting the degassed benzene into the crystal growing apparatus are described in Appendix A.

3.3 Crystal Growth

During the orientation procedure (Section 3.4) and the subsequent preparation of the benzene single crystals for ultrasonic measurements (Section 3.5), a significant part of the original piece of crystal was trimmed away because of the cutting and melting operations involved. It was therefore necessary initially to grow large pieces of single crystalline benzene. The final oriented sample was 1.9 cm in diameter and 1.5 cm long. The crystal-growing apparatus and procedure used were adopted from a method developed by Liebermann[6] and Rasmussen.[7,8] The crystals are grown from the melt in a sealed container, by using a cold copper probe as the nucleation point for the crystal seed. Once the seed is formed, the crystal is grown by slowly varying the temperature of the melt, the probe, and/or the ambient air. The actual temperatures and their rates of change vary for each type of material in ways that must be determined principally through extensive

trial-and-error experimentation. Once the procedure is established, large pieces of single crystal can be grown (typically 10 × 10 × 5 cm).

The fundamental condition for crystallization to occur from a melt is that the total free energy of the solid-liquid system be decreased. For each volume of crystal that is created there is a decrease in the specific free energy of the solid and an increase in its surface free energy, the latter being a function of the surface tension at the solid-liquid interface. Hence, there is a critical size for the nucleus and a concomitant critical change in free energy which must be established for the volumetric effect to outweigh the surface effect. When this condition is fulfilled, the nucleus will support stable crystalline growth. Zhdanov[49] shows that for a given substance the critical change in free energy is decreased by (1) supercooling the liquid and (2) providing an external surface for nucleation.

Brice[50] shows that, in general, the rate of crystal growth is inversely proportional to the shear viscosity of the liquid and directly proportional to the amount of supercooling. He also points out that the temperature distribution within the solid-liquid system is a major factor in the quality of crystals grown and is one that can readily be controlled experimentally. If one considers the liquid-solid interface as a plane surface, the heat flow equation per unit area is

$$\kappa_s \frac{dT_s}{dx} = \Delta H_V f + \kappa_L \frac{dT_L}{dx} \qquad (3.1)$$

Here κ_s and κ_L are the thermal conductivities of the solid and liquid and dT_s/dx and dT_L/dx the corresponding temperature gradients. ΔH_V is the change in the specific enthalpy, i.e., the latent heat of fusion per unit volume, and f is the rate of linear growth in the x direction. Equation 3.1 shows that as the crystals grow in the x direction the latent heat

of fusion must be dissipated; this requires that the solid-liquid interface be cooled as the crystal grows. The heat can be dissipated through the solid, provided the proper temperature gradients exist. Ideally, the temperature gradient of the system should be such that a minimum temperature is at the center of the solid mass, a positive gradient exists between the center of the solid and the solid-liquid interface, and a positive gradient (smaller than that in the solid) exists from the interface to the outer extremity of the system. If the heat of fusion is not dissipated completely, the interface may become slightly warmer than some part of the liquid farther out in the melt. The result is a negative temperature gradient in that part of the melt, which leads to growth of unusable crystals.

In general, the intrinsic properties of surface tension, viscosity, and thermal conductivity of a liquid determine the difficulty of crystal growth for a given experimental apparatus. Experimentally, one has control over the temperature gradients and their time rates of change in the system and, to some extent, the degree of supercooling of the liquid. The presence of a cold probe in the liquid enhances nucleation of the seed crystal and also provides a path for the dissipation of the latent heat of fusion.

The entire crystal growing apparatus is built into a commercial refrigerator and is shown in Fig. 2. A large copper block (3/4 in. thick by 7.5 in. long by 6 in. wide) was made to attach onto the cooling coils of the refrigerator. Attached to the block is a tapered, stainless steel lid assembly which is used to seal a small pyrex bell jar. A copper probe is threaded through the copper block, passes through the lid, and extends into the jar. Two glass tubes and a thermocouple probe also pass through the lid-and-block assembly into the jar. A plexiglass box containing several heater elements

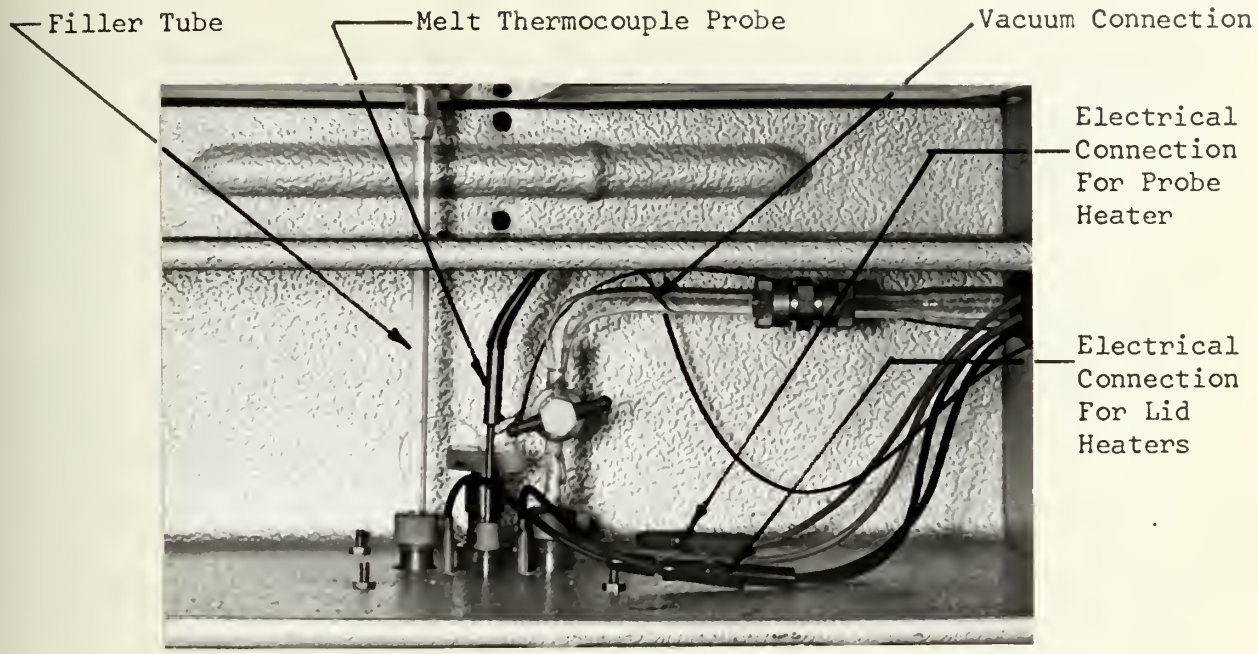

Fig. 2a. Refrigerator freezer compartment.

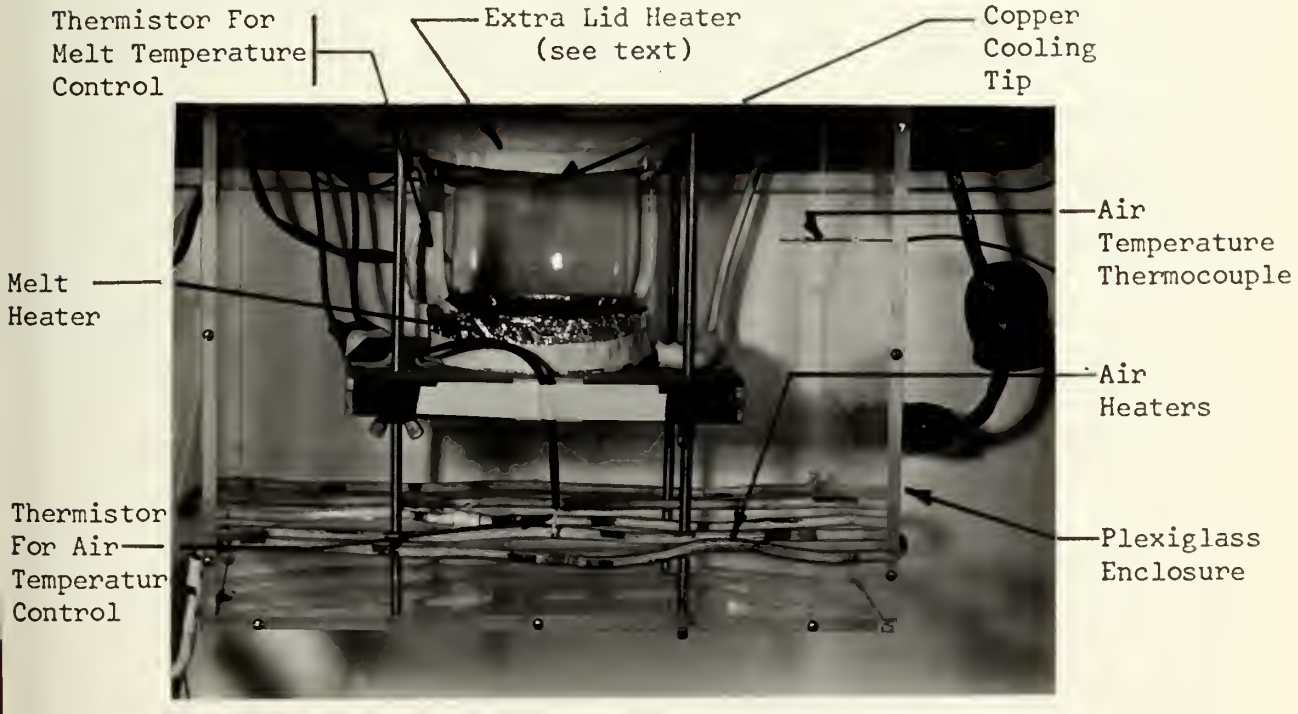

Fig. 2b. Crystal growing jar and associated equipment.

Fig. 2. Crystal growing apparatus.

encloses the entire apparatus and is used to control the ambient air temperature that surrounds the jar. The temperatures of the probe, the surface of the lid, the ambient air, and the liquid in the jar (the melt) are controlled by electric heaters to accomplish crystal growth.

The details of the copper block and stainless steel lid assembly are shown in Fig. 3. The large thermal mass of the block minimized temperature fluctuations in the copper cooling tip. The lid is tapered to ensure that the cooling tip is the only nucleation point in the liquid and its surface temperature is always kept above the freezing point of benzene by an internal heater element. The latter condition precludes crystallization of benzene vapor on the lid which, if allowed to occur, would interfere with the initial stages of crystal growth on the probe.

The copper cooling probe is threaded through the copper block and passes through a teflon bushing inside the lid (see Fig. 3). A viton O-ring in the bushing seals the area between the probe and the bushing from the atmosphere. A copper-constantan thermocouple and an electric heating element are embedded inside the probe. The part of the probe going through the teflon bushing has a 1/2-inch diameter and the tip of the probe was machined to a hemisphere of radius 1/4-in. The probe tip was polished to a fairly smooth surface with emery cloth and Alumina polishing compound.

One of the glass tubes which passes through the block-lid assembly is used to fill the jar. The filling tube goes through the freezer compartment, through the top of the refrigerator, and terminates outside the refrigerator at the joint J_1 shown in Fig. 1 (see also Fig. 2a). The other glass tube which passes through the block-lid assembly passes from the freezer compartment through the right side of the refrigerator and is connected to the

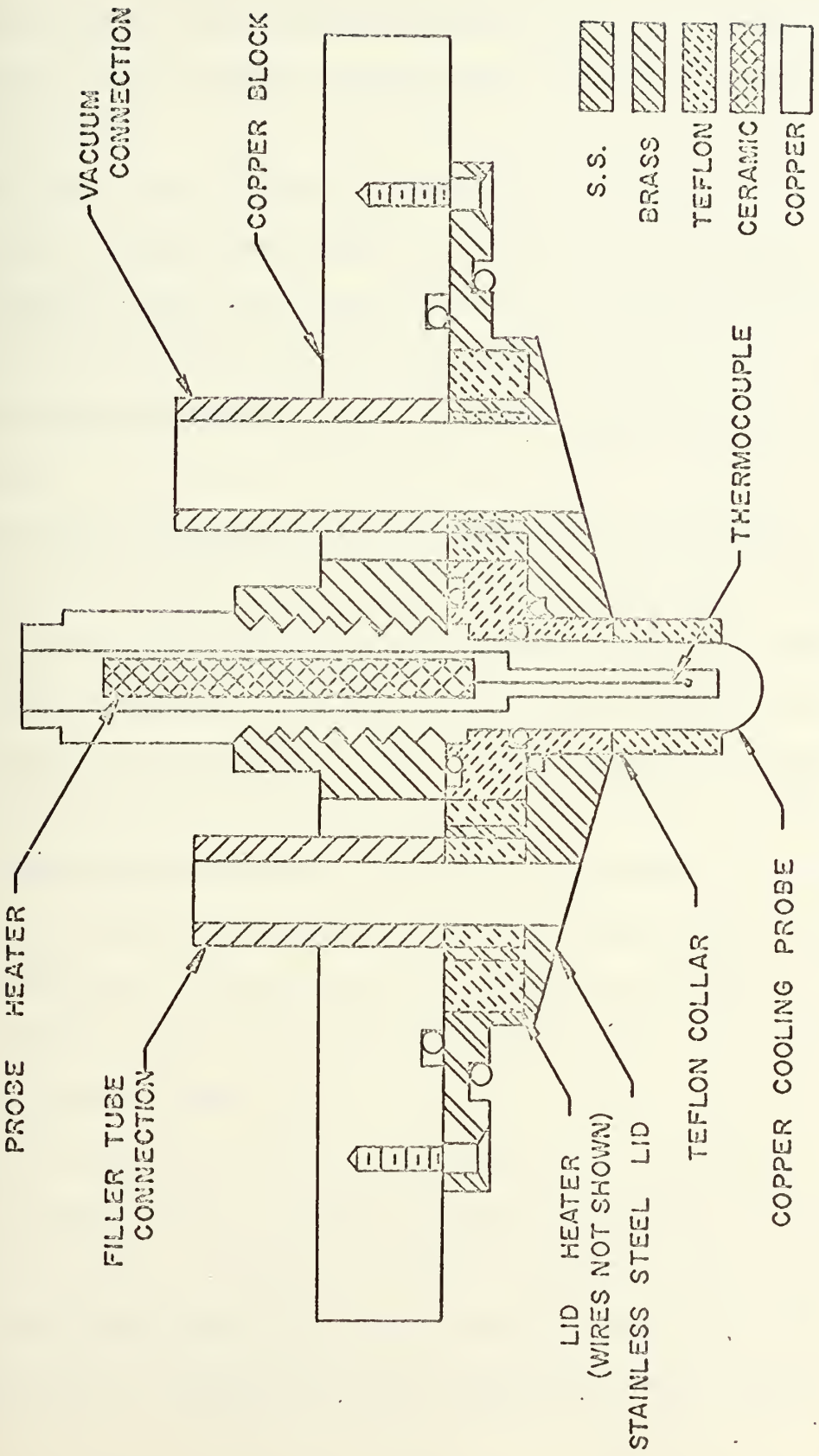

FIGURE 3. CROSS SECTION OF LID ASSEMBLY

vacuum system. The area between the outside surface of each tube and their respective passage in the lid-block assembly is sealed by a quick-disconnect O-ring seal (CAJON Ultratorr Fitting) which is soldered into the top of the copper block.

The thermocouple probe which passes through the lid-block assembly is a 1/8-inch O.D. stainless steel sheath which has an iron-constantan thermocouple embedded inside. The probe is six inches long and can be positioned within the melt or inside the lid at any desired vertical level. The outer surface of the probe sheath is also sealed with a quick disconnect O-ring connection.

The crystal growing jar (see Fig. 2b) is a small pyrex bell jar with a capacity of approximately 600 ml (purchased from the American Scientific Company, catalog number JR-4875). The jar is set in a heater element which conforms to the contour of the jar base. The heater element is in turn set on a plywood base 3/4-in. thick. Four threaded rods which are attached to the copper block pass through the wooden base, and the jar is sealed to the lid by tightening the wing nuts on the rods at the bottom of the wooden base. All seals in the jar-lid assembly are made with viton O-rings and without any vacuum grease. The jar heater is controlled by a thermistor sensing element which is taped on the outside wall of the jar and is thermally insulated from the ambient air.

The air temperature around the jar assembly is controlled by a grid of heating elements which are threaded through the lower sides of the plexiglass box (see Fig. 2b). A thermistor extends down from the wooden base and is positioned in the middle of the heater grid; its control unit will be described below. A linearly polarized light source, which is used to check

visually for flaws during crystal growth, is attached to the inside back wall of the box; when the box is in place, the light source is directly behind the center of the jar. The four threaded rods pass through the bottom of the box and allow securing the box in position. A copper-constantan thermocouple, inserted through the center of the right side of the box, is used to monitor the air temperature at that point.

There are four heaters in the apparatus that require control. Power to the probe and lid heaters is provided by Variacs to establish the temperature gradient within the cooling probe. The air and melt temperatures and the temperature gradients in the liquid are controlled by half-wave SCR (silicon control rectifier) proportional controllers in conjunction with the thermistor sensing elements. The SCR units were designed and built in this laboratory by Cuomo[51] and Blinick[52] after the original design of Scott.[53]

The temperature gradient in the liquid had a radial component due mainly to the ambient air temperature, and a vertical component due to the melt heater. It was found that once all the heater controls were set to their optimum position (to be described later), only the melt-heater control had to be varied during crystal growth. A motor drive unit, attached on the melt temperature SCR controller, continuously decreased the melt temperature at a very slow rate. The fastest rate compatible with good crystal growth was found to be 0.12°C/hr; it was achieved by turning the SCR heater control at a rate of 0.36 rpd.

All temperatures were monitored with a Mosley 7100B strip-chart recorder which could be read to within ±0.005 mV on its most sensitive scale. Because of the large thermal inertia of the copper block, the probe and lid temperature did not exhibit temperature fluctuations in excess of ±0.1°C when at

equilibrium. Fluctuations in the melt temperature and the air temperature were approximately ±0.25°C and ±1°C, respectively.

Initial experiments with the apparatus showed the need to incorporate slight modifications in the equipment described. It was found that the best crystal growth was obtained when the tip of the copper probe penetrated approximately one inch into the liquid. In this position, the lid temperature did not much influence the probe temperautre. However, so much surface area was in the liquid that three or four single crystal seeds would usually form and this limited the ultimate size of a piece of single crystal that could be grown. Consequently, a teflon collar was put around the probe tip to reduce the area available for nucleation. Subsequently, one or, at most, two single crystal seeds would form.*

An additional jar heater was wrapped around the top of the jar (see Fig. 2b) and was controlled by the same power source as that for the lid heater. It served to prevent crystallization on the jar walls immediately below the outer extremity of the lid; the lid heater was not able to do this. Considerable improvement in crystal growth was realized thereby.

It was originally intended to use the stainless steel thermocouple probe to monitor the melt temperature as it was changed; however, it was found that when the melt temperature reached approximately 3.5°C, crystals started to form on the probe which interfered with the main crystal on the copper probe. Therefore, once the amount of supercooling (≈1.5°C) and the optimum

---

*It is believed that a cone shaped probe with a small tip radius would overcome the problem to some extent for the tip of the cone would present an even smaller nucleation area. See Rasmussen.[7,54]

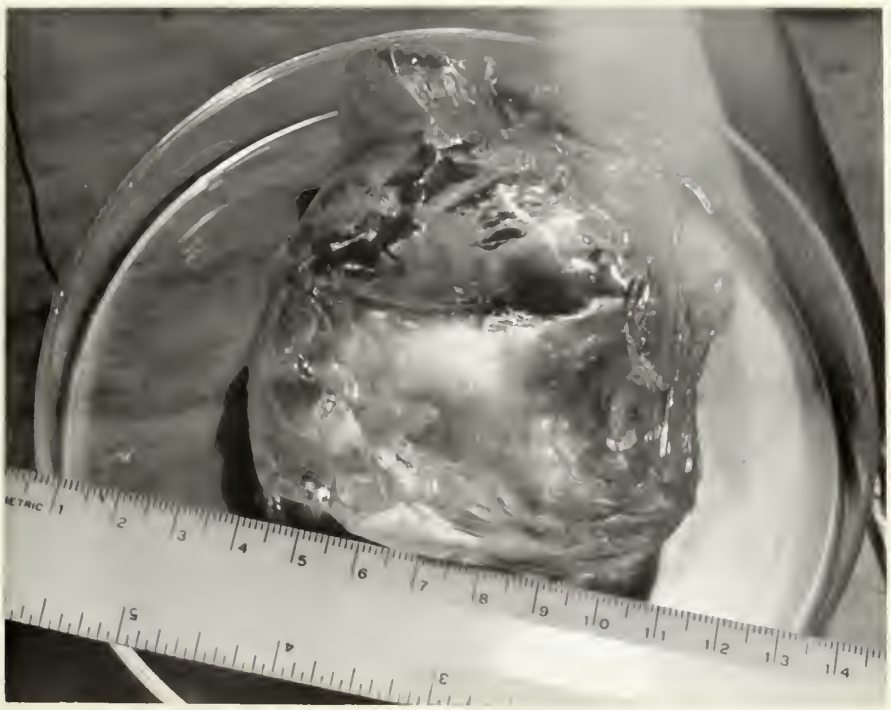

Fig. 4. Single crystal of benzene immediately after being removed from crystal growing jar. (Approximate dimensions 7 × 7 × 10cm).

rate of decrease in the melt temperature (0.12°C/hr) were determined, the thermocouple probe tip was positioned inside the lid to monitor the lid temperature.

Since all the temperatures are interdependent, it was necessary to determine experimentally which combination of Variac and SCR controller settings yielded the best crystal growth. The actual procedure that was used and some problems associated with the apparatus are discussed in Appendix B. The method used to cut the crystal and prepare it for optical orientation is described in Appendix C. Fourteen crystals were grown with the apparatus; each one yielded crystals large enough for two or three samples. A piece of single crystal, which had just been removed from the jar, is shown in Fig. 4. Its approximate dimensions were $7 \times 7 \times 10$ cm.

3.4 Orientation of Single Crystalline Benzene

Since it was intended to measure α in known crystallographic directions, the next step was to determine these in the crystal sample whose growth was described in Section 3.3. Benzene is an orthorhombic crystal; it therefore has three axes, "a", "b", and "c", which are mutually perpendicular but each with different length of unit cell. Attempts to determine the axial directions were first made with the Laue back-reflection X-ray technique; however, these were unsuccessful, the interpretation of the complex X-ray patterns being excessively difficult. Fortunately, benzene crystal is transparent, colorless, and strongly birefringent (biaxial). Hence, methods of optical orientation with polarized light were available (Mullens[55]).

The orthorhombic structure happens to be the only one for biaxial crystals in which all three principal crystallographic axes coincide, respectively, with the three "indicatrix axes." In general, the biaxial indicatrix

is a triaxial ellipsoid in which the three mutually perpendicular semiaxes are equal in magnitude to the three principal indices of refraction, $n_x < n_y < n_z$. Two optic axes and the acute bisectrix (the bisector of the angle between the optic axes) lie in the n_x, n_z plane, the optic plane. For the orthorhombic case, the acute bisectrix coincides with one of the axes of the crystal, and the optic plane coincides with one of the (100) planes. Since all three of the crystal axes are mutually perpendicular, one must lie in the optic plane, perpendicular to the axis defined by the acute bisectrix, while the third axis must be perpendicular to the optic plane. Mullens[55] has determined that for benzene the acute bisectrix and the optic plane correspond, respectively, to the b axis and the a-b plane of the crystal.

A beam of plane-polarized (p-p) light entering a birefringent crystal is split into two components that travel at different speeds. One of these components is perpendicular and the other parallel to the principal section; i.e., to the plane containing one of the optic axes and the propagation vector of the light passing through the crystal. If the birefringent crystal is set between two polars of a polarizing microscope (i.e., a polarizer and an analyzer) that are maintained crossed at 90°, maximum extinction of the light will occur when the crystal is rotated to a position for which the planes of vibration of the light components in the crystal coincide with the planes of vibration of the polars. At this point a relationship between the microscope axes and the principal section has been established: one of the optic axes will lie in a plane parallel to one or the other of the vibration planes of the polars.

The polarizing microscope used to achieve this first result (as well as

the subsequent orientation operations) is a fairly conventional compound instrument with the following auxiliary features: (1) The sample is held in a multiaxes stage which allows the crystal to be rotated about three mutually perpendicular axes. (2) A special objective lens (30X) is used which allows enough separation between the lens and the microscope stage to permit insertion of the multiaxes stage on the microscope stage. (3) There are perpendicular crosshairs in the eyepiece (ocular) which correspond to the directions of the vibration planes of the polars when the latter are held crossed at 90°. One of the polars (the polarizer) is located below the microscope stage and the other (the analyzer) is located between the objective lens and the eyepiece. The two polars can be crossed at any arbitrary angle but are usually used in the 45° or 90° position. (4) A removable lens (Bertrand lens) can be inserted between the analyzer and the ocular. The microscope can be used as a conoscope or an orthoscope depending on whether the Bertrand lens is inserted or removed, respectively.[56] The conoscopic mode was used in this experiment.

After the crystal is mounted on the multiaxes stage and placed on the microscope stage, a convergent beam of p-p white light is brought to focus on the bottom face of the sample. This beam diverges as it passes upward through the crystal; upon leaving, it passes through the objective lenses, the analyzer (crossed at 90° to the polarizer) and the Bertrand lens. The result is an interference fringe pattern which is focused at a point between the Bertrand lens and the ocular. The size and resolution of the pattern seen through the ocular depend on the magnifying power of the objective and the ocular.

Because the beam of polarized light diverges while passing through the crystal, some part of it will be parallel (or nearly so) to one of the optic axes. Along any optic axis, light of either polarization travels with the same speed; hence, this particular direction will be shown by a black dot surrounded by fringes, because the polars are crossed. Superimposed are dark bands called isogyres which start from the optic axes as sharply defined (straight or curved) lines, but become progressively broader away from this axis. When the acute bisectrix of the crystal is aligned parallel to optic axis of the microscope, the isogyres form a cross which coincides with the crosshairs in the ocular. The two optic axes patterns are equally spaced about the center of the cross on one of the isogyres. When this pattern is observed with all the axes on the universal stage in their zero positions, the crystal is oriented with its b axis along the optic axis of the microscope, its a axis along the isogyre containing the optic axes figures, and its c axis along the other isogyre of the cross. The acute bisectrix pattern is shown in Fig. 5. In Fig. 5 the a axis is parallel to the E-W

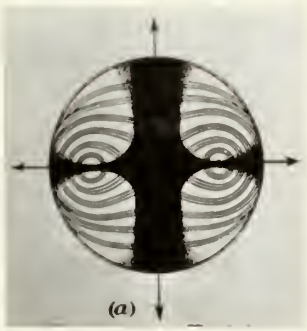

Fig. 5. Acute bisectrix pattern (from Hartshorne and Stuart [58]).

direction, the b axis is normal to the plane of the paper at the center of the cross, and the c axis is in the N-S direction.

For a complete theory of the interference patterns observed with a conoscope see References 57 and 58. For a description of the manipulations involved in this experiment see Appendix D. The procedure used enabled orientation to within ±2°.

3.5 Sample Preparation

The methods used to prepare the sample for ultrasonic measurements were patterned after those of Heseltine and Elliot.[59] An oriented piece of crystal is cut into a cylindrical sample and frozen into an annular brass sample holder. The faces of the sample are lapped to make them flush with the flat sides of the sample holder and are sealed with thin pieces of mylar. The mylar seals prevent sublimation of the sample and on one face provides a bonding surface and a ground connection for the ultrasonic transducer. The sample holder is mounted onto a specially designed housing which incorporates the electrical connections necessary to excite the transducer and provides the means for positioning the sample holder in a dewar assembly which, in turn, enables one to make ultrasonic measurements as a function of temperature.

All the sample preparation is done in the refrigerated cold box with the mechanical apparatus shown in Fig. 6. This apparatus is made entirely of brass and is used in a vertical or a horizontal position. The main components consist of the dovetailed track, the cutter-planer housing, the sample holder housing, the planer, two cylindrical cutting tools, and an L-shaped stand which supports the track in the vertical position. A breakdown of these components is shown in Fig. 7.

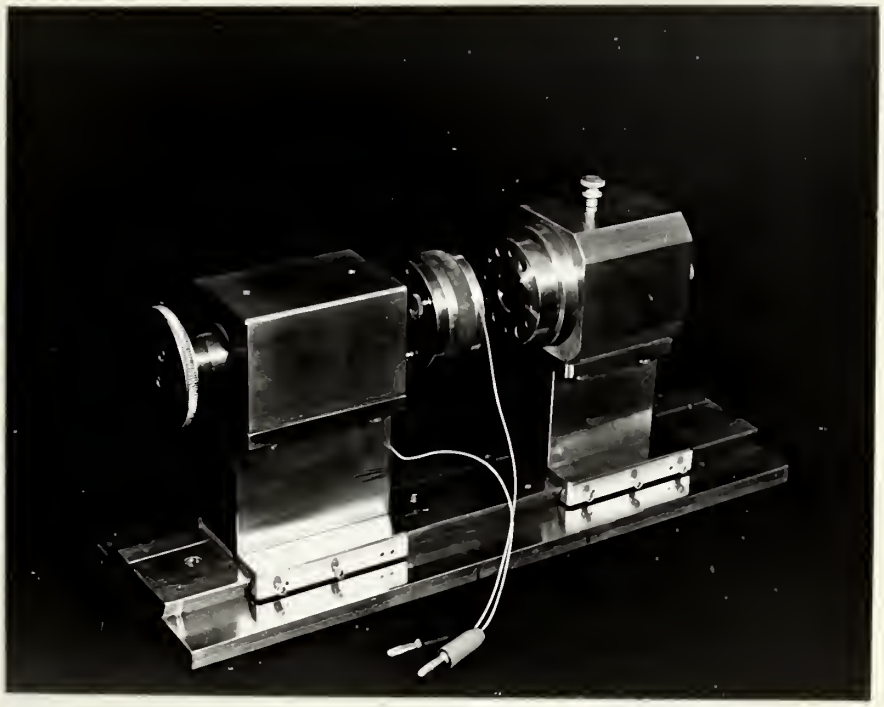

Fig. 6a. Mechanical apparatus in horizontal position (Used to melt flat face on sample).

Fig. 6b. Mechanical apparatus in vertical position (Used to cut cylindrical sample).

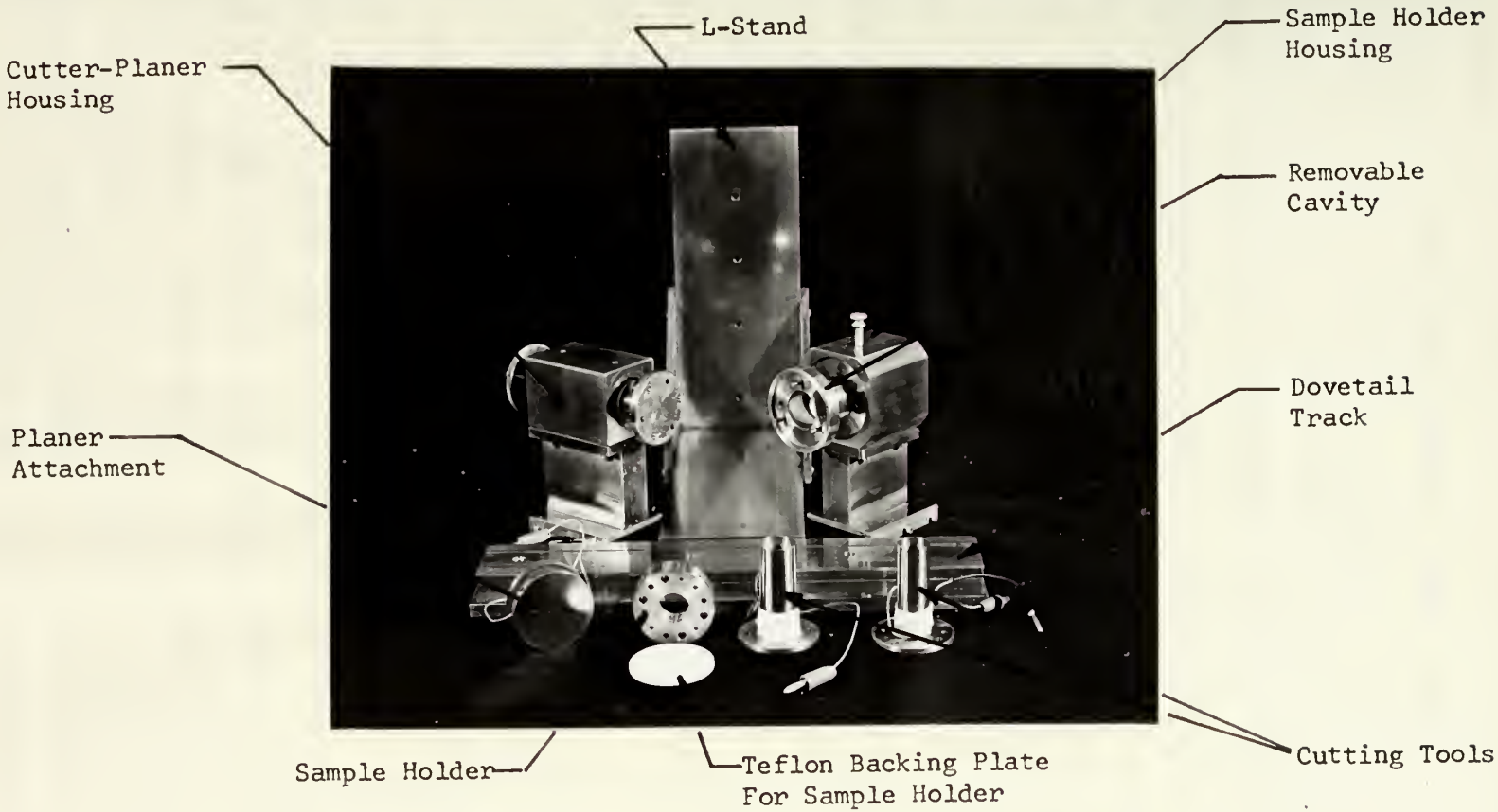

Fig. 7. Parts breakdown of mechanical apparatus.

The cutter-planer housing and the sample holder housing fit onto the track and can slide along the track axis or be held stationary by tightening set screws in the base of each housing. Both housings are machined so that their vertical edges are exactly perpendicular to the track axis; hence, parallel to each other. A piston which is two inches longer than the cutter-planer housing fits into a cylindrical hole in the center of the housing and is free to move along the track axis. A mounting plate on one end of the piston enables either the planer or a cutting tool to be attached to the piston. The planer is a flat brass disc which is heated by a nichrome wire heating element embedded behind it. The cutting tools are thin-walled (1/64-in. thick) brass tubes (3/4-in. and 7/8-in. diameter) which are heated by a nichrome wire heating element wrapped around the upper end of each tube. Inside the sample holder housing there is a removable cavity (see Fig. 7). The cavity provides the means to attach the sample holder to the housing during the sample facing procedure and is removed during the sample cutting procedure.

The sample holder (see Fig. 7) is a brass ring which has a 2-in. O.D., is 0.593 in. (1.54 cm) thick, and has a 3/4-in. diameter hole bored through the center. Several additional holes are incorporated which are used (1) to mount the sample holder on the removable cavity, (2) to attach a cover plate over the mylar seal on the reflecting surface of the sample, (3) to mount the sample holder on the ultrasonic cavity (to be described later), and (4) to insert a thermocouple into the sample holder.

The procedure used to cut and polish the sample with the mechanical apparatus is described in Appendix E. The final sample is 1.54 cm long and 1.9 cm in diameter and has one face (the reflecting surface) sealed with a

piece of 1/4-mil thick mylar. The next step is to bond the transducer onto the opposite face of the transducer.

3.6 Transducer Bonding Technique

To obtain a good coupling of the sound energy from a transducer into a solid the bond between the two must be able to support the type of mechanical displacement induced by the transducer and be as thin as possible, the latter condition being necessary to ensure that a minimum of energy be lost in the bond itself. The bonding agents and procedures used generally depend on the nature of the bonding surface and the type of transducer being employed, i.e., it is usually more difficult for a bond to support shear waves than longitudinal waves.

The frequency dependence of the sound absorption yields useful information concerning the properties of the material being investigated. The upper frequency limit at which sound absorption measurements can be made is principally determined by the intrinsic attenuation of the sample, i.e., the higher the intrinsic absorption the lower the upper frequency limit. When measurements are made as a function of temperature, the relative values of α for different frequencies at the same temperature and the change in the relative values of α with changing temperature are of primary interest. When this type of measurement is being made, the most consistent results are usually obtained if a single transducer is used and is operated at its fundamental frequency and at as many odd harmonic frequencies as is possible, given the intrinsic attenuation of the sample. Transducers with different fundamental frequencies used on the same sample can lead to erroneous results. (This point will be discussed later.)

Benzene is very soft and fragile; consequently, it cannot withstand a great deal of pressure before it becomes strained or cracked. Because the sound absorption in benzene is so high, a transducer with a relatively low fundamental frequency (2.0 MHz) had to be used to determine the frequency dependence of the absorption with temperature. Low fundamental-frequency transducers are inherently thicker than the higher fundamental-frequency transducers (5 MHz and above) normally used with solids and, in general, are more difficult to bond onto a sample. Hence, the fragile benzene surface and the need for a thick transducer necessitated the use of a peculiar bonding technique to obtain a usable ultrasonic signal.

A brief description of the bond will be given here; the details are presented in Appendix F. The transducer is bonded onto a piece of 1/4-mil thick aluminum-coated mylar with Nonaq stopcock grease at room temperature. The transducer-mylar combination is, in turn, bonded onto the benzene sample with a glycerine-water solution. The latter bond is made in the cold box at about -10°C. The mylar seals the sample from the atmosphere and provides an electrical path from the ground electrode of the transducer to the sample; the latter is at ground potential when the ultrasonic measurements are made.

Once a bond was made, it would last for approximately five days before it began to deteriorate. It was found that a bond could be broken and remade with a fresh transducer-mylar combination two to three times. The low and high temperature limits of the ultrasonic measurements were restricted by the characteristics of the bond. The lower limit appears to depend on the linear expansion coefficient of the benzene along its three principal axes. Although it could not be precisely determined, it is believed that the bond broke as a result of the benzene-mylar combination pulling away from the

transducer due to thermal contraction. The linear expansion coefficient is greatest along the c axis[60] and the bond broke at a higher temperature along this axis than along the a or b axis. Consequently, measurements along the c axis were only taken down to 180°K whereas the lower limit along the a and c axes was 170°K. The high temperature limit was due to an apparent change in the bond characteristic when the sample temperature was raised from 250°K to 260°K. Measurements were taken at intervals of 10°K, first with the temperature decreasing and then with the temperature increasing. If the temperature was allowed to go above 250°K after one cycle and subsequently brought below 250°K to initiate another cycle, it was found that the measurements of the two cycles were inconsistent. However, if an upper limit of 250°K was used, the measurements of succeeding cycles were consistent to within 3-4%.

An x-cut, coaxially plated quartz transducer with a fundamental frequency of 2MHz was used. The transducer has a 1/2-in. overall diameter and a 3/8-in. active diameter. Transducers with fundamental frequencies of 2.5 MHz and 5.0 MHz were also employed; however, inconsistent results were obtained with the three transducers and are attributed to the difference in the transducer thicknesses. (This point is discussed more fully in Section 4.2 and Appendix G.) Since the transducer with the lowest fundamental frequency yields the most information within a given frequency interval, the 2 MHz transducer was used exclusively for the measurements.

3.7 Ultrasonic Measurement Procedure

The prepared sample is mounted onto the ultrasonic cavity as shown in Fig. 8. The ultrasonic cavity provides the electrical connections necessary

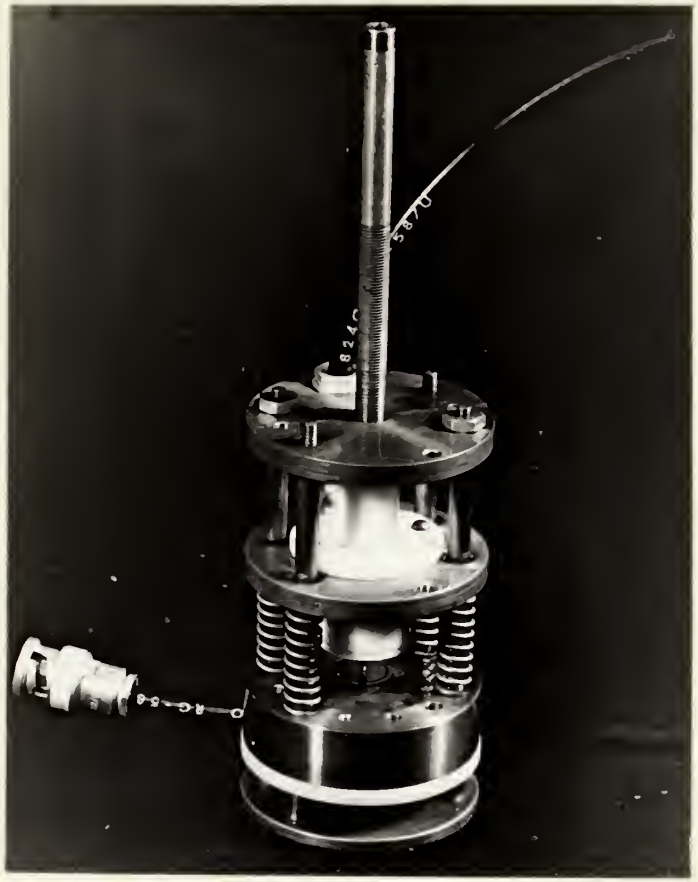

Fig. 8. Ultrasonic cavity (see Fig. 10).

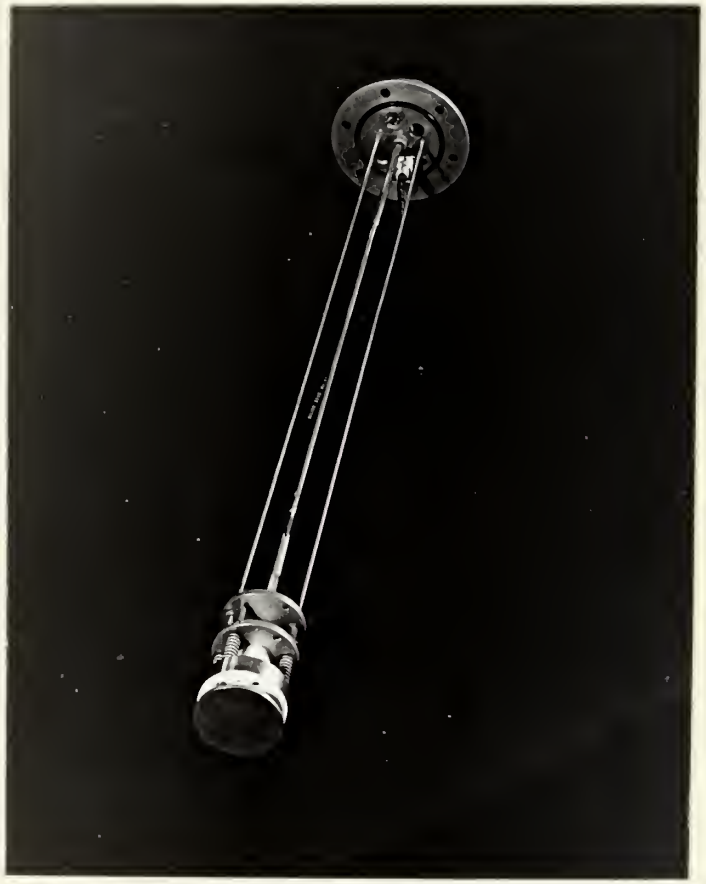

Fig. 9. Ultrasonic cavity attached to the dewar mounting plate.

to excite the transducer and is designed to fit into a dewar to enable measurements to be made as a function of temperature. The sample holder slides over the four posts of the cavity base and rests on the bottom plate. Four coil springs, one on each post, provide spacing between the spring-loaded center electrode and the transducer. The top plate is secured to the four posts and has a screw threaded through its center which allows pressure to be exerted onto the electrode plate which, in turn, adjusts the pressure that the electrode exerts on the transducer. It was found that only a light pressure on the transducer was necessary to obtain a good ultrasonic signal. The ground connection to the transducer is provided by the aluminum coated mylar which is in contact with the brass sample holder, i.e., the whole cavity assembly except for the center electrode is at ground potential. A coaxial cable is connected to the electrode plate and there are access holes in each plate to allow a thermocouple to pass through and be inserted into a hole in the sample holder.

The ultrasonic cavity is attached to the mounting plate of the dewar assembly with two stainless steel rods as shown in Fig. 9. The rods are first attached to the upper plate of the cavity and then screwed into the bottom of the mounting plate. The coaxial cable from the cavity is connected to the mounting plate and the thermocouple passes through an access hole in the top of the plate.

A schematic of the dewar assembly is shown in Fig. 10. A liquid helium dewar was modified to allow the ultrasonic cavity to be inserted into a temperature controlled environment. A small brass can which is wrapped with heater tape is located in the lower part of the inner dewar. Two copper-constantan thermocouples are embedded between the can and the heater tape.

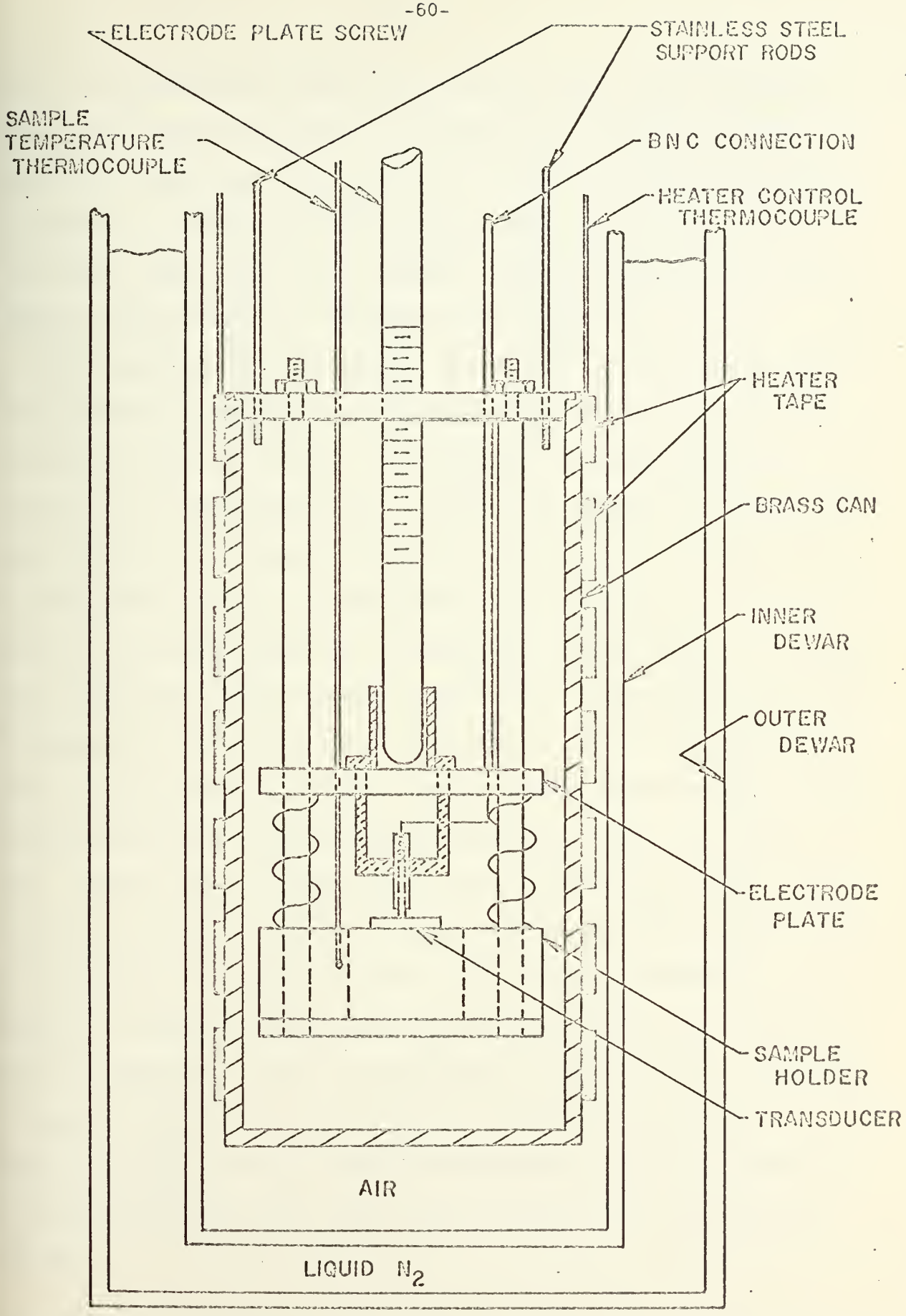

FIGURE 10. SCHEMATIC OF SAMPLE INSIDE OF DEWAR ASSEMBLY

One of the thermocouples is used as the sensing element for an SCR proportional controller which controls the current in the heater and the other measures the temperature of the outside of the can. The ultrasonic cavity is suspended in the can by the mounting plate which, in turn, is secured to the upper flange of the dewar assembly. The outer dewar is filled with liquid N_2 which provides the refrigerant for the system.

The temperature inside the can is controlled by a commercially manufactured feedback control system. A block diagram of the main components of the system is shown in Fig. 11. (All components were manufactured by R. I. Controls, Inc., Minneapolis, Minn.) The Data Trak programmer unit supplies command signals to the Thermac Controller. The Thermac Controller provides the Power Controller with an input signal which is proportional to the difference in the command signal of the programmer (corresponding to the desired system temperature) and the feedback signal from the system being controlled (corresponding to the actual system temperature). The Power Controller is a full wave SCR proportional controller which supplies the amount of current to the heater required to bring the system temperature back to the desired value. The Data Trak programmer gives either a steady state command signal for constant temperature control or a programmable, rate signal which changes the temperature as a function of time. With this system extremely stable temperature control and smooth rates of temperature change can be realized. When the temperature inside the dewar assembly is at equilibrium, temperature fluctuations would not exceed ±0.1°K. The equipment is capable of even better temperature control; however, there is a considerable amount of thermal lag in the system because of the large amount of brass used in the mechanical apparatus.

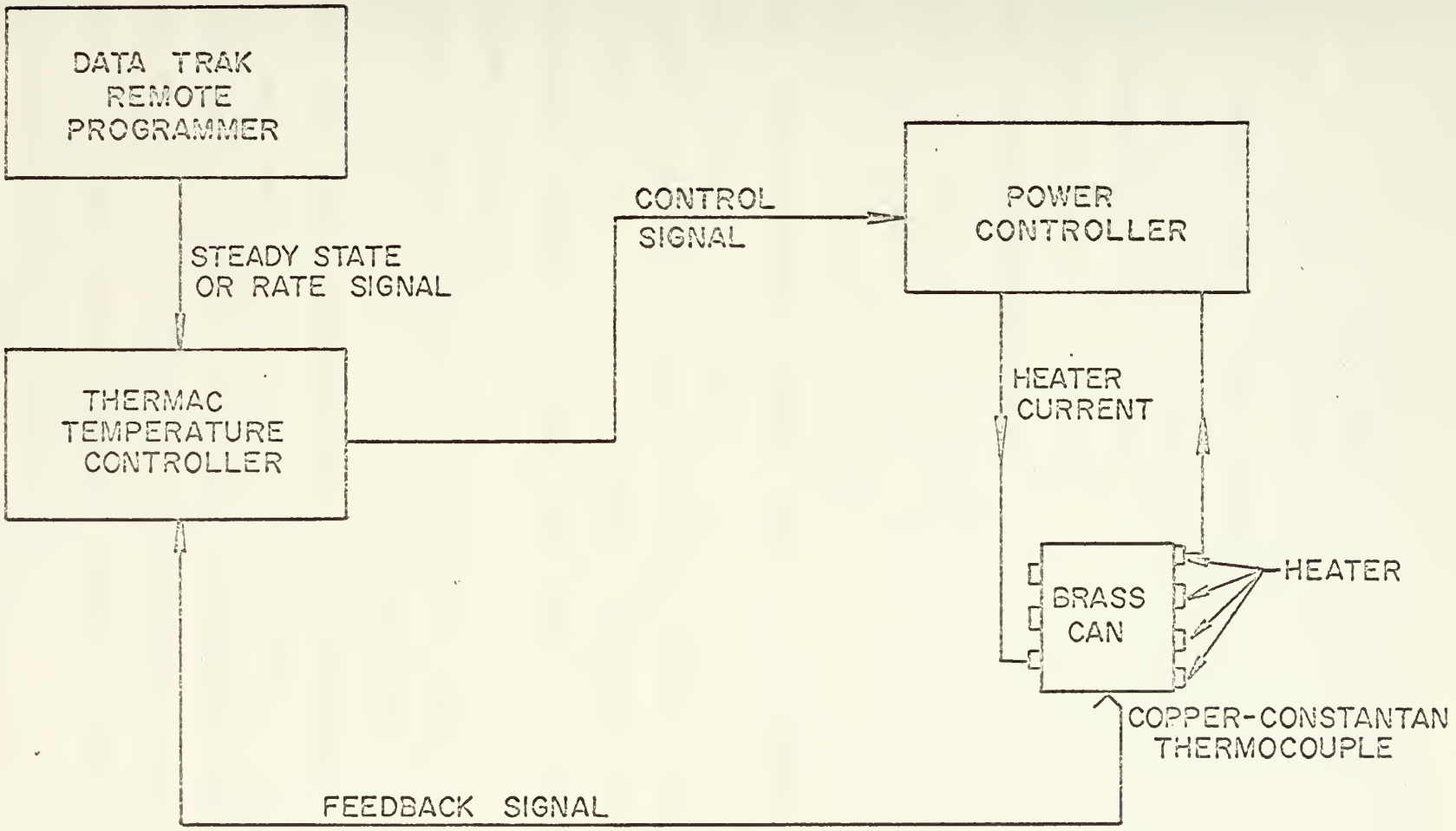

FIGURE 11. BLOCK DIAGRAM OF TEMPERATURE CONTROL SYSTEM

Prior to transferring the sample from the cold box into the dewar, it is important that the temperature inside the can be stabilized at about -10°C. If the sample is subjected to a thermal shock, the bond may be destroyed and/or the sample may crack. (Note: The temperature at the thermocouple next to the surface of the can is normally lower than the temperature inside the can; consequently, a relation between the two must be determined experimentally.) Once the sample is in the dewar, the sample temperature is monitored with the copper-constantan thermocouple in the sample holder. The thermocouple is connected to a Mosely 7100B strip-chart recorder which can be read to within ±0.005 mV (∿ ±0.1°K). After the sample is initially put into the dewar, the temperature is allowed to stabilize for approximately 15 minutes. When equilibrium is reached, the Data Trak programmer is turned on and the temperature is decreased at a rate of 5-8°K per hour. Upon reaching a desired temperature, the system is allowed to come to equilibrium for 25-30 minutes prior to making any measurements. Measurements were taken every 10° between 170-250°K. (The lower limit along the c axis was 180°K as indicated in Section 3.6.)

A block diagram of the electronic system used to make the ultrasonic measurements is shown in Fig. 12. All the components except the oscilloscope (Fairchild, Model 766H) were manufactured by the MATEC Corporation of Warwick, R. I. The model numbers of the equipment used are shown in Fig. 11; in some cases more than one component is incorporated into the same unit. The master synchronizer triggers the oscilloscope, the pulsed oscillator, and the pulse comparator. The latter two are alternately triggered to allow the wave forms generated by each unit to be alternately displayed on the oscilloscope; the persistence of the cathode ray tube of the oscilloscope makes the waveforms

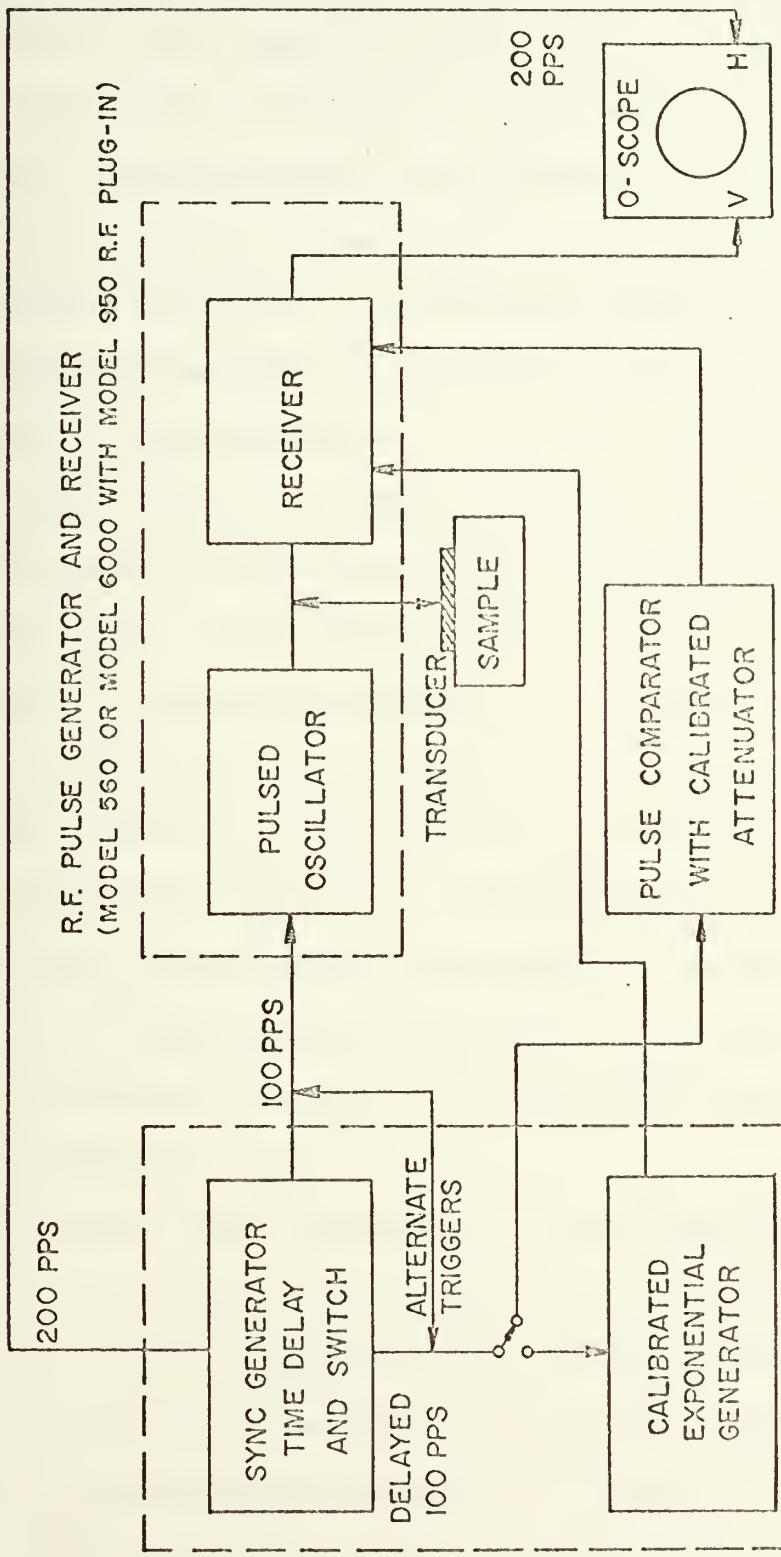

FIGURE 12. BLOCK DIAGRAM OF ELECTRONICS SYSTEM

appear as if they are superimposed. The pulsed oscillator supplies an electrical pulse of short duration (∿ 5 μsec) to the transducer which converts the electrical energy into acoustical energy with a frequency equal to the transducer fundamental frequency or an odd harmonic of the fundamental. The acoustical energy is reflected off the back face of the sample and is received by the transducer. The electrical signal generated by the transducer is amplified and demodulated in the receiver and the echo pattern is displayed on the oscilloscope.

The pulse comparator provides a calibrated comparator pulse which can be used to measure the difference in the attenuation between any two pulses in the echo train. The calibrated exponential generator provides an alternate method of attenuation measurement. An exponential waveform is superimposed on the echo train and is adjusted to make the peaks of the pulses in the echo train fall on the exponential. This method provides a convenient means of checking the quality of a pattern (which should be exponential) which, in turn, can be related to the quality of the bond and the extent that diffraction and nonparallelism effects have on the attenuation. A more detailed description of the electronic components and their uses is found in the literature.[61,62]

The specifications for the Model 950 low frequency plug-in, which is used with the Model 6000 Generator and Receiver unit, state the frequency range to be 1-20 MHz; consequently, for measurements above 20 MHz a Model 560 Transmitter and Receiver was used (frequency range 10-320 MHz). In practice, it was found that acceptable patterns were obtained with the Model 950 up to 26 MHz; consequently, it was possible to double-check measurements between 10-26 MHz. Measurements with the two units usually agreed to within 2-3%.

The attenuation measurements were made as a function of frequency at each temperature. The measurements were made at a frequency of 6 MHz or higher, the upper limit depending on the orientation. No data were obtained at 2 MHz, for preliminary measurements showed the attenuation values obtained were inconsistent with those of higher frequencies. This is attributed to the large diffraction loss at this frequency which could not be accurately accounted for with the correction procedure used. (This point will be discussed further in Section 4.2.)

For highly attenuating materials, there are relatively few pulses in the echo train; consequently, an accurate attenuation measurement with the exponential generator is not practicable. Therefore, the pulse comparator method was used in this case. A change in the relative value of attenuation with temperature is most accurately obtained by taking the difference in the attenuation between two echos in the pattern. The use of two pulses has the inherent advantage that any change in the electrical characteristics of the electronic components is automatically accounted for, i.e., a change in the electrical characteristics will have an equal effect on each pulse in the pattern and will not influence a difference measurement between two peaks.

The mechanics of making a measurement with the pulse comparator are relatively simple. The height of the comparator pulse is matched to the height of the first pulse in the pattern. Then the comparator pulse is positioned next to another pulse farther out in the echo train and is attenuated in calibrated steps until it is the same height as the second pulse selected. The amount of attenuation inserted can be read directly off the dials on the pulse comparator unit to within ±0.1 db. Because the attenuation in benzene is so high, only two peaks were available for measurement in

the patterns for 14 MHz and higher; consequently only the first two peaks were used at all frequencies. Pictures of typical patterns obtained with a 2 MHz transducer are shown in Fig. 13. The patterns shown depict the attenuation along the b axis at 170°K and 250°K at 6, 10, and 14 MHz.

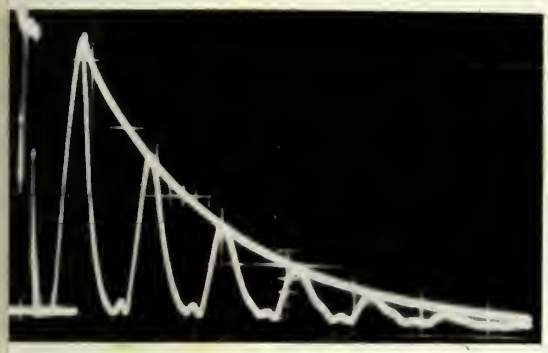

6 MHz. - 250°K

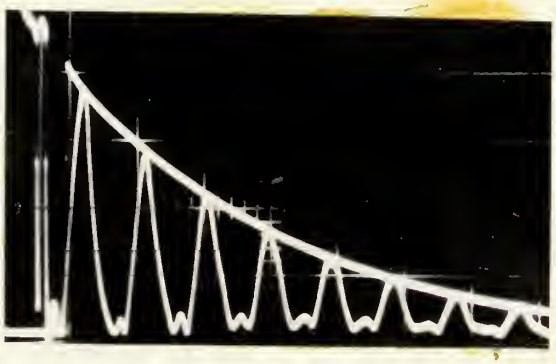

6 MHz. - 170°K

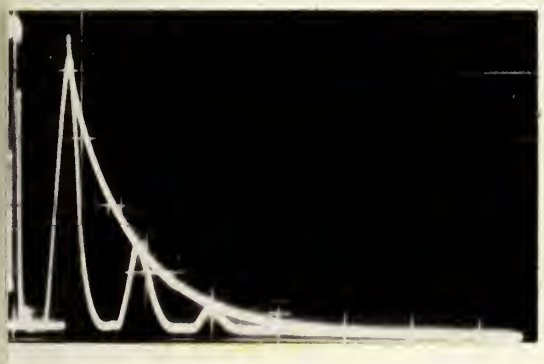

10 MHz. - 250°K

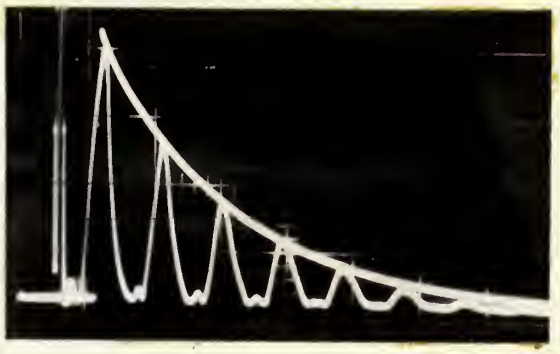

10 MHz. - 170°K

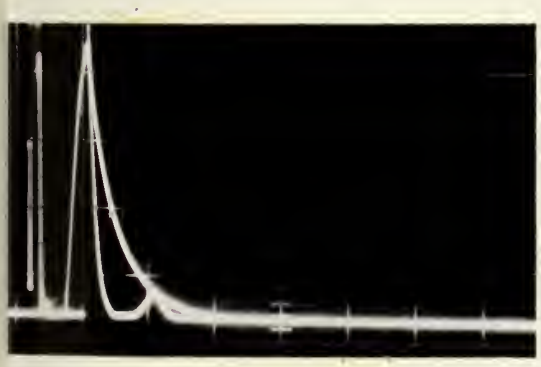

14 MHz. - 250°K

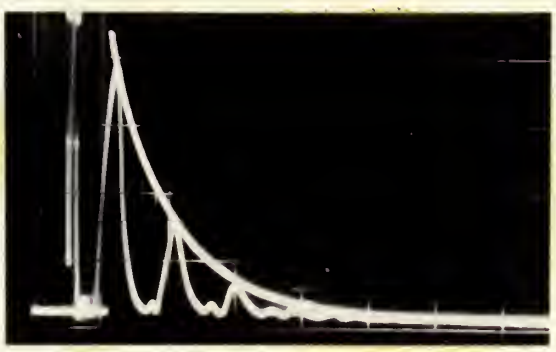

14 MHz. - 170°K

Fig. 13. Observed ultrasonic absorption patterns for benzene, b-axis, 170°K and 250°K. (Scale: 2 volts/cm vertical and 10μ sec/cm horizontal.)

4. Experimental Measurements

4.1 Experimental Results

Initially measurements were taken with transducers having fundamental frequencies of 2.0, 2.5, and 5.0 MHz. However, as mentioned in Section 3.5, the results obtained with the three transducers were inconsistent. Although the frequency dependence appeared to be the same for the three cases, the absorption values did not agree to within experimental error, i.e., the curves obtained on an α versus ν plot for each transducer would be displaced with respect to each other by a distance which fell outside the experimental error. This anomaly was first attributed to a bond loss; however, further experimentation did not bear this out. Regardless of whether each transducer type was bonded onto different samples or successively bonded onto the same sample, the results were the same. Since so many different bonds yielded the same discrepancy between the attenuation values, it was concluded that the bond characteristics were not the predominant factor causing the inconsistency. Although it was not proved conclusively, the discrepancy seems to be associated with the differences in the transducer thicknesses. Experimental measurements which tend to support this conjecture are presented in Appendix G. Because of this effect all the measurements presented here were taken with a 2.0 MHz transducer since it yields the most information within a given frequency interval.

The data presented here were taken with five separate samples. One sample was oriented along the a-axis, two along the b-axis, and two along the c-axis.* During each run the sample temperature was lowered in ten

*During the course of the experiment measurements were taken on 21 samples. Various combinations of bonding techniques and transducers were tried before reproducible bonds could be made and good ultrasonic patterns were obtained.

degree intervals to the minimum value. At each interval the temperature was allowed to come to equilibrium for 25-30 minutes; then the measurements were taken. After the minimum temperature was reached, measurements were taken in the same manner with increasing temperature up to 250°K. The cycle was repeated three times, which resulted in six sets of attenuation measurements at each temperature.

The average sound absorption values for the a, b, and c axes, which have been corrected for diffraction effects, are tabulated in Tables II, III, and IV, respectively. Very weak signals were obtained at 30 MHz and higher; consequently, measurements could only be made to within ±1 db (normal accuracy is ±0.1 db). As a result, the data for 30 MHz and above are somewhat erratic and not as reliable as those for the lower frequencies. The standard deviation for each point is not greater than 7%. (Errors and corrections are discussed in Section 4.2).

The data are plotted as functions of α/ν (which is defined as μ' henceforth) versus ν in Figs. 14, 15 and 16. One usually plots the absorption per wavelength $\alpha\lambda \equiv \mu$ versus ν when analyzing relaxation effects associated with α ; however, accurate velocity data were lacking for each frequency at which absorption measurements were made. If it is assumed that the velocity dispersion is a small effect compared to the relaxation phenomena associated with the sound absorption, the μ' versus ν plot should give essentially the same relative functional behavior as the μ versus ν presentation. (Note: The solid curves are drawn through the experimental points; the dashed curves will be discussed in Section 5).

The temperature dependence of the attenuation along the three axes for 6, 10 and 14 MHz is shown in Fig. 17. The values along the a-axis at

Table II

Sound Absorption (cm^{-1}) Along the a Axis

Temp. (°K)	Frequency (MHz)							
	6	10	14	18	22	26	30	34
250	0.200	0.484	0.861					
240	0.191	0.422	0.774	0.968				
230	0.173	0.391	0.702	0.832	0.861			
220	0.166	0.356	0.623	0.723	0.821	0.932		
210	0.169	0.343	0.639	0.662	0.750	0.881		
200	0.152	0.313	0.630	0.576	0.635	0.752		
190	0.146	0.272	0.563	0.596	0.593	0.721	0.725	0.774
180	0.149	0.263	0.521	0.536	0.578	0.679	0.625	0.681
170	0.120	0.228	0.455	0.458	0.458	0.595	0.581	

Table III

Sound Absorption (cm^{-1}) Along the b Axis

Temp. (°K)	Frequency (MHz)					
	6	10	14	18	22	26
250	0.160	0.408	0.763			
240	0.141	0.370	0.625	0.833		
230	0.123	0.310	0.508	0.700	0.936	
220	0.110	0.267	0.472	0.682	0.937	
210	0.0940	0.217	0.420	0.614	0.794	0.968
200	0.0860	0.193	0.363	0.563	0.720	0.900
190	0.0790	0.173	0.350	0.494	0.597	0.816
180	0.0715	0.149	0.326	0.444	0.549	0.672
170	0.062	0.121	0.284	0.400	0.970	0.542

Table IV

Sound Absorption (cm^{-1}) Along the c Axis

Temp. (°K)	Frequency (MHz)								
	6	10	14	18	22	26	30	34	38
250	0.231	0.452	0.765	0.806					
240	0.226	0.416	0.760	0.776	0.923				
230	0.224	0.402	0.659	0.742	0.925	0.994			
220	0.218	0.396	0.646	0.675	0.699	0.808			
210	0.211	0.373	0.617	0.636	0.631	0.759			
200	0.217	0.373	0.556	0.575	0.621	0.705	0.990		
190	0.215	0.341	0.544	0.539	0.619	0.668	0.777	0.805	
180	0.194	0.328	0.485	0.493	0.537	0.521	0.655	0.776	0.930

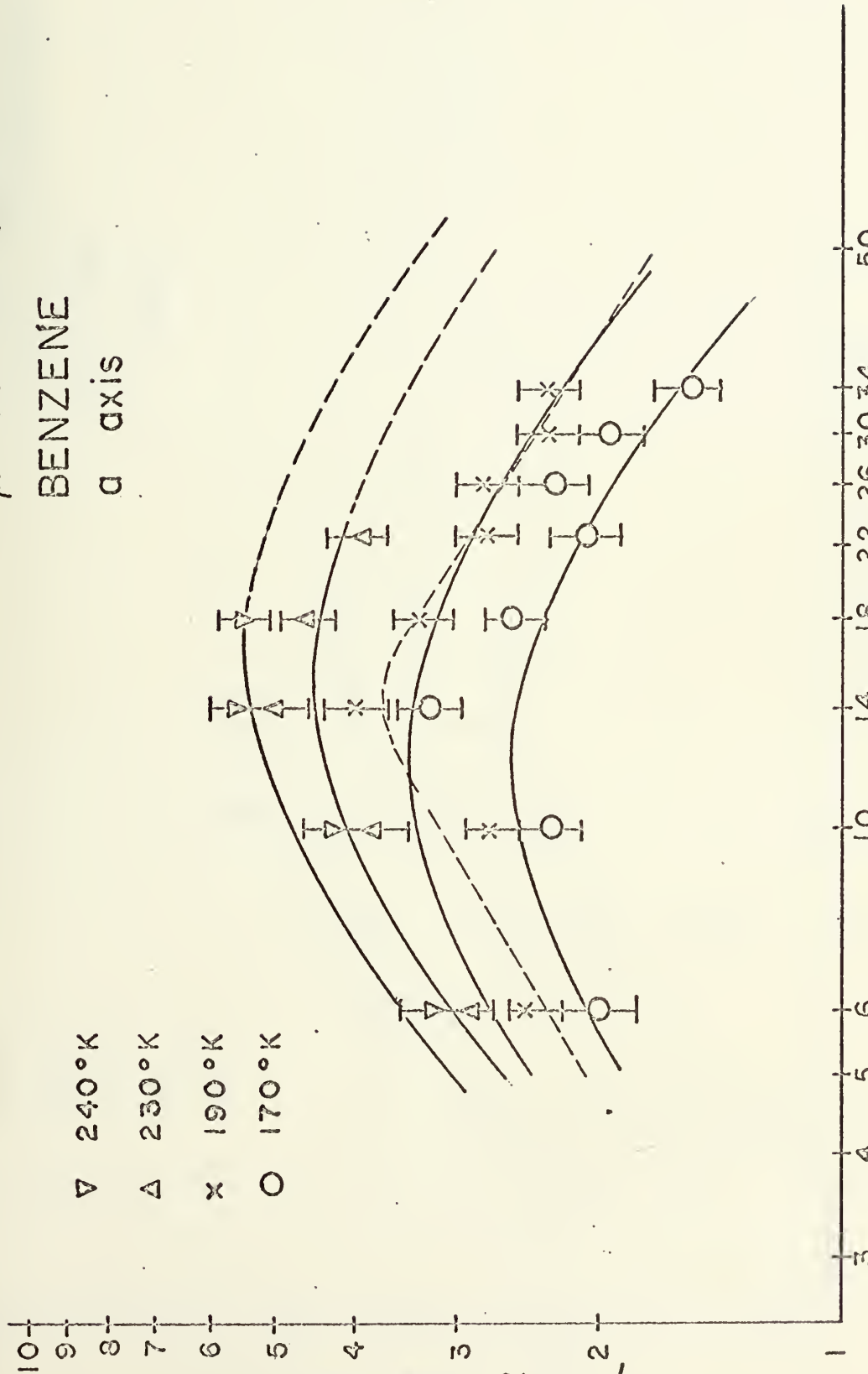
μ' vs. FREQUENCY
BENZENE
a axis
▽ 240°K
△ 230°K
× 190°K
○ 170°K
μ' x 10⁰ (CM⁻¹ SEC)
FREQUENCY (MHz)
1
2
3
4
5
6
7
8
9
10
3
4
5
6
10
14
18
22
26
30
34
50

Figure 14

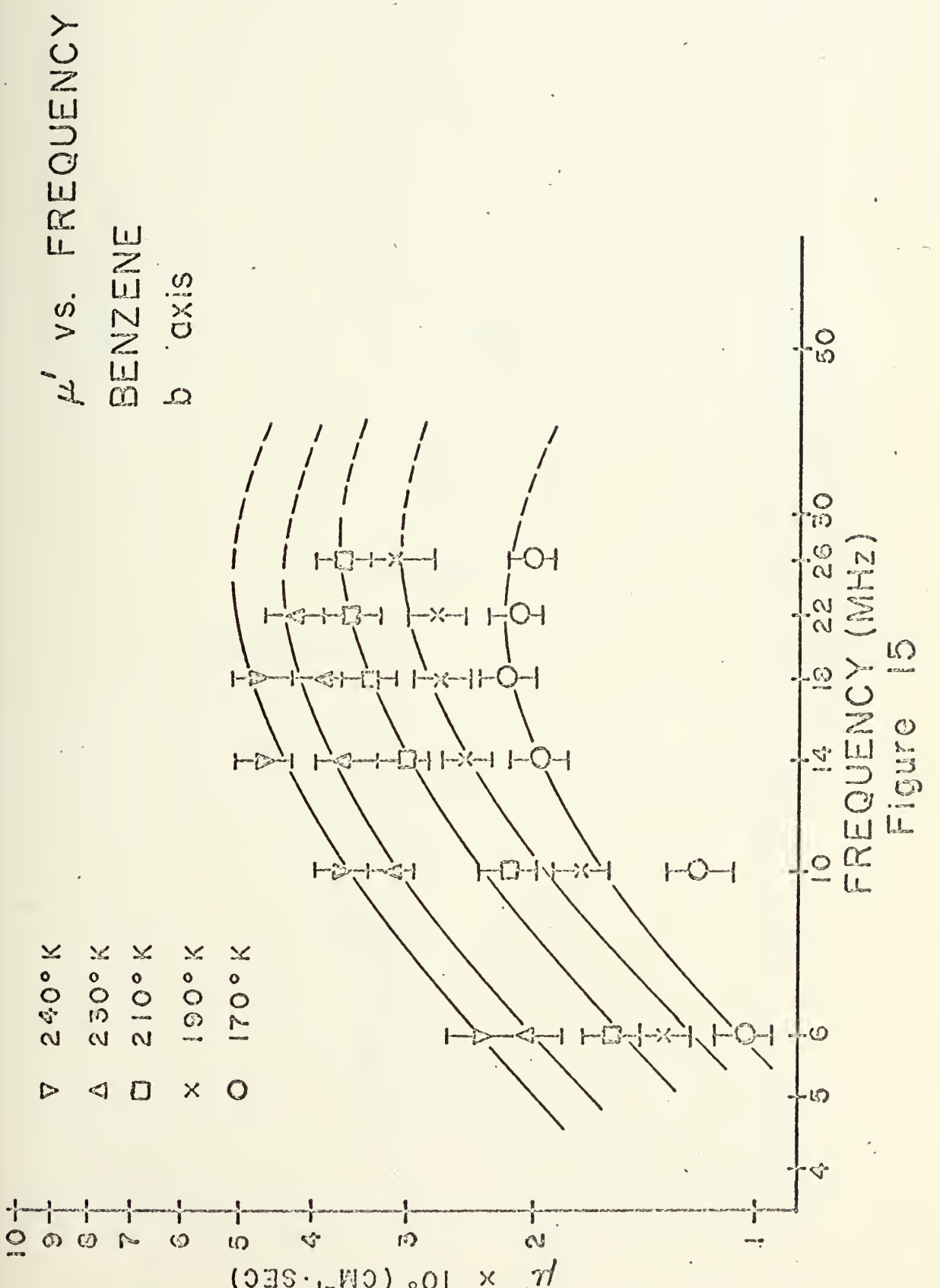
μ' vs. FREQUENCY
BENZENE
b axis
▽ 240° K
△ 230° K
□ 210° K
× 190° K
○ 170° K
μ' x 10⁸ (CM⁻¹·SEC)
FREQUENCY (MHz)
4
5
6
10
14
18
22
26
30
50
1
2
3
4
5
6
7
8
9
10

Figure 15

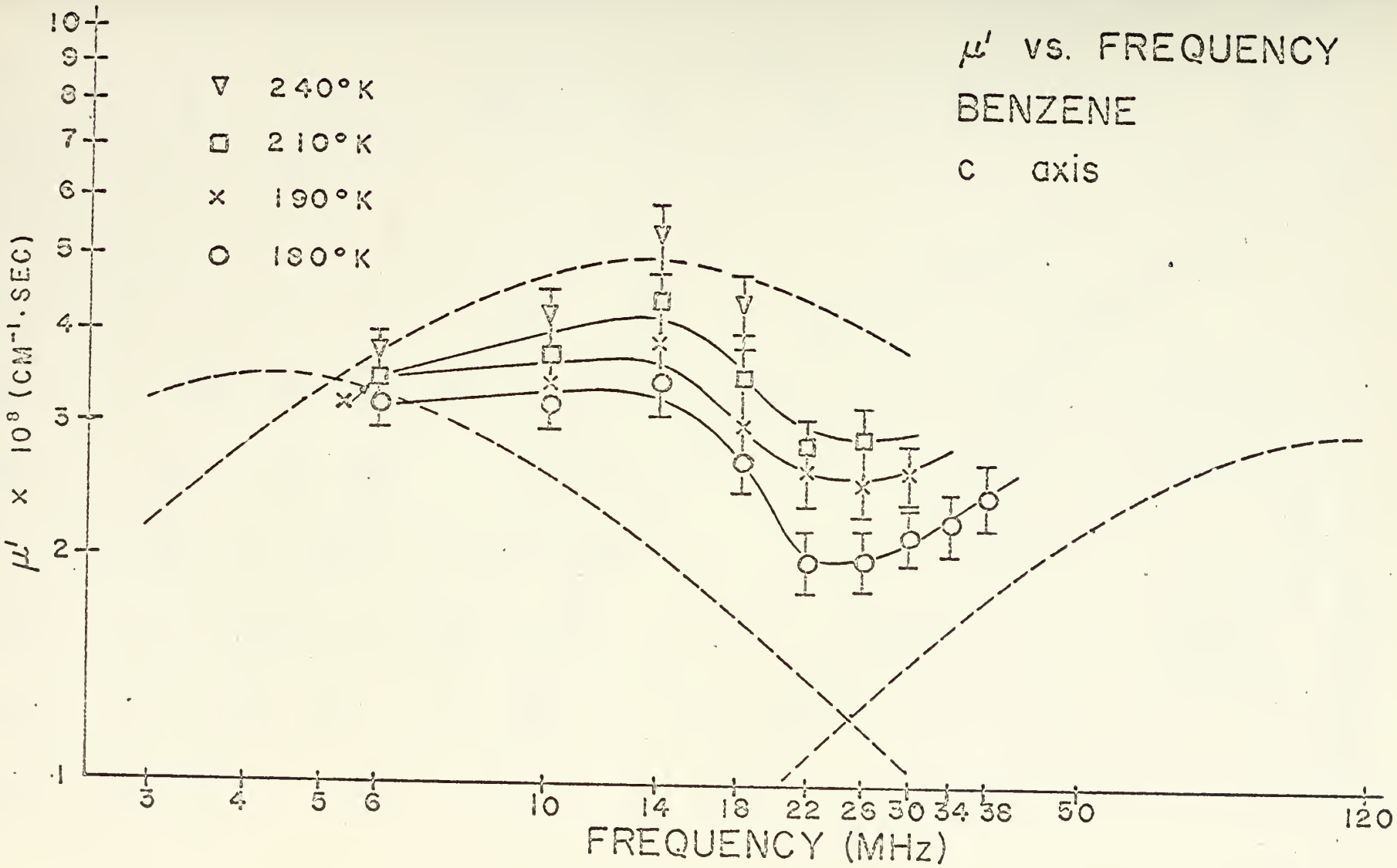
μ' vs. FREQUENCY
BENZENE
c axis
240°K
210°K
190°K
180°K
μ' × 10⁸ (CM⁻¹·SEC)
10
9
8
7
6
5
4
3
2
1
3
4
5
6
10
14
18
22
26
30
34
38
50
120
FREQUENCY (MHz)

Figure 16

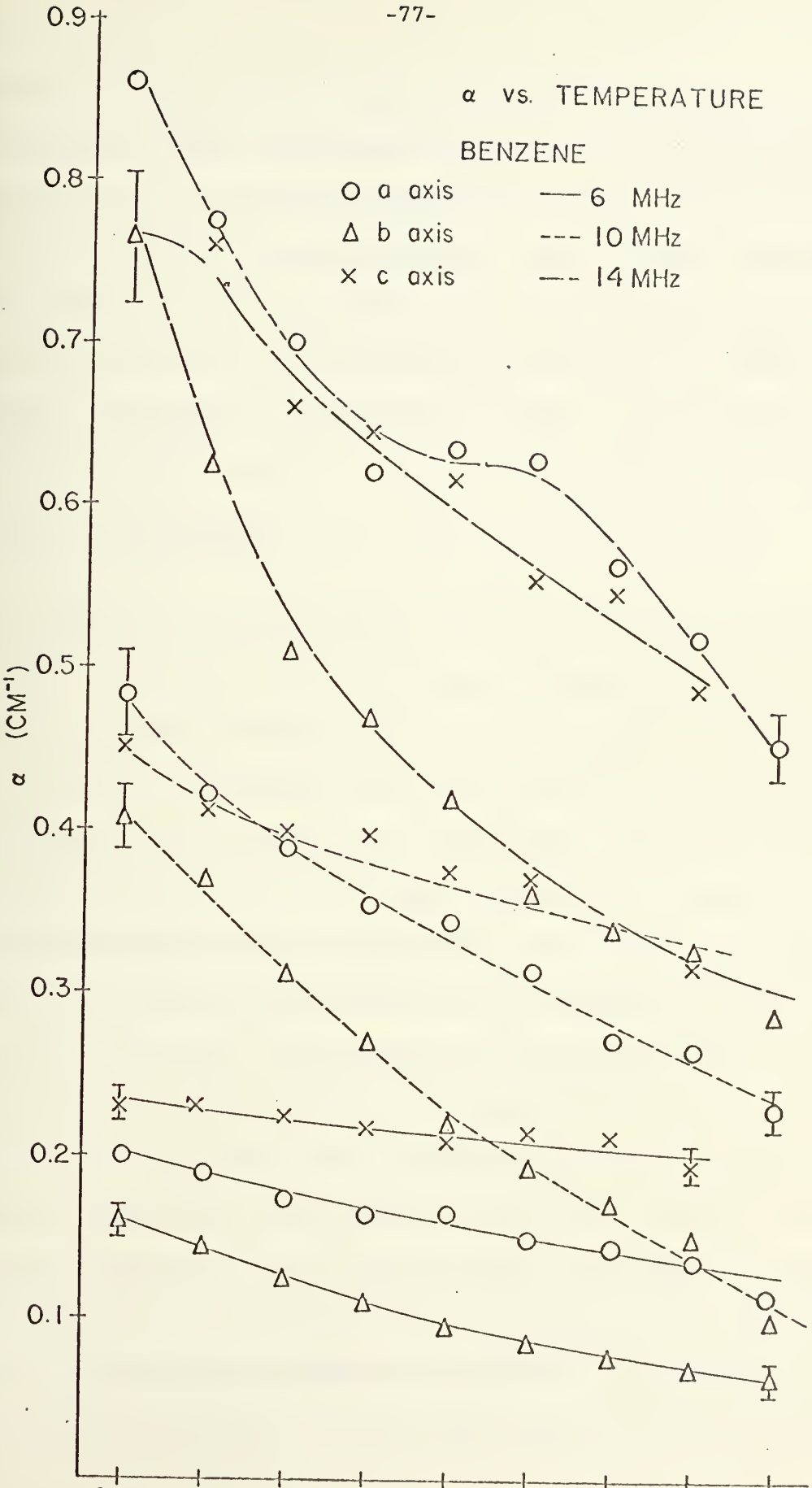
α vs. TEMPERATURE
BENZENE
O a axis
Δ b axis
× c axis
— 6 MHz
--- 10 MHz
— - 14 MHz
α (CM⁻¹)
0.9
0.8
0.7
0.6
0.5
0.4
0.3
0.2
0.1
250 240 230 220 210 200 190 180 170
TEMPERATURE (°K)

Figure 17

14 MHz for 200, 210, and 220°K display an anomalous behavior. α remains almost constant at these temperatures whereas for all the other measurements (a, b, and c axes) α decreases monatomically with decreasing temperature at a given frequency in the same temperature range. Whether the anomalous effect is real or not is questionable. Since the remainder of the data tends to contradict it, it is believed that the values of α along the a-axis for 14 MHz at 200 and 210°K may be too high. The results will be discussed in detail in Section 5.

4.2 Errors and Corrections

In addition to the normal errors due to the experimental apparatus and the scatter of the data, there are a number of loss mechanisms peculiar to the use of ultrasonic techniques which cause the measured sound absorption to be greater than the actual value for the material under consideration. Included among these are losses due to diffraction, transducer bonding, nonparallelism between the sample faces, transducer thickness, reflection, and electromechanical conversion (insertion loss). The relative importance of each of the effects depends primarily on the magnitude of the intrinsic absorption of the sample, the frequency range of the experiment, and the specific acoustic impedances of the transducer material and the sample. For the case of solids where sound absorption measurements are made as a function of temperature, magnetic field, or some other variably parameter, an accurate estimate of all the loss mechanisms is difficult to obtain. Consequently, the relative change in α as a function of the parameter of interest is obtained and an approximate estimate of the magnitude of each loss mechanism is calculated or found experimentally. The errors and

corrections pertinent to this experiment will be discussed below.

The error associated with the experimental equipment depends on a knowledge of the sample thickness and how accurately the difference in the magnitude of two peaks in each echo pattern can be measured. The sample thickness was measured with a micrometer with within ±0.02 cm and was corrected for thermal contraction by using the values of the linear expansion coefficients given by Cox et al.[60] The attenuation could be measured to within ±0.1 db below 30 MHz and to within ±1.0 db at 30 MHz and above. The accuracy of the measurements for 30 MHz and above was limited by the low signal-to-noise ratio of the patterns obtained at these frequencies. For the lowest values of attenuation measured, i.e, at 6 MHz and 170°K, the error was calculated to be 4.7% of the measured values. For 30 MHz and above, the error estimated is 7.4%. Hence, the systematic error is less than or equal to the 7% error associated with the scatter of the data; consequently, the latter quantity is the predominant error of the measurement.

The largest correction--that for diffraction--was calculated by using the method of Seki, Granato, and Truell[63] as modified for highly attenuating materials by Papadakis.[64] Because of the high absorption of benzene, the diffraction correction was significant only for the measurements taken at 6, 10, and 14 MHz. The maximum corrections for these three points were 29%, 10.3%, and 5.7% of the measured values, respectively (b-axis 170°K). At 18 MHz and above the correction was less than 2%.

Although an estimate of the bond loss was obtained experimentally, an idea of the effect of the mylar interface can be obtained by considering the standard three-layered-media acoustic transmission problem.[65] The bond in this case can be divided into three three-layered-media combinations:

(1) transducer-Nonaq-mylar, (2) Nonaq-mylar-glycerine, and (3) mylar-glycerine-sample. If a good bond has been made, the Nonaq and glycerine interfaces should be thinner than the mylar (less than 1/4-mil). In general, it is found that the effect of the intermediate layer depends on the magnitude of the propagation vector of the sound, $k = 2\pi/\lambda$, and ℓ , the thickness of the layer. If the quantity $k\ell << 1$, the intermediate layer is acoustically transparent. For the mylar layer, the maximum value of $k\ell$ was 1×10^{-2} for the frequencies used in this experiment. Consequently, if the nonaq and glycerine bonds provide good coupling of the sound energy into and out of the mylar seal, the latter should not have appreciably interfered with the passage of the sound wave between the transducer and the sample.

To determine the actual effect of the bond, measurements were made on a sample which was first air backed (sealed with clear mylar) and then backed with a dummy transducer that was bonded onto the reflecting surface of the crystal with the same glycerine-mylar-Nonaq bond used for the active transducer. The latter configuration yielded higher attenuation measurements; the excess was attributed to the bond loss. The dummy transducer had a fundamental frequency of 5 MHz and was one inch in diameter. A transducer with a larger diameter than that of the sample was used to eliminate the problem of having to center the transducer in the middle of the sample so that it would be in line with the active transducer. Alignment would be necessary with a transducer which had a smaller diameter than that of the sample to ensure that the sound beam is coupled into the dummy transducer and not reflected off the benzene surface.

Measurements were taken between 230-250°K on a nonoriented sample in

the two configurations described. The excess absorption due to the dummy transducer was approximately 10%. Hence, the bond losses were not a major part of the apparent attenuation and the relative behavior of the sound absorption with temperature should be that characteristic of the sample and not that of the bond.

In general, losses due to nonparallelism of the sample faces are significant at high frequencies and for materials with low intrinsic attenuation. The frequency at which nonparallelism becomes a predominant loss mechanism must be calculated for each case. For highly attenuating materials an estimate of the losses due to nonparallelism is given by[66]

$$\alpha' = \frac{8.68\pi^2\nu^2R^2\theta^2n}{s^2L} \quad . \tag{4.1}$$

α' is the attenuation in db/cm due to nonparallelism, R the radius of the active area of the transducer, θ the amount of nonparallelism between the two sample faces expressed in radians, n the echo farthest out in the echo train used for measurement, s the sound velocity, and L the sample thickness. The value of θ for this experiment was estimated to be 6.67×10^{-4} radians. Substitution in Eq. 4.1 indicates that the attenuation due to nonparallelism at 38 MHz at 180°K is 1.5% of the measured value. This represents the maximum error due to nonparallelism.

It was mentioned above that inconsistent results were obtained when transducers with different fundamental frequencies were used. The same effect was observed by Sylwestrowicz[67] who made sound absorption measurements on three different types of materials with five different fundamental-frequency transducers. A set of measurements was taken on each material with each transducer. For a given type of material, the frequency dependence

of the absorption was the same for the five transducers but there was a significant difference in the magnitude of the apparent attenuation; the thickest transducer (lowest fundamental frequency) yielded the highest value of attenuation. For example, the absorption value measured at the third harmonic of a 5 MHz transducer was higher than that obtained with a 15 MHz transducer operated at its fundamental.

Because the "thickness" effect becomes more predominant with thicker transducers, it was a significant factor in this experiment. The 2.0 MHz transducer is much thicker than transducers usually employed in making sound absorption measurements in solids (normally transducers with fundamental frequencies of 5 MHz and higher are used). An attempt was made to obtain an estimate of the thickness effect by applying Sylwestrowicz's procedures to this experiment. Measurements were taken with 2.0, 2.5, and 5.0 MHz transducers on a benzene sample at 250°K. The details of the procedure and the experimental results are given in Appendix G; a possible cause for the effect is also discussed in that appendix.

The experimental results indicated that with a 2.0 MHz transducer, the thickness effect accounted for about 30% of the apparent attenuation. The experimental values quoted in Section 4.1 were not corrected for this effect, however, because the "thickness effect" experiment was carried out on one axis at one temperature. The fact that such an effect appears to exist is brought out to emphasize the relative nature of sound absorption measurements in solids as a function of temperature. One must be careful when comparing measurements of different investigators to keep the thickness effect in mind, especially when transducers with fundamental frequencies below 5 MHz are used.

Finally, mention should be made of losses due to reflection and electromechanical conversion. For the case of a solid with an air-backed reflecting surface, the mismatch of the acoustical impedances between the sample material and the air is so great that a reflection coefficient of unity can be assumed, i.e., there are no losses due to reflection. The reflecting surface of the sample in this experiment was covered with mylar; however, the mylar was so thin that any sound energy absorbed in it would be negligible compared to that of the benzene. Thus, it was assumed that the sample was essentially air-backed and the reflection losses were negligible.

Attenuation due to insertion loss can also be neglected in this case. This loss can be expressed as the amount of acoustical energy extracted from the sample per reflection that is converted into electric energy and depends primarily on the electromechanical coupling coefficient of the transducer employed. For a quartz transducer operating under the conditions of this experiment the insertion loss was calculated to be 0.06%.

Thus, the predominant error in the experimental measurements resulted from the scatter of the data with additional uncertainty for the low frequency measurements (6 and 10 MHz) introduced by diffraction and for the high frequency values by nonparallelism (1.5% at 38 MHz) and the low signal-to-noise ratio of the patterns obtained (30 MHz and above). The bond loss was found not to predominate over the intrinsic attenuation and the "thickness effect" was shown to influence only the magnitude of the measurements and not the relative frequency behavior with temperature. It is estimated that the total error of the measurements is approximately 7% at 26 MHz and below and not greater than 10% for 30 MHz and above.

5. Discussion of Results

5.1 General

The sound absorption measurements obtained in this experiment were recorded at higher frequencies and lower temperatures then previous measurements in solid benzene, and, more significantly, were made along known crystallographic directions. A different relaxation behavior was observed along each axis which indicates that the sound absorption depends on the orientation of the molecules in the unit cell. The lack of relaxation effects in the same frequency range in the liquid state further indicates that the sound absorption mechanism must be related to the structure of the solid, i.e., the ultrasonic beam induces the lattice vibrations to interact with each other or causes interactions between the lattice and internal oscillations. If α were due to intermolecular vibrations only, a reasonable agreement with the theory of Woodruff and Ehrenreich[43] would be expected. However, as pointed out in Section 2.3, Woodruff and Ehrenreich's theory predicts the magnitude of α to be less than 1% of the observed value and transition times which are three to four orders of magnitude faster ($\sim 10^{-13}$ sec) than observed in this experiment ($\sim 10^{-9}$ sec). Hence, Liebermann's postulate that sound absorption in molecular solids arises from the interaction between the inter- and intramolecular vibrational modes would appear to be appropriate.

The large values of α observed in this experiment are consistent with the magnitude of the sound absorption observed in previous ultrasonic attenuation investigations in organic molecules. However, the frequency dependence of α above 14 MHz and its temperature dependence below 250°K

depart significantly from what has been observed experimentally and from that predicted by both the Liebermann and Danielmeyer analyses. In all previous investigations, with the exception of the most recent by Wilson and Yun[11] in naphthalene (discussed later), α exhibited an approximate frequency-squared dependence and was practically independent of temperature within the limits of the experimental measurements. The upper frequency and lower temperature limit of these measurements were as follows:

Benzene[6]	10.7 MHz	215°K
Cyclohexane[7]	8 MHz	185°K
Carbon tetrachloride[8]	13.5 MHz	227°K
p-dichlorobenzene[9]	65 MHz	220°K
Naphthalene[9]	95 MHz	200°K.

In general, the values of α obtained in this work at 14 MHz and below show a partial agreement with the ν^2 dependence of previous investigations; however, above 14 MHz, relaxation effects predominate. Therefore, a discussion of the data at 14 MHz and below will be given first; then the relaxation effects observed along each axis will be discussed and finally, an attempt will be made to relate the behavior of α to the molecular structure within the unit cell of benzene.

5.2 Sound Absorption Behavior Between 6 MHz and 14 MHz

The temperature dependence of α for each axis at 6, 10, and 14 MHz is shown in Fig. 17. In general, the change in α with temperature is the greatest for the b-axis and the least for the c-axis but the rate of change for each axis increases with frequency. At 6 MHz the value of α for the c-axis changes by 4.4% between 215°K (the lower temperature limit of

Liebermann's experiment) and 250°K. This compares favorably with Liebermann's result of α exhibiting only a slight temperature dependence; however, the remainder of the data in Fig. 17 contradicts the temperature dependence observed in all previous investigations (except for the most recent values for naphthalene[11]). In the latter case, the values of α also decrease with temperature down to the point where relaxation effects are observed (170°K) but the rate of decrease does not change as rapidly with increasing frequency as it does in the present work.

It can be seen from Fig. 17 that the relative magnitude of the attenuation is the greatest for the c-axis and the least for the b-axis at 6 and 10 MHz. The same relative relation holds for the magnitude of the linear expansion coefficients β' along each of the axes, i.e., the largest value of β' is that for the c-axis (2.21×10^{-4}/°C)[60] and the smallest for the b-axis (1.06×10^{-4}/°C)[60], a ratio of 2.09. Between 180°K and 250°K the ratio of α for the c-axis to that of the b-axis ranges from 1.5 to 2.7 at 6 MHz and 1.1 to 2.3 at 10 MHz. Although β' is not the only parameter affecting the sound attenuation, the linear expansion coefficient appears to give a qualitative relationship of the relative magnitudes of the attenuation along the different axes at 6 and 10 MHz. In general, linear expansion in a solid results from the anharmonicity of the potential energy which describes the binding forces of the atoms or molecules in the substance under consideration. For molecular solids α would also appear to depend on the anharmonic terms of the intermolecular potential; consequently, some correlation between α and β' would be expected, i.e, the molecular arrangement within the unit cell does influence the sound absorption. At frequencies above 10 MHz the relative relation between α and

β' does not hold; however, as will be discussed later, the crystal structure influences the sound absorption at these frequencies as well.

Comparison of the frequency dependence of the absorption values obtained at 14 MHz and below with that obtained from Liebermann's values for benzene can be made by calculating the slopes of the lines that result from a logarithmic plot of α versus ν. The slope should be close to two if α exhibits approximate frequency-squared dependence. At 250°K the slopes obtained from the data of this experiment between 6 and 14 MHz are 1.73, 1.85, and 1.42 for the a, b, and c axes, respectively. At 170°K the slopes obtained from the data in the same frequency range are 1.60 and 1.83, respectively, and for the c-axis at 180°K, 1.08. Hence, the frequency dependence along the b-axis exhibits essentially no change between 170°K and 250°K whereas it changes by 7.5% and 24% from the high temperature values for the a and c axes, respectively. From Liebermann's measurements on nonoriented benzene crystals at 6.4 and 10.7 MHz at 273°K, the slope is 1.90. If it is assumed that the slopes change linearly with temperature, the extrapolated values for the a, b, and c axes at 273°K become 1.76, 1.85, and 1.52, respectively. Hence, of all the measurements, the frequency dependence of α for the b-axis agrees most favorably with that observed by Liebermann and the temperature dependence compares least favorably with Liebermann's results, i.e., there is a 62% change in α between 170°K and 250°K (6 MHz). The agreement of the frequency and temperature dependences for the c-axis values are reversed, i.e, agreement of the frequency dependence is the worst and that of the temperature dependence is the best.

The fact that the slopes of the lines on the $\log \alpha$ vs. $\log \nu$ plots for the a and c axes decrease with decreasing temperature suggests that

presence of relaxation effects; this is borne out by the data obtained above 14 MHz (see Figs.14-16). Wilson and Yun[11] observed the same behavior for naphthalene; i.e., the slope changed from 1.74 at room temperature to approximately one in the temperature range where relaxation effects were observed (170°K).

5.3 Pertinent Facts Concerning Relaxation Theory

Prior to discussing the experimental results for the higher frequencies, a brief description of the standard relaxation curve on a μ (absorption per wavelength) versus ν plot will now be given. The standard formula for the attenuation per wavelength (Eq. 2.37) can be rewritten in the form

$$\mu = \frac{\pi r}{(1-r)^{1/2}} \frac{\omega\tau_m}{1+\omega^2\tau_m^2} \tag{5.1}$$

where $\tau_m = \tau_{ps}(1-r)^{1/2}$. Thus, μ can be separated into two terms, one which involves only the relaxation strength r and the other which involves $\omega\tau_m$. The latter term controls the shape of the curve on the μ versus ν plot. If the quantity $\omega\tau_m/(1+\omega^2\tau_m^2)$ is plotted as a function of $\omega\tau_m$, a broad bell-shaped curve is generated which has a maximum value at $\omega\tau_m = 1$. In the region where $\omega\tau_m << 1$ the curve is a straight line with a slope of one and where $\omega\tau_m >> 1$ the curve is also a straight line but with a slope of minus one. The curve thus formed is the "standard relaxation curve" for a single relaxation process. The position at which $\omega\tau_m = 1$ on the μ versus ν plot defines the maximum absorption per wavelength μ_m and the relaxation frequency ν_m. The change of μ_m and ν_m with temperagure can be used to obtain information about the reaction mechanisms which

take place in the relaxation region. If velocity dispersion is small, μ can be replaced by μ', i.e. (α/ν), and the μ' versus ν plot should exhibit the same characteristics as the μ vs. ν presentation.

A single relaxation process will occur if there is a maximum value of sound absorption per wavelength that results from the exchange of energy between one lattice vibrational mode and one optical vibrational mode. As discussed in Section 2.2, in many cases in liquids and gases the entire optical spectrum of a substance will relax as a group; such a relaxation will also generate a standard relaxation curve on the μ vs. ν plot. If there is more than one relaxation process occurring at frequencies which are relatively close together, i.e, which differ by less than a factor of about 10, the standard relaxation curve will become distorted. One can usually obtain a reasonable reproduction of the distorted curve by adding two or more standard relaxation curves with different values of μ_m and ν_m. However, multiple relaxation processes are quite complicated and the addition procedure only gives an indication that such a process exists; it does not yield any information as to how the interaction is taking place; i.e, whether the processes are interdependent or independent of each other. Hence when the additive procedure is used, it must be kept in mind that the values of μ_m and ν_m of the individual components of the sum describe only the simplest possible interaction that is likely to occur.

5.4 Relaxation Effects in Benzene

Figure 14 shows the μ' vs. ν curves for the a-axis. The standard relaxation curve has been drawn through the experimental points for 170, 190, 230, and 240°K. (The trend of the curves at the lower temperatures

was used to draw the curves for the upper temperatures.) The curves indicate that the relaxation frequency ν_m changes from 17 MHz to 12 MHz and μ'_m decreases by 58.5% from its value at 240°K. The shift of ν_m to a lower value at the lower temperature is characteristic of vibrational relaxations, i.e., normally the transition times will increase with decreasing temperature.

All the points do not fall on the curves as drawn, however. The data from 18 MHz to 34 MHz fit very well as does the 6 MHz point, but the 10 MHz and 14 MHz points are below and above the curves, respectively. The discrepancy at 14 MHz becomes more pronounced as the temperature is decreased. A better fit to the points would be given by a curve which peaks more sharply than the standard relaxation curve; the dashed curve drawn through the points for 190°K represents such a behavior.

The experimental points for 190°K have been replotted in Fig. 18. The curve drawn was obtained by adding the contributions of the three standard relaxation curves shown and appears to fit the experimental data somewhat better than the standard curve. This suggests the possibility of multiple relaxations occurring in the same frequency region. For the example shown, the relaxation frequencies would be 9, 14, and 24 MHz and the relaxation strength of the center curve is about 80% higher than the other two. As indicated earlier, this is only representative of the type of multiple relaxations which might occur.

The data for the b-axis are shown in Fig. 15. Every experimental point except one (10 MHz @ 170°K) falls on the standard relaxation curves drawn. Once again the trend of the low temperature data was used to draw the curves for the high temperature data. The points at 170°K fall on the back side

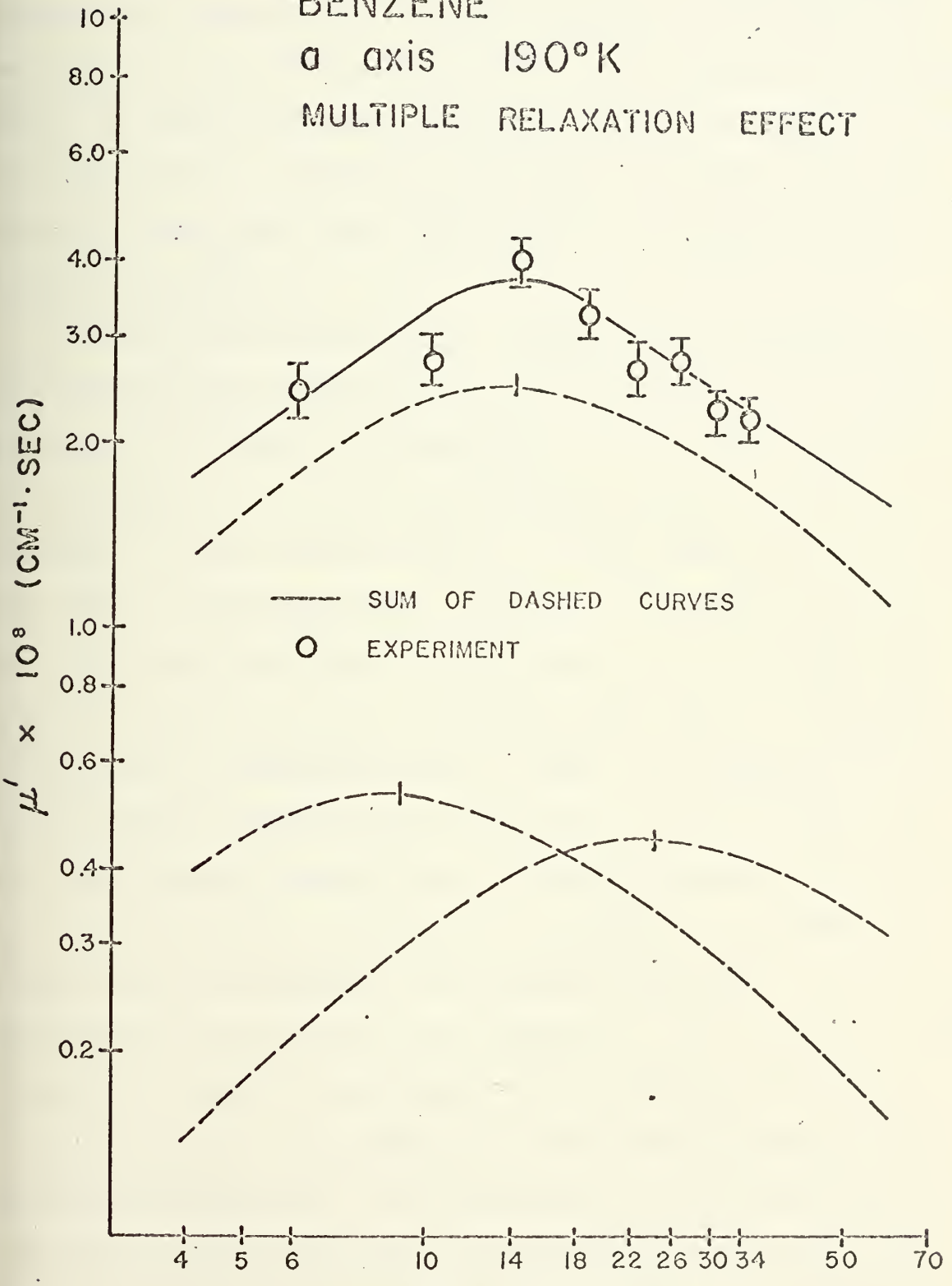
μ' vs. FREQUENCY
BENZENE
a axis 190°K
MULTIPLE RELAXATION EFFECT
μ' x 10⁸ (CM⁻¹·SEC)
10
8.0
6.0
4.0
3.0
2.0
1.0
0.8
0.6
0.4
0.3
0.2
SUM OF DASHED CURVES
EXPERIMENT
4
5
6
10
14
18
22
26
30
34
50
70
FREQUENCY (MHz)

Figure 18

of the standard curve which gives a good indication that a relaxation is present. The curves indicate a relaxation frequency of 26 MHz at 240°K and 20 MHz at 170°K with a change of 53.5% in μ'_m over the same temperature range. The shape of the curves indicate the presence of a single relaxation along this axis, i.e., either one lattice mode is exchanging energy with one optical mode or the entire optical spectrum is relaxing as a group with a single relaxation time.

The c-axis curves shown in Fig. 16 exhibit the most distortion of all the curves obtained, especially at the lower temperatures. The experimental points for 240°K roughly fit a standard curve centered at 14 MHz; however, as the temperature is lowered another relaxation appears to influence the absorption. At 180°K the points from 26 to 38 MHz appear to be on the upward slope of a second relaxation. In Fig. 16, two standard relaxation curves have been drawn in below the experimental curves. By adding the components of these two curves, the resultant curve (see Fig. 19) qualitatively follows the experimental points at 180°K. This suggests that there is a low frequency relaxation at 4.5 MHz with $\mu' = 3.5 \times 10^{-8}$ cm^{-1} sec and a high frequency relaxation with a relaxation frequency of 120 MHz and $\mu'_m = 3.0 \times 10^{-8}$ cm^{-1} sec. Once again, the behavior of ν_m follows the pattern which is characteristic for vibrational relaxations. At 240°K the high frequency relaxation peak is at a value of ν_m and μ'_m such that the values of μ' associated with that curve do not influence the values of μ' of the relaxation curve centered at 14 MHz (within the range of the experimental measurements). As the temperature is lowered both relaxation peaks shift to a lower frequency. The influence of the upper peak starts to appear at 210°K and becomes stronger as the temperature is lowered further.

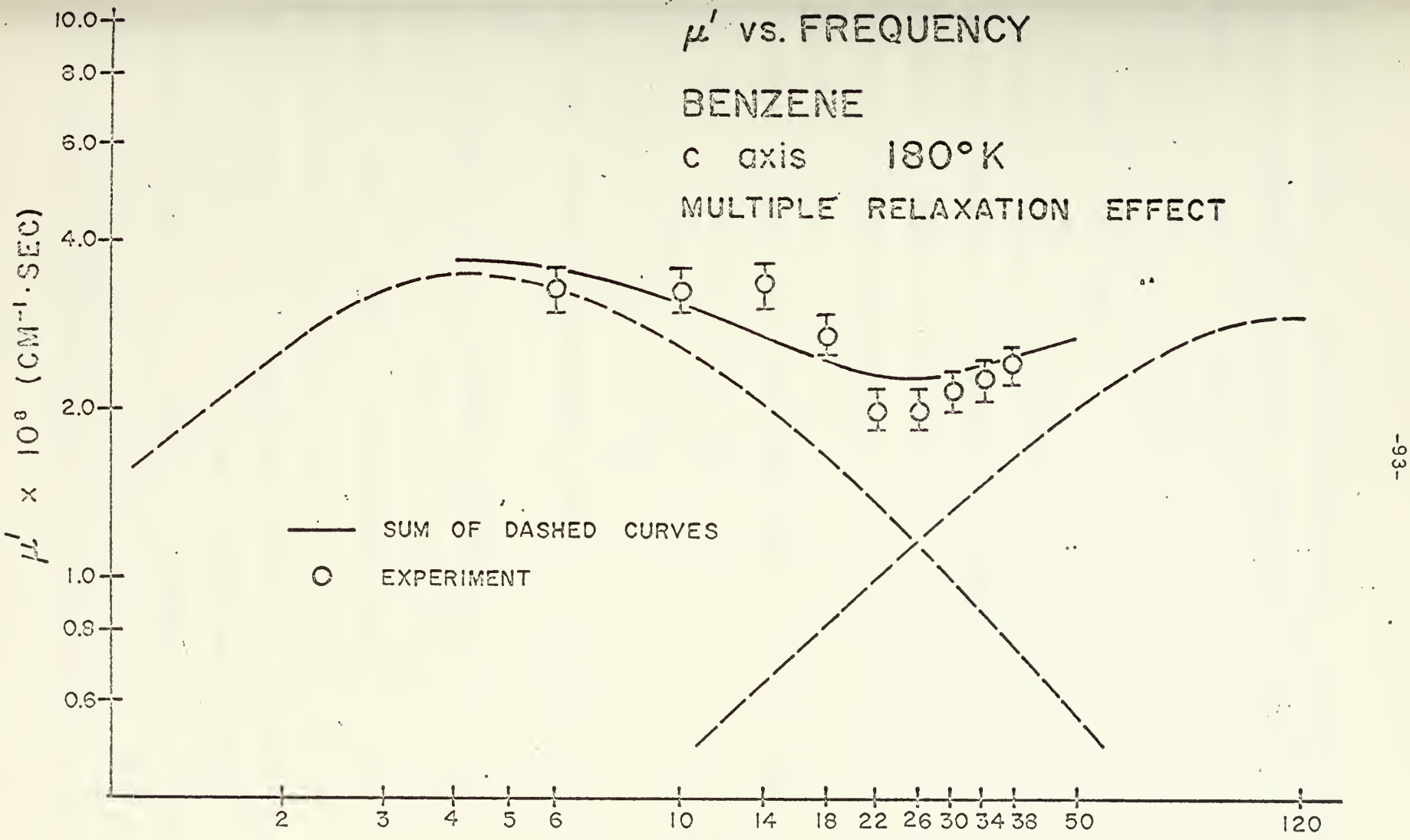
μ' vs. FREQUENCY
BENZENE
c axis 180°K
MULTIPLE RELAXATION EFFECT
μ' × 10⁸ (CM⁻¹·SEC)
10.0
8.0
6.0
4.0
2.0
1.0
0.8
0.6
SUM OF DASHED CURVES
EXPERIMENT
2
3
4
5
6
10
14
18
22
26
30
34
38
50
120
FREQUENCY (MHz)

Figure 19

The exact behavior of the upper relaxation cannot be determined because of the limited experimental information. However, the low frequency relaxation appears to be centered at 14 MHz at 240°K and at 4.5 MHz at 180°K; μ'_m changes by 32.8% over the same temperature range.

5.5 Comparison With Theory

Neither Liebermann's nor Danielmeyer's theory predicted the existance of relaxation effects in the frequency and temperature ranges of this experiment. In Section 2 it was pointed out that both theories contained a number of fundamental weaknesses and did not adequately describe the sound absorption process in molecular crystals; however, since they are the only theoretical treatments available, a brief comparison will be made between each theory and the experimental results. In so doing, modifications will be made in the theories to take into account the anisotropic properties of the solid wherever possible and factors in the equations for α and τ that may be treated as experimentally adjustable parameters will be pointed out.

A comparison of the experimental relaxation times, i.e., where $\omega\tau_m = 1$, for each axis and those calculated from Liebermann's and Danielmeyer's theories is shown in Table V. The comparison is made for temperatures of 180°K and 240°K, the temperature range which is common to the data for all three axes and for which an experimental value of ν_m could be obtained for each axis. (Fewer points were obtained at 250°K than at 240°K and below; consequently, a value of ν_m could not be determined for each axis at 250°K). Equations 2.5 and 2.26 were used to calculate τ for Liebermann's and Danielmeyer's theory, respectively (ν_D was considered to be constant

Table V

Comparison of Experimental and Theoretical Relaxation Times

	Temp. (°K)	τ_a	τ_b	τ_c	τ
		(sec × 10^9)			
Experimental	240	9.35	6.15	11.4	
	180	13.4	8.00	35.5	
Danielmeyer's	240	0.26	2.47	.0103	
Theory	180	0.45	4.74	.0073	
Liebermann's	240				0.94
Theory	180				3.70

for the present case). Since Danielmeyer's theory is derived from a solid state viewpoint, it is possible to modify it slightly to account for anisotropy. To calculate τ from Eq. 2.26 one must first calculate the value of the coupling parameter B contained in the factor K (see Eq. 2.23). B is related to the Grüneisen constant by Eqs. 2.20 and 2.21. Hence, the Grüneisen constant can be calculated as a function of temperature for each principal direction from Eq. 2.21. (In doing this β must be replaced by $3\beta'$ for each direction and χ_T^{-1} by the experimentally determined values of the bulk modulus (Heseltine et al.[14])). Once this is done, Eq. 2.20 can be used to calculate the value of B as a function of temperature using the value of c_{ii}^s, which is appropriate for a longitudinal sound wave propagated along the axis under consideration (elastic constants also given by Heseltine et al.[14]). Since the coupling parameter A contained in Liebermann's equation for τ (Eq. 2.5) is derived from the Lennard-Jones potential a quantitative relation between A and the elastic and thermodynamic

properties of the crystal cannot be made; consequently, the value of A originally calculated for benzene by Liebermann was used. The relaxation time predicted by the modified Danielmeyer theory for the b-axis agrees fairly well with the experimental values for the same axis. Agreement for the a and c axes is much poorer. The value of τ predicted by Liebermann's theory agrees to within one order of magnitude with all the experimental values. Except for τ_c, both theories predict an increase in the relaxation time with decreasing temperature as is indicated by experiment. τ_c indicates the opposite behavior and results from the fact that the values of K for the c-axis decrease much more slowly with temperature than for the other two axes. This allows the exponential factor $e^{\theta/T}$ (see Eq. 2.29) to have a greater influence on the change of τ with decreasing temperature.

Better agreement between the value of τ_a and τ_c obtained from experiment and those predicted by Danielmeyer's theory can be obtained by treating B as an adjustable parameter. In Eq. 2.20 only c_{11}^s and c_{33}^s were used to calculate the values of B for the a and c axes, respectively; however, as pointed out in Section 2.2, B is related to the second and third order elastic constants. For an anisotropic solid the value of B may be quite different from that given by Eq. 2.20. If the value of B calculated for the a-axis is divided by two, the predicted values of τ_a fall into the same order of magnitude as the experimental values. For the c-axis, the value of B for 240°K and 180°K must be divided by about 3 and 3.5, respectively so that the predicted values of τ_c will be of the same order of magnitude as the observed values and also increase with decreasing temperature

The above discussion assumed ν_D to be constant; however, as mentioned in Section 2, when ν_D is treated as a function of temperature, Liebermann's theory predicts the attentuation to decrease with increasing temperature and Danielmeyer's theory predicts an increase in the relaxation time with increasing temperature (increase of α with increasing temperature). Although Danielmeyer's results is plausible, it does not agree with the relaxation behavior observed. For a decrease in the relaxation time with increasing temperature would shift the relaxation peak to a lower frequency as the temperature is increased, which is just opposite the normal behavior in vibrational relaxations and from that experimentally observed.

Another parameter which can be compared with the theory is the change in μ_m' for each direction as a function of temperature. To do this the relaxation strength in Eq. 5.1 must be modified to take the sound velocity into account. In general μ_m occurs when $\omega\tau_m = 1$ and for this case Eq. 5.1 becomes

$$\mu_m = \frac{\pi r}{2(1-r)^{1/2}} \tag{5.2}$$

From Danielmeyer's theory the relaxation strength is given by Eq. 2.38 and for benzene yields values of $r << 1$ ($\sim 10^{-3}$); therefore, the r in the denominator of Eq. 5.2 can be neglected. Equation 5.2 can be rewritten in terms of μ_m' as

$$\mu_m' \approx \frac{\pi}{2}\left(\frac{r}{s}\right) \equiv \frac{\pi}{2} r' \tag{5.3}$$

Here s is the longitudinal sound velocity along the principal axis for which the absorption measurements are being made.

Equation 2.38 shows that r is temperature dependent, i.e., the specific heats and the factor ζ_s, which is related to the elastic constants

(Eq. 2.39), change with temperature. Hence, μ_m' can be calculated for each direction at different temperatures which enables a comparison of the change in the relative values of μ_m' with temperature.

Since ζ_s is based on an isotropic solid, a slight modification is necessary to use it in the present case. The principal axes of the orthorhombic structure are two-fold symmetric; hence, there are two shear velocities for each principal direction. To calculate ζ_s for a given direction for benzene, the average value of the two shear velocities was used. Equation 2.39 becomes

$$\zeta_s' = 1 - \frac{2}{3}\left[\frac{c^s_{t_1} + c^s_{t_2}}{c^s_\ell}\right] \tag{5.3}$$

Here $c^s_{t_1}$ and $c^s_{t_2}$ are the elastic constants associated with the shear velocities which propagate along one of the principal axes; c^s_ℓ is the corresponding elastic constant for longitudinal waves. Hence, to calculate μ_m' Eq. 2.37 is modified to become

$$\mu_m' \simeq \frac{\pi}{2} r_m' = \frac{\pi}{2s} \frac{(C_p - C_v)\zeta_s' C_v^i}{C_v(C_p - \zeta_s' C_v^i) - C_p(1-\zeta_s')C_v^i} \tag{5.4}$$

By using the experimental values of the sound velocities[14] and specific heats[19], μ_m' can be calculated from Eq. 5.4 for any temperature between 170°K and 250°K.

A comparison of the change in μ_m' between 180°K and 240°K that was experimentally observed and that calculated from Eq. 5.4 is given in Table VI. It can be seen that the predicted change in μ_m' is from 1.55 to 2.12 times greater than that obtained from the observed values. A better agreement could be obtained in two ways. First, the factor ζ_s' can be treated as an

Table VI

Comparison of the Theoretical and Experimental

Change in μ_m' With Temperature

	Temp (°K)	Axis a	b	c
μ_m'(exp)	240	0.54	0.48	0.50
($cm^{-1}sec \times 10^7$)	180	0.32	0.27	0.34
μ_m'(th)	240	4.40	5.95	5.15
($cm^{-1}sec \times 10^7$)	180	1.22	1.90	1.67
$\Delta\mu_m'$(exp)		44.4%	43.8%	32.0%
$\Delta\mu_m'$(th)		71.5%	68.0%	68 %
Ratio $\frac{\Delta\mu_m'(exp)}{\Delta\mu_m'(th)}$		1.61	1.55	2.12

experimentally adjustable parameter since it is probably related to the elastic constants of the material in a more complicated way than is described by Eq. 5.3. It would be possible to adjust ζ_s' for each axis and for each temperature to obtain the change in μ_m' that is experimentally observed. However, this procedure does not yield any information concerning the details of the physical processes involved.

A second way to obtain better agreement is to consider the possibility of partial relaxation effects; i.e., the energy that is coupled into the internal modes does not relax with all the modes at one time as assumed by Danielmeyer. This type of behavior has been experimentally observed for vibrational relaxations in liquid sulfur dioxide (Bass and Lamb[68]) and liquid methylene chloride (Andreae[69]).

For liquids and gases the relaxation strength and the internal specific heats are related by an expression similar to Eq. 2.38[68]. However, rather than use the total internal specific heat, the contribution of the internal specific heat due to each mode is determined from the Einstein relationship (Eq. 2.3) and μ_m is calculated for the mode under consideration from the result. Absolute sound absorption measurements are usually made in liquids; consequently, it can be determined if the total internal specific heat relaxes at the experimentally observed relaxation time by comparing the numerical value of μ_m obtained from experiment to that calculated from theory. For liquid sulfur dioxide and methylene chloride it was found that $\mu_m(\text{exp})$ was less than $\mu_m(\text{th})$ when the latter was calculated by use of the total internal specific heat. However, if only the contributions to C_v^i due to certain internal modes were used to calculate $\mu_m(\text{th})$, excellent agreement between theory and experiment was obtained. For sulfur dioxide

there are four internal modes (one of which is degenerate) and it was found that only two contribute to the observed relaxation. For methylene chloride only eight of the nine internal modes participate in the observed relaxation.

5.6 Relationship of α to the Molecular Vibrations

A procedure similar to that employed for liquids could be used to calculate $\mu_m'(th)$ in the present case by replacing C_i in Eq. 5.4 by the C_i (calculated from Eq. 2.3) for the internal modes of crystalline benzene. A comparison between $\mu_m'(th)$ calculated in this manner and $\mu'(exp)$ could be made on a relative basis for two different temperatures as was done in Table VI. Before going into the details of this calculation, a brief description of the benzene molecule will be given.

Cox et al.[60] determined that the benzene molecule is accurately planar with one carbon atom at each vertex of a regular hexagon. One hydrogen atom is bonded to each carbon atom and the C-H bonds extend radially outward from the center of the hexagon along lines joining the center and the vertices of the hexagon. A schematic diagram of the molecule is shown below.

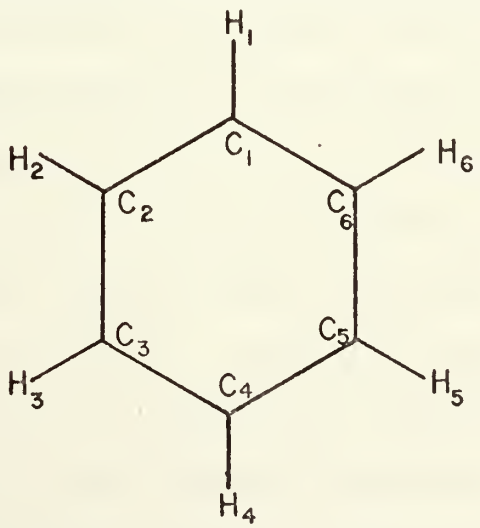

Fig. 20. Benzene Molecule

The numbering system is that used by Cox to describe the position of the atoms when the molecule is in the unit cell of crystalline benzene (discussed later). The internal oscillations of the benzene molecule can be divided into in-plane and out-of-plane vibrations, the latter usually correspond to the lower frequencies in the optical spectrum; hence, are the ones with weaker bonds. Examples of the out-of-plane vibrations would be the C-H out-of-plane bending mode and the C-C-C-C skeletal out-of-plane mode. The weakest in-plane vibration is the C-C-C bending mode which tends to change the obtuse angles of the type C_1-C_2-C_3. The strongest bond of all the internal vibrations, i.e., that with the highest frequency, is the C-H in-plane stretching vibration. There are a total of thirty normal modes for the internal oscillations of the benzene molecule (for a complete description of each mode see Wilson et al.[70]). In the gaseous and liquid states ten of the modes are degenerate; however, in the solid state the degeneracies are lifted and there are thirty nondegenerate internal modes[3].

Many spectroscopic experiments have been performed on crystalline benzene; consequently, the internal vibrational frequencies are well known. By using the most recent Raman[71] and infrared[72] data for benzene δC_i was calculated for the internal modes in the lower part of the optical spectrum and for the highest internal mode. Then r'_m was calculated using the definition in Eq. 5.4 except that C_v^i was replaced by the appropriate δC_i. From this a value of $\mu'_m(th)$ can be calculated for each internal mode. The results are shown in Table VII. The modes are listed in order of increasing wavenumber, the value in parentheses corresponds to the standard numbering system for the normal modes first introduced by Wilson.[70] Also, the type of vibration is indicated; i.e, C-H bending, etc.

Table VII

Comparison of $\mu_m'(th)$ for Individual Internal Modes and $\mu_m'(exp)$

Mode	Wave-number (cm^{-1})	Mode type	Temp. (°K)	δC_i (cal/mole-°K)	a-axis μ_m' ($cm^{-1}sec$) $\times 10^8$	a-axis $\Delta\mu_m'$ (%)	b-axis μ_m' ($cm^{-1}sec$) $\times 10^8$	b-axis $\Delta\mu_m'$ (%)	c-axis μ_m' ($cm^{-1}sec$) $\times 10^8$	c-axis $\Delta\mu_m'$ (%)
Expt'l			240		5.4	44.4	4.8	43.8	5.0	32.0
			180		3.2		2.7		3.4	
1(ν_{16})	404.0 I	$C_\perp$ a	240	1.04	4.15	49.3	5.9	44.0	5.03	41.8
			180	0.818	2.12		3.3		2.93	
2(ν_{16})	419.2 I	$C_\perp$ a	240	1.03	4.07	49.1	5.86	45.0	4.98	43.8
			180	0.79	2.07		3.22		2.79	
3(ν_6)	605.0 R	$C_{\parallel}$ b	240	0.775	3.03	68.2	4.33	56.2	3.68	64.2
			180	0.375	0.96		1.50		1.30	
4(ν_{11})	679.0 I	$H_\perp$ c	240	0.565	2.22	70.4	3.13	67.0	2.64	66.0
			180	0.262	0.66		1.03		0.89	
5(ν_4)	709.1 *	$C_\perp$ a	240	0.532	2.12	73.5	2.95	69.8	2.49	68.8
			180	0.230	0.56		0.89		0.78	

Table VII (continued)

Mode	Wave-number (cm^{-1})	Mode type	Temp. (°K)	δC_i (cal/mole-°K)	a-axis μ'_m ($cm^{-1}sec$) $\times 10^8$	a-axis $\Delta\mu'_m$ (%)	b-axis μ'_m ($cm^{-1}sec$) $\times 10^8$	b-axis $\Delta\mu'_m$ (%)	c-axis μ'_m ($cm^{-1}sec$) $\times 10^8$	c-axis $\Delta\mu'_m$ (%)
6(ν_{10})	852.3 R	$H_\perp$ c	240	0.317	1.21	77.5	1.73	75.8	1.48	75.8
			180	0.109	0.27		0.42		0.36	
7(ν_{10})	864.0 R	$H_\perp$ c	240	0.32	1.26	80.8	1.78	78.5	1.53	78.5
			180	0.95	0.24		0.38		0.33	
8(ν_{17})	970.0 I	$H_\perp$ c	240	0.199	0.76	81.1	1.08	81.3	0.92	78.2
			180	0.054	0.14		0.20		0.22	
9(ν_{17})	982.0 I	$H_\perp$ c	240	0.143	0.73	83.5	1.05	81.8	0.91	83.5
			180	0.048	0.12		0.19		0.15	
10(ν_1)	982.0 R	C-C d	240	0.198	0.75	86.5	1.08	82.3	0.91	82.4
			180	0.048	0.12		0.19		0.16	
⋮										
30(ν_2)	3062.5 R	C-H e	240	$< 1\times10^{-7}$						
			180	$< 1\times10^{-7}$						

R - Raman (Reference 71)
I - Infrared (Reference 72)
* - Calculated (Reference 3)

a. Skeletal out-of-plane vibration
b. C-C-C in-plane vibration
c. C-H out-of-plane bending vibration
d. C-C stretching vibration
e. C-H stretching vibration

It can be seen in general that the change in μ_m' between 180°K and 240°K becomes greater as the internal vibrational frequency increases. For the a and b axes the changes in μ_m' for the lowest optical mode are within a few percent of the experimentally observed values. The correlation for the c-axis is not as good; however, it is much better than that obtained in Table VI. Hence, Table VII gives an indication that the lower frequency internal modes are the ones which play the principal role in the relaxations which are observed. Also, it should be noted that the values of the $\mu_m'(th)$ calculated with the δC_i are of the same order of magnitude as the $\mu_m'(exp)$ whereas the values of $\mu_m'(th)$ calculated with the total internal specific heat are one order of magnitude greater than $\mu_m'(exp)$ (compare Tables VI and VII). Although it was indicated in Section 4.2 that the experimental values of α could be as much as 40% higher than the absolute values, i.e., due to the thickness effect and experimental error, the fact that the measured values are significantly less than those predicted by using the total internal specific heat gives further support to the idea of partial relaxation processes.

5.7 Relationship of α to Crystal Structure

An intuitive argument as to why one might expect the low frequency internal modes to participate in the relaxation processes rather than the other modes can be obtained by trying to visualize the effect of the sound waves on the molecules in the benzene unit cell. The arrangement of the benzene molecules in the unit cell as seen looking down the b and c axes is shown in Fig. 21. The crystal structure of benzene is simple orthorhombic with a space group of Pbca which means there is a molecule

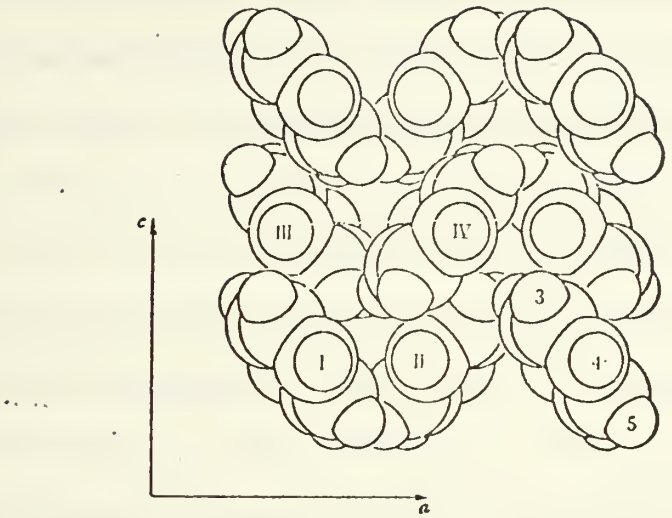

Fig. 21a. Diagram of the crystal structure of benzene viewed down the b-axis.

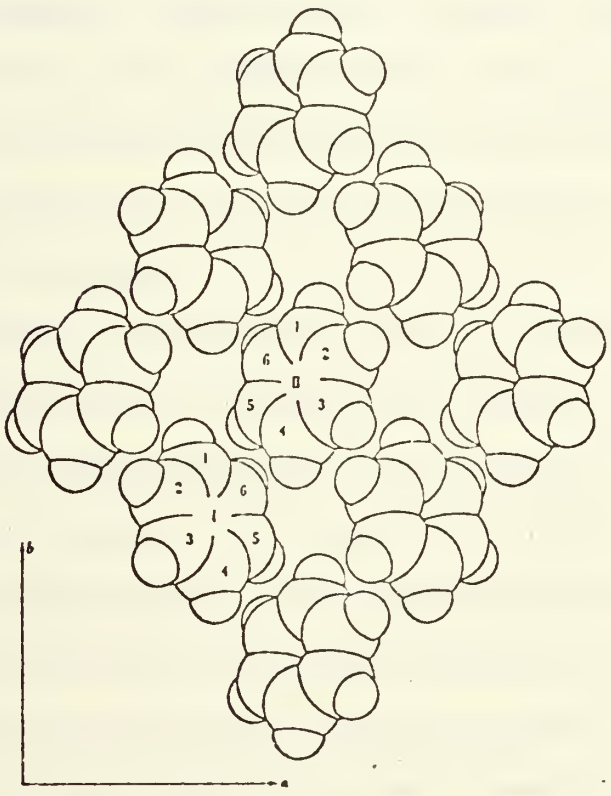

Fig. 21b. Diagram of the crystal structure of benzene viewed down the c-axis.

Fig. 21. Crystal structure of benzene (from Cox, Cruikshank, and Smith [60]).

positioned at each corner and in the center of each face of the unit cell. (The structure can be thought of in simpler terms as face centered orthorhombic). Hence, there are four molecules per unit cell; each molecule has twelve nearest neighbors. The four molecules have been designated I, II, III, and IV in Fig. 21a. The molecular planes are almost parallel to the b-axis and molecules of type I and II are inclined about 45° to the a and c axes and are at right angles to each other. (The same relative orientation exists for molecules of type III and IV.) The H_6 hydrogen atom (see Fig. 21b) of molecule I is located between the H_4 and H_5 hydrogen atoms of molecule II; consequently, the C-H bonds of the two molecules intermesh in a bevel gear arrangement. The bevel gear arrangement forms a line along the a-axis in the shape of a corrugated sheet. Molecules III and IV form a similar sheet which appears to be stacked on top of the sheet formed by the type I and II molecules. Thus, there are a series of corrugated sheets perpendicular to the c-axis.

Lattice vibrations in a molecular solid can be divided into translational and rotational modes. In benzene the rotational modes are the lattice vibrations with the highest frequencies[3]; thus, are the ones in the upper part of the acoustic spectrum. Cox et al.[60] have determined that at thermal equilibrium the molecules rotate about mutually perpendicular axes in the molecular plane and about the sixfold axis perpendicular to the molecular plane. The latter rotation has the greatest amplitude of all the rotational modes and causes the type I and II molecules to oscillate back and forth in opposite directions; i.e., as two gears would if one of the gears were set into simple harmonic motion. This action causes all the molecules in the same sheet to oscillate in the same manner.

If a longitudinal sound wave is propagated along the c-axis (see Fig. 21a), the ensuing compressions and rarefications will tend to induce the molecular planes to oscillate about axes which are parallel to the b-axis. Thus, the corrugated sheets will be flattened out in the regions of compression and will tend to their equilibrium positions in the regions of rarefaction. Such a motion would tend to distort the benzene ring and also cause the nearest neighbor H-H distances to be displaced from equilibrium. One would expect that the internal modes most affected would be the skeletal out-of-plane vibrations, the C-C-C in-plane vibration, and the C-H out-of-plane bending vibrations. From Table VII it can be seen that these three modes are the lowest in the optical spectrum. Thus, there is a possibility that relaxations are taking place between an excited state of the rotational lattice modes and excited states of the lower modes in the optical spectrum.

A similar situation would exist when a longitudinal wave is propagated along the a-axis. The molecular planes would be induced to oscillate about axes parallel to the b-axis and in regions of compression would be squeezed together in an "accordion-like" fashion. Since the interatomic bonds that are formed by atoms that are closest together in nearest neighbor molecules, i.e. H_6 atom of molecule I (H_6^{I}) and the H_4^{II} and H_5^{II} atoms, are much stronger than those bonds formed by atoms which are farther apart, this type of motion would tend to distort the molecular plane (skeletal out- of-plane vibration) and induce the C-H bonds to be bent out of the molecular plane. Once again, there is the possibility that lattice rotational mode is exchanging energy with the lower modes in the optical spectrum.

A longitudinal sound wave propagated along the b-axis would induce

the molecule to oscillate about its sixfold axis. This would cause the "gears" in each sheet to oscillate in phase, i.e., the type I and II molecules would oscillate in opposite directions. Such a motion would tend to change the H-H distances between nearest neighbor molecules but the rotational motion should not cause the molecular ring to be distorted as in the previous two cases. However, the molecular ring could be distorted by the translational motion of the molecules which would cause the C-C-C in-plane vibration to become excited. Thus, the sound wave along the b-axis appears to affect the molecules in a much different manner than when propagated along the a and c axes. The observed relaxation for the b-axis is also different from those of the other two axes. Figure 15 gives the indication that a single relaxation is taking place. This could be a result of the interaction of a lattice mode with either a C-H bending mode or the C-C-C in-plane mode. It is more likely that the entire optical spectrum is relaxing as a group; however, the comparison in Table VI tends to contradict this possibility. If one believes that Eq. 5.4 gives a reasonable value for $\mu_m'(th)$, then a relaxation between one rotational lattice mode and one low frequency optical mode is indicated.

The above discussion, which attempts to relate the action of the sound wave on the molecular structure is of course oversimplified. The actual interaction in the crystal is certainly much more complicated; however, if molecular resonance is the primary sound absorption mechanism in organic crystals, one can see that the molecular arrangement within the unit cell should be an important factor in the sound absorption behavior. It would be interesting to make sound absorption measurements on an oriented organic crystal with cubic structure. In such a case, the elastic constants along

all the (100) axes would supposedly be the same and any difference in the sound absorption behavior along each principal axis would be a result of the molecular arrangement.

The agreement between theory and experiment is not particularly good. Table V shows an order of magnitude agreement between some of the theoretically predicted and experimentally observed relaxation times; however, these values were calculated under the assumption that ν_D is independent of temperature. When the temperature dependence of ν_D is taken into account, Liebermann's theory predicts relaxation times which lead to values of $\alpha(T)$ which contraduct experimental results (see page 11). Danielmeyer's theory predicts the value of τ to decrease with decreasing temperature which is also in opposition to the experimental result. However, both relaxation time theories were based on the high-temperature Debye approximation, i.e., $\theta_D << T$. The lower temperature limit in this experiment (170°K) was close to θ_D for benzene (150°K); consequently, the theoretical formulas for τ should not be expected to be valid in that temperature region.

The comparison shown in Table VI suggests that Danielmeyer's assumption that the entire optical spectrum relaxes with a single relaxation time is questionable. One would expect better agreement between the theoretically predicted and experimentally observed change in μ_m'. Closer agreement was obtained by considering the possibility of partial realxation processes (Table VII). The analysis presented in Tables VI and VII depends on the validity of Danielmeyer's expression for r (Eq. 2.38). Since Eq. 2.38 is based on well-known concepts of solid state and relaxation theory, at least an order-of-magnitude agreement between $r'(exp)$ and $r'(th)$ should

be expected (using both C_v^i and δC_i). To apply the theory to a specific crystal structure, however, a more realistic expression for the factor ζ_s (Eq. 2.39) must be obtained. By considering an anisotropic solid, such an expression could be derived using Danielmeyer's approach.

5.8 Suggestions for Future Research

Further theoretical and experimental work concerning sound absorption in molecular crystals is desired. The existing theories contain too many generalizations to enable accurate predictions of the sound absorption behavior. One of the basic problems in the derivation of transition probabilities was the lack of an accurate expression for the intermolecular potential. The potential obtained by Williams[22] (Eq. 2.8) should be useful in this regard. As a first approximation one could take the third derivative of Eq. 2.8 (restricting the summation to include only interatomic distances of the nearest neighbor molecules ($\sim 4A^\circ$)) and use first-order time-dependent perturbation theory to calculate τ. Further refinement could be made by separating each interatomic distance, i.e., r_{HH}, r_{CC}, and r_{CH}, into components along each axis, then taking the third derivative of each resulting expression. To calculate τ, however, the Debye approximation for the density of states would still probably have to be used. The resultant relaxation time could be related to the complex sound velocity in an anisotropic crystal by using an approach similar to that used by Danielmeyer (see page 23).

Further experimentation would be desirable with organic substances which have simpler molecular structure and are cubic in the solid state. Carbon tetrachloride (CCl_4) fulfills these criteria and large single crystals

of CCl_4 have been grown.[8] However, CCl_4 freezes at -23°C and undergoes a phase transition at -48°C. The low freezing point would present experimental difficulties during orientation and the phase transition would limit the temperature range of the experiment to about 25°.

Although a more complex molecule than benzene, cyclohexane forms as fcc and its freezing point is 6.2°C. Hence, the crystal growing apparatus and the sample preparation procedure developed for this experiment could be used. Orientation would have to be accomplished using X-ray techniques, however, since cubic crystals cannot be oriented with a polarizing microscope (cubic crystals appear to be isotropic when examined with polarized light).

Further absorption and velocity measurements on benzene would be desirable. Velocity measurements made as a function of frequency would indicate the importance of dispersion in the region where relaxations were observed in this work. Absorption measurements at higher frequencies would be possible at lower temperatures and may show the existence of relaxation phenomena in the 100 MHz region as was qualitatively indicated in this work for the c-axis. Shear wave absorption measurements should give further indication as to the importance of the molecular arrangement in the unit cell. The corrugated-sheet arrangement described earlier indicates that molecules of adjacent sheets are much more loosely bound than those within the same sheet. This suggests the possibility that the sheets may be able to slide with respect to each other; i.e., that the a-b crystallographic plane is a slip plane. If dislocation damping is a significant sound absorption mechanism in benzene, transverse waves that are polarized in the slip plane should yield higher absorption values than transverse waves

polarized perpendicular to it. All the experimental apparatus developed for this experiment could be used to make shear wave measurements in benzene except that an improved transducer bonding technique would have to be developed. (Preliminary work with thick shear wave transducers indicated that the bonding technique described in Section 3.6 would not support shear waves.)

Hence, there are at least four experiments, which would yield useful information about the properties of molecular crystals, that could be performed by using all or part of the apparatus and procedures developed for this work:

(1) Sound velocity measurements on oriented benzene crystals in the same temperature and frequency range of this experiment.

(2) Longitudinal-wave sound absorption measurements on oriented benzene crystals below 170°K. (Requires development of a new bonding technique.)

(3) Shear wave sound absorption measurement on oriented benzene crystals below 170°K. (Also, requires an improved bonding technique.)

(4) Longitudinal wave absorption measurements on oriented cyclohexane crystals. (Requires development of an X-ray orientation technique.)

Appendix A

Procedures Used With the Vacuum Sublimation Apparatus

To start the sublimation process (see Fig. 1 in Sec. 3.2) all the teflon stopcocks are closed except T_6, T_7, and T_8. The storage tube is put into position by connecting the joint J_3. The system is then evacuated to a pressure of 10^{-3} mm Hg (1μ), which seals J_3. Approximately 200 ml. of liquid benzene are put into the supply tube and this tube is attached at J_2. The benzene is then slowly frozen by means of liquid N_2; the liquid N_2 is then removed and the stopcock T_5 is opened. The initial surge of air and benzene vapor is trapped by the cold trap immediately in front of the rough vacuum pump. When the pressure becomes less than 2 mm Hg (2000μ), the sublimate trap is cooled by liquid N_2. The level of the liquid N_2 must be maintained slightly below the lower end of the inner tube. If the level is higher, the inner tube will very rapidly become clogged and the maximum capacity of the trap will not be utilized. When about half of the sublimand in the supply tube is gone, stopcocks T_5 and T_8 are closed. The remaining sublimand is kept frozen with liquid N_2. Liquid N_2 is then removed from the sublimate trap and transferred to the storage tube. The resulting pressure difference between the storage tube and the sublimate trap causes the sublimate to be "vacuum transferred" into the storage tube. When the transfer is complete, stopcock T_7 is closed and T_5 and T_8 are opened. The liquid N_2 is removed from the supply tube and transferred to the sublimate trap; then the remainder of the sublimand is sublimated. During this step, the benzene in the storage tube is kept frozen with liquid N_2. When the sublimand is completely gone, the sublimate is again "vacuum transferred" to the storage tube.

It takes approximately four hours to process 100 ml. of sublimand and about the same amount of time to transfer to the storage tube. Since the capacity of the crystal-growing jar is approximately 550 ml., it is necessary to degas about 600 ml. of liquid benzene. In order to do this, three storage tubes were constructed and a different storage tube was attached to J_3 each time the supply tube was refilled. Thus, the above procedure is repeated three times. The supply tube, sublimate trap, and the storage tube (in position for transfer) are shown in Fig. A-1. A special clamp had to be constructed to hold the supply tube in position at J_2. The storage tube, supply tube, and clamp are shown in Fig. A-2.

Once the benzene is degassed, it has to be put into the crystal-growing jar without allowing air to get into the system (see Fig. 1). Before putting the benzene into the crystal grower, the entire system is evacuated, by use of both the diffusion pump and the roughing pump. Stopcocks T_4 and T_8 are opened and the remaining ones left closed. [It was found that the lowest pressure attainable with the teflon stopcocks in the system (without vacuum grease) was 5×10^{-6} mm Hg.] After the pressure has reached the lowest value, T_4 is closed and the diffusion pump is turned off. A storage tube is then put into the filling position as shown in Figs. 1 and A-3. T_3 is opened to allow the air between T_1 and T_2 to be evacuated and J_1 to be sealed. T_3 is then closed, and T_1 is opened just enough to start the benzene to flow. T_2 is opened to allow the benzene to be pulled into the crystal-growing jar by gravity and pressure differential. After the flow is started, T_1 is fully opened.

When the transfer is complete (it takes about 1 minute), T_1 and then T_2 are closed and the empty storage tube is removed. Any residual liquid

benzene left between J_1 and T_2 is swabbed with cotton Q-tips; then another storage tube is put into position and the transfer process is repeated. During transfer with the third storage tube, the flow is controlled with T_1 and T_2 to obtain the proper liquid level in the crystal grower as described in Appendix B.

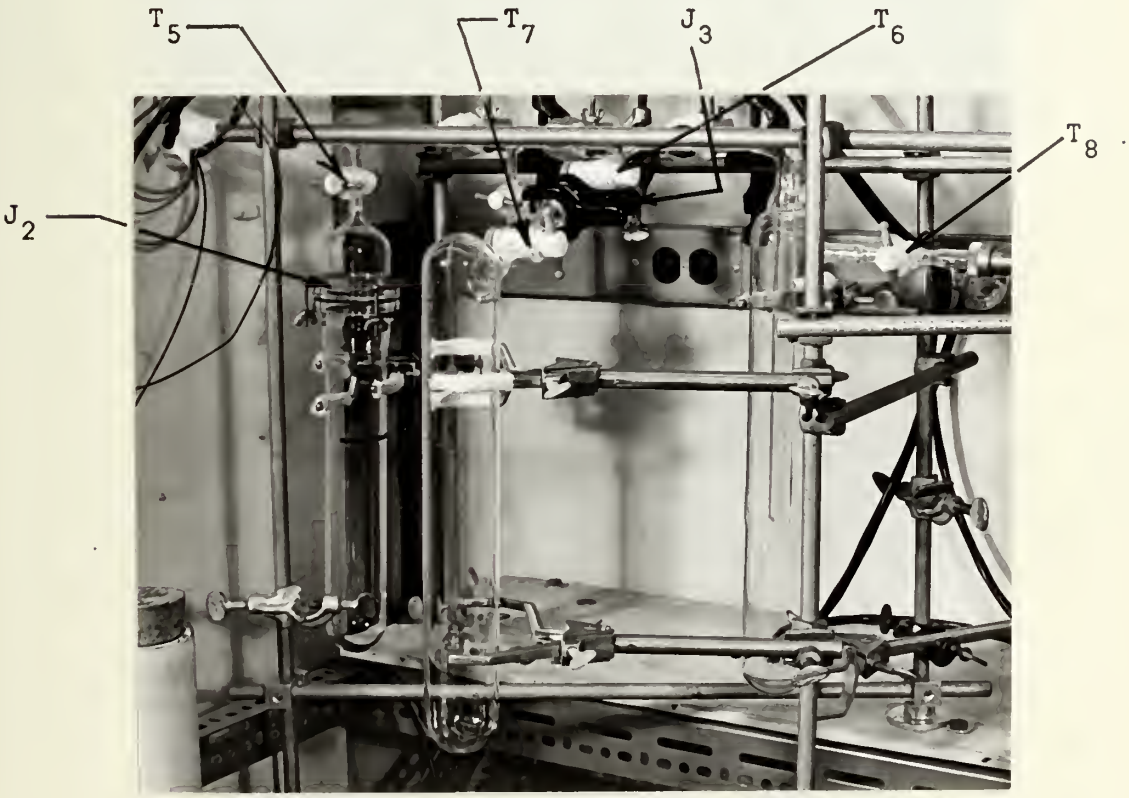

Fig. A-1. Vacuum sublimation apparatus (Also see Fig. 1).

Fig. A-2. Storage Tube, Clamp, and Supply Tube

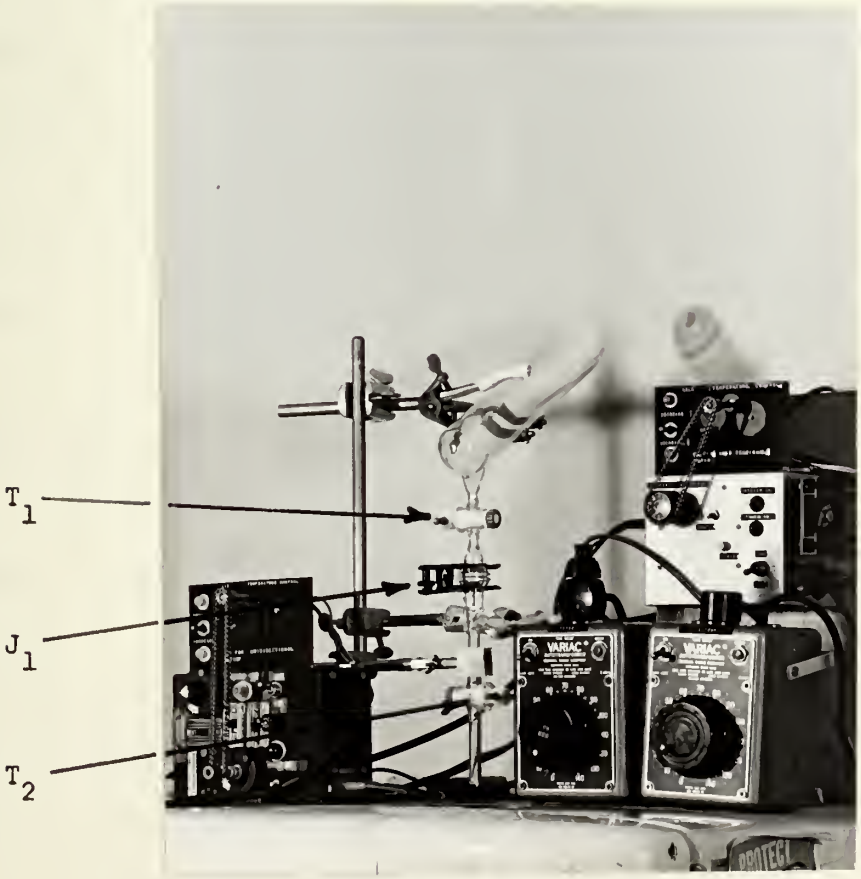

Fig. A-3. Storage Tube In Filling Position
(Also see Fig. 1)

Appendix B

Crystal Growth Procedure and Associated Problems

To start the growth procedure, the jar is filled to a level which covers about half the teflon collar. (The crystal growing apparatus and filling procedures are described in Section 3.3 and Appendix A, respectively). The refrigerator and the two SCR controllers are turned on immediately after the jar is filled. The controllers are set to establish an initial equilibrium air temperature of approximately 4°C and a melt temperature of 3.5°C at the copper probe tip after the refrigerator has cooled down to its lowest temperature (-5°C). (This corresponds to settings of 7.95 and 6.50 on the air and melt SCR controllers, respectively.) After the refrigerator has been in operation for one hour, the probe and lid temperature Variacs are turned on. (This is not done earlier, as a safety precaution, since benzene is extremely inflammable and has a low flash point of - 11.1°C.) The Variacs are set to establish an initial equilibrium temperature of 1°C on the probe and a lid temperature of 8.5°C (settings of 9.8 volts and 20.0 volts respectively). It takes approximately three hours for all the temperatures to come to equilibrium. Thereafter the seed growth is commenced. The melt temperature is then decreased, using the motor drive on the SCR controller, and a seed should form within twenty-four hours. However, the first seed usually is polycrystalline and consequently it has to be partially melted by means of the melt heater control. The melt temperature is raised to a point where the seed is just barely visible; then the melt temperature is again reduced. Usually this procedure will yield one or two single crystal on the probe tip but three or four attempts may be necessary to obtain one that is satisfactory. After the seed is formed, the melt temperature is

decreased continuously for a period of 48 hours. At the end of this period the crystal on the probe should occupy about one-third of the volume of the jar. During this same period the probe and air temperatures will also decrease, but as long as the initial equilibrium temperatures have been established the crystal on the probe should grow satisfactorily. However, as the melt temperature is decreased, the jar walls become cool enough to allow crystals to form on the inside of the walls.

The melt temperature is decreased for another 24 hours. During this period the probe and wall crystals will start to meld into one another. When this occurs, the melt heater control no longer has much effect on the crystal growth and the crystals will grow without any further temperature changes. It takes approximately another 48 hours for crystallization to be complete throughout the jar. Hence it takes about five days to complete the crystal-growing run once the seed is formed. Obtaining a good seed crystal is the most critical part of the procedure. If more than two or three single-crystal seeds are allowed to grow, the individual crystals obtained will generally not be large enough to use.

The formation of crystals on the jar walls is undesirable. Many different temperature combinations were tried to prevent this from happening. However, whenever the jar walls were heated enough to prevent crystillization, the crystal on the probe would be limited to a smaller size than obtained with wall crystallization. Thus, the wall crystallization had to be accepted as one of the limitations of the apparatus. In a few of the runs, the probe and wall crystals melded into one large single crystal which occupied almost the entire volume of the jar, but generally the wall and probe crystals would be separate single crystals. Even then, it was not

unusual to obtain a large piece of single crystal from the wall crystallization.

To prevent the wall effect the apparatus would have to be modified in two main ways. First, the volume of the jar should be reduced to about half its present size in order to make the melt temperature controller effective throughout the growing process. Second, the jar walls should be thinner. The walls of the present apparatus are relatively thick (~ $\frac{1}{8}$ in.) which causes a great deal of heat to be dissipated in the walls -- at some point, enough to sustain crystallization. Thinner walls would be more responsive to the melt temperature control and would require less heat to warm them sufficiently to prevent crystallization; thus, there would be less effect on the probe crystal. These changes were not accomplished because the crystals which were grown were large enough for the purposes of this work.

Once crystallization was complete throughout the jar, the entire jar is removed from the refrigerator and transferred to the glove box. The procedure used to separate the single crystals from the solid mass of benzene is described in Appendix C.

Appendix C

Crystal Cutting Methods

Two methods were used to separate the single crystals from the frozen mass which resulted from the crystal-growing procedure described in Appendix B. First, it was found that if the frozen mass were left inside the cold box (- 10°C) for about an hour, sublimation along the crystal boundaries would occur more rapidly than from the crystal surfaces. As a result the boundaries become clearly visible and if a thin stainless steel spatula is inserted into a boundary at two or three points, the entire piece of single crystal would break away from the mass. However, if the crystal does not break off easily, this procedure should not be used, because additional force could possibly produce strains in the crystals.

The second and more common method was to use a hot-wire cutter to cut out the single crystal pieces. Previous investigators have used sharp knives and even hacksaws to cut organic crystals, but it was feared that such a procedure would lead to severe straining of the crystals. The hot-wire cutter was made in the form of the miniature jig saw shown in Fig. C-1. The base is made of plywood and covered with a piece of plate glass. A nichrome wire (number 18 gauge), held taut in a teflon collar by a large cantilever leaf spring, passes through the base to an electrical connection on the back. The other end of the wire goes from the teflon collar, over the spring, and to another electrode on the back side. The large wire size is used to make the cut wide enough to preclude refreezing the two pieces back together once the cut is made. The two electrodes are connected to a Variac and just enough current is passed through the wire to melt the crystal slowly as the crystal is pushed through. The crystals were cut into cubes

with sides 3.5 to 4.0 cm in length. Smaller pieces or odd shaped ones can also be used if the initial orientation procedure described in Appendix D. reveals that the crystal is oriented close to the b-axis.

To prepare a piece of crystal for optical orientation, two flat, parallel sides must be melted onto the sample. This is done with the vertical planing apparatus shown in Fig. C-2. The vertical planer is the same pieces of apparatus shown in Fig. 7a except that the sample holder housing has been removed and the track is held in the vertical position.

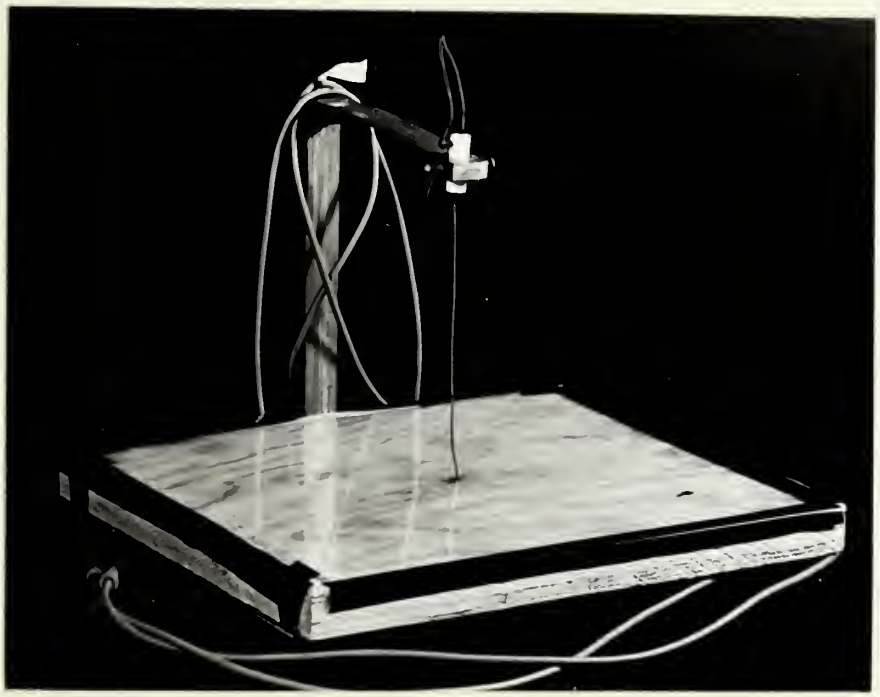

Fig. C-1. Hot wire cutter

Fig. C-2. Vertical planing apparatus.

Appendix D

Optical Orientation Procedure

A Vickers' M-72C Research Polarizing Microscope was used in conjunction with two multiaxes universal stages to accomplish orientation of the crystal (see Section 3.4). Coarse orientation was performed with a locally manufactured three-axis universal stage which was patterned after a similar device used by Heseltine and Elliot[59] and which is shown in Fig. D-1. The three-axis universal stage or the "rough universal stage" (R.U.S.) consists of two gimbal rings which are mounted inside a piece of large diameter aluminum tubing and which rotate about mutually perpendicular horizontal axes. Another ring is set inside the inner gimbal and is free to rotate about an axis perpendicular to the plane of that gimbal. Once coarse orientation is obtained, the cyrstal is mounted in a 5-axis Leitz Universal stage (L.U.S.). Each gimbal on the L.U.S. is graduated in one-degree increments which allows fine alignment of the crystal to be accomplished. A 10x objective lens is used during the coarse orientation and a 30x objective is used with the L.U.S. The R.U.S. is used because it can accommodate a larger piece of crystal than the L.U.S. Once the coarse orientation procedure is complete, enough crystal has usually been melted away to allow it to fit into the L.U.S. The microscope with the L.U.S. attached is shown in Fig. D-2. (Note: It is convenient to designate the directions of the vibration planes of the polars when crossed at 90° as N-S and E-W. Thus, the crosshairs in the ocular and the horizontal axes of the universal stage can also be described as N-S and E-W.)

In the procedures described below the terms isogyre, optic axis figure, and acute bisectrix figure are used frequently. Although briefly described

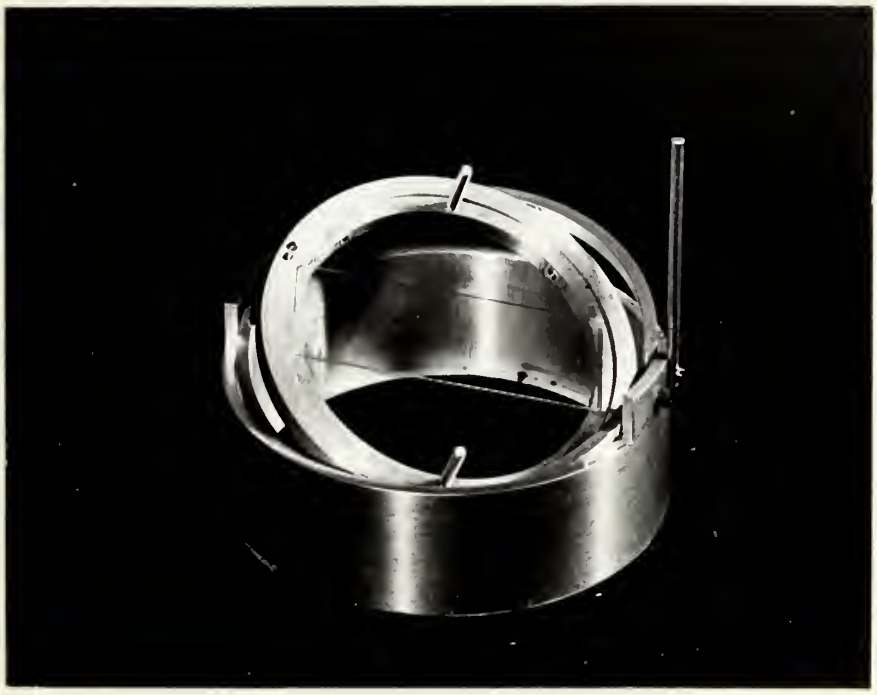

Fig. D-1. Three-axis universal stage.

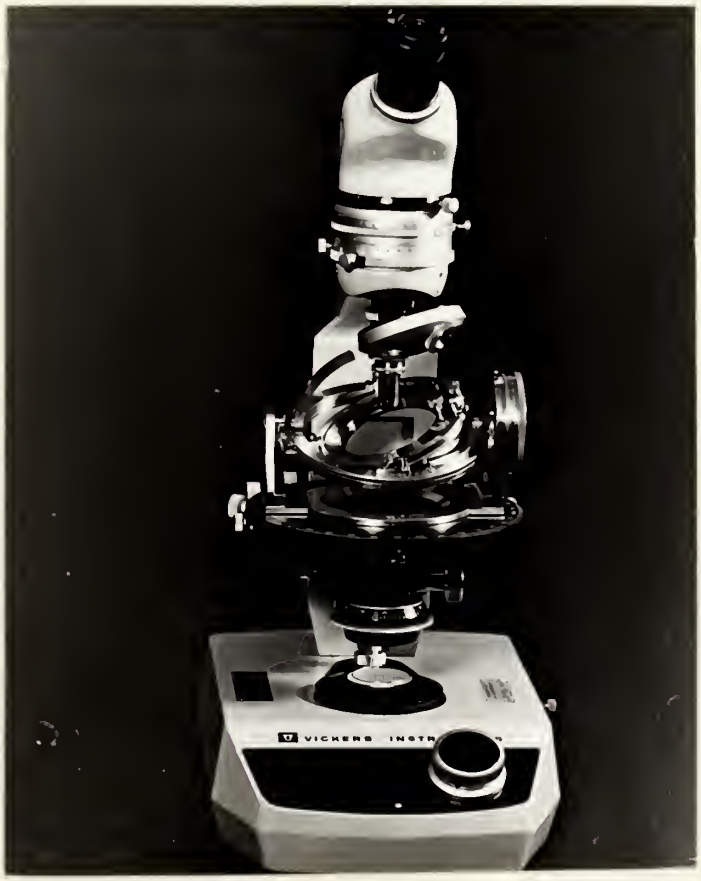

Fig. D-2. Vickers' M-72C research polarizing microscope with Leitz 5-axis universal stage.

in Section 3.4, a much more detailed description of these terms and the interference patterns associated with them is given by Wahlstrom[57] and Hartshorne[58]. These references should be studied prior to attempting the orientation procedure.

The first step in the optical orientation procedure is to take a relatively large piece of single crystal (3.5-4 cm cube) and melt two parallel faces on it with the vertical planing apparatus described in Appendix C (see Fig. C-2). After the surfaces are prepared they quickly become opaque because of sublimation. To keep the faces optically clear, glass microscopeslides -- initially at room temperature -- are frozen onto each face. These slides also provide a means for suspending the crystal in the center of the R.U.S.

The R.U.S., holding the randomly oriented crystal, is put onto the microscope stage. (The microscope is located inside the refrigerated glove box at this point.) The gimbals of the R.U.S. are rotated until maximum extinction occurs. (There is a possibility of seeing an isogyre during this observation; however, usually extinction will occur.) Once the maximum extinction position is found, the extinction directions, which correspond to the polar axes, are marked on the glass slide. The R.U.S. is removed from the microscope stage and two new parallel surfaces are melted onto the crystal, parallel to one of the extinction directions. The orientation procedure is repeated. If an isogyre is not seen now, a third pair of parallel faces is melted onto the crystal, parallel to the other extinction direction previously determined. As discussed in Section 3.4, one of the optic axes should be observed during one or the other of these observations.

Once an optic axis is found, the crystal is transferred to the L.U.S. To ensure that the L.U.S. is centered with respect to the microscope stage, the L.U.S. is fastened onto the microscope stage with two set screws. The holes in the base of the L.U.S. and in the microscope stage are aligned so that the L.U.S. will be centered when the set screws are secured.

The next eight steps in the orientation procedure will be explained with the aid of Fig. D-3. A schematic drawing of the position of the crystal relative to the L.U.S. is shown for each step. (Note the drawing is two-dimensional whereas the actual L.U.S. has three degrees of freedom.) The top and bottom faces of the crystal as they appear in step 1 have been designated A and B, respectively, and maintain the same identity throughout the procedure. A top view of the glass slide which is frozen onto side A and/or B is shown with the position of the reference marks used in each step.

Two reference marks are used. One coincides with the zero index mark on the inner ring of the L.U.S. and is used to keep the crystal in the same relative position with respect to the ring throughout the procedure. This mark will be called the "index reference mark". (Note: The crystal can be held secure in the L.U.S. by first putting a thin coat of vacuum grease on the inner ring and then pressing the glass slide, which has previously been frozen onto the sample, into place.) The second reference mark is made in a N-S direction and is used to ensure that the relationship between the N-S and E-W directions of the crystal with respect to the horizontal plane of the L.U.S. in step 8 is the same as in step 1. If it is not, one can easily become confused and there is a possibility that subsequent corrections will be made in the wrong direction.

The procedure is as follows (see Fig. D-3):

Step 1 -- The crystal is suspended in the L.U.S. by the microscope slide attached to side A and the combination is put onto the microscope stage. The gimbals of the L.U.S. are rotated to bring one of the optic axes as close to the center of the field of view as possible and to make the isogyre parallel to one of the crosshairs in the ocular. The N-S and the index reference marks are put on slide A as indicated. (The initial direction of the N-S reference mark is arbitrary but once a direction is chosen, it must be maintained throughout the sequences. The N-S index mark should not be made until the desired pattern is centered in the field if view).

Step 2 -- The L.U.S. is removed from the microscope stage and the crystal is set on top of the L.U.S. in the same relative position as it had while suspended. The N-S reference mark is unchanged. The index reference mark is transferred to slide B.

Step 3 -- The N-S reference mark is transferred from slide A to slide B. Slide A is removed by pressing a small flat piece of metal, which is at room temperature, against the slide; the heat transfer will melt the bond between the slide and the sample in about 2-3 seconds.

Step 4 -- A horizontal surface is melted onto side A with the vertical planer; then a glass slide is attached to the new surface and the N-S reference mark is transferred from slide B to slide A.

Step 5 -- The N-S and E-W gimbals on the L.U.S. are set to their zero positions. Reference marks are unchanged.

Step 6 -- The crystal is turned over so that side A rests on top of the L.U.S. The same N-S reference mark is on slide A as in steps 4 and 5;

Illustration of Steps Used During Orientation Procedures

Front View of Crystal on Universal Stage (U-stage)

Top View of Reference Marks on Glass Slides (A or B as indicated)

Step 1

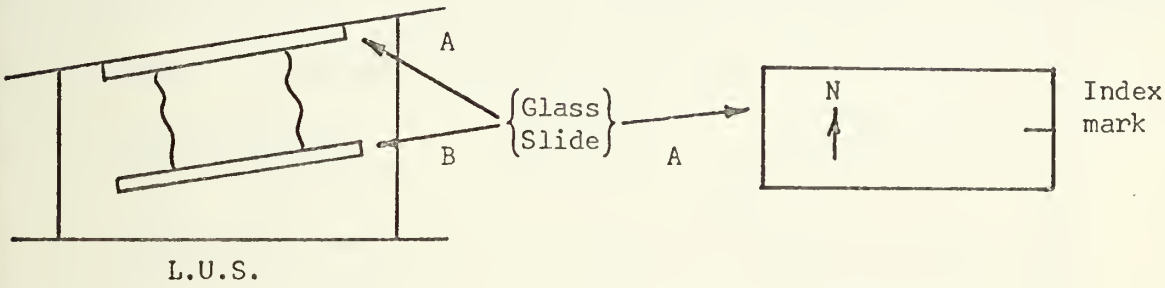

Crystal is suspended in L.U.S. in an orientation at which on isogyre, optic axis pattern, or an acute bisectrix pattern has been observed with the microscope. If orientation is close to b axis, angles have been corrected for refraction. Reference marks on slide A in the N direction and in line with index on inner ring of the L.U.S.

Step 2

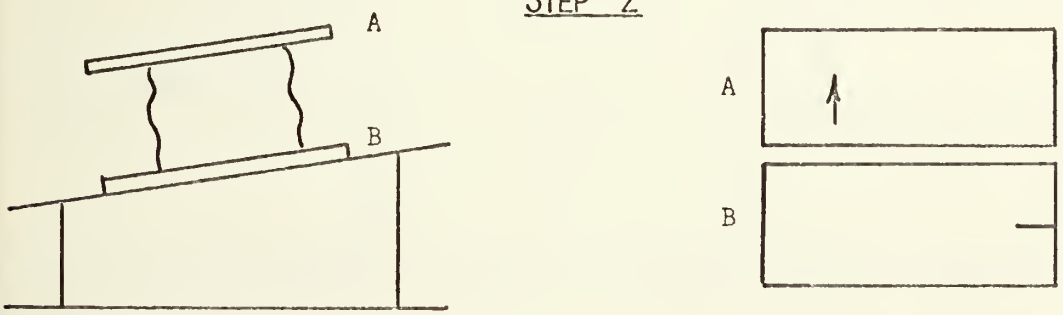

Crystal is set on top of L.U.S. in same relative position as it had when suspended. Reference mark on slide A in N direction. Index reference mark is transferred to slide B.

Figure D-3

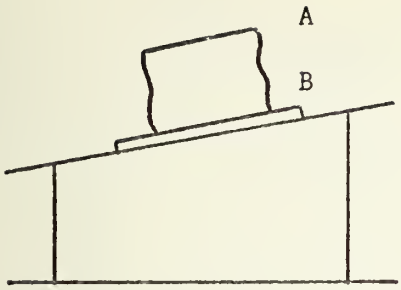

STEP 3

N-S reference mark from slide A is transferred to slide B. Index reference mark unchanged. Slide is taken off side A.

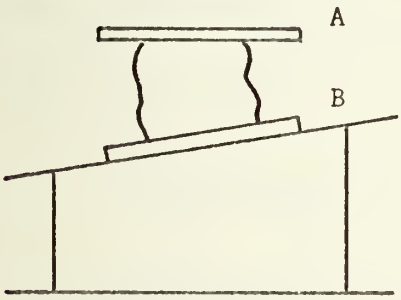

STEP 4

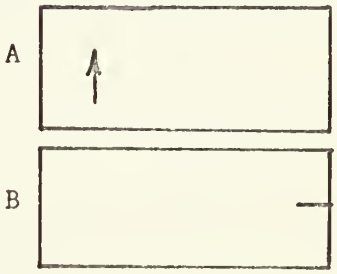

A new horizontal surface is melted onto side A with the vertical planer. A slide is frozen onto the new surface and the N-S reference mark is transferred to slide A.

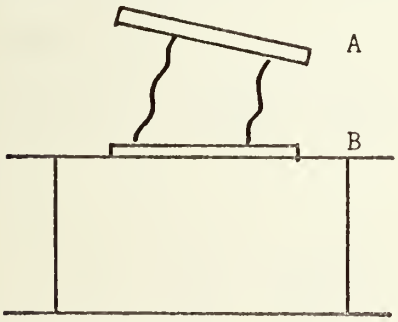

STEP 5

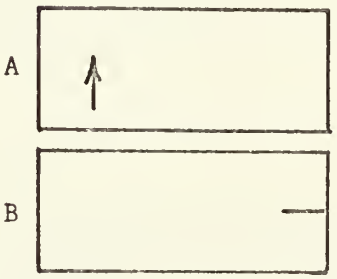

The N-S and E-W gimbals on the L.U.S. are set to zero. Reference marks are unchanged.

FIGURE D-3 (CONT'D).

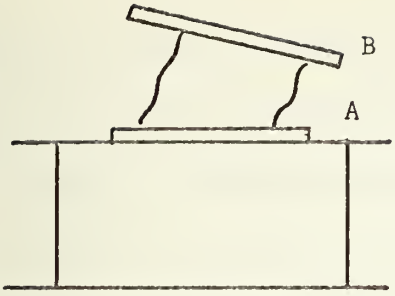

STEP 6

Crystal is turned over so that side A rests on top of the L.U.S. The same N-S reference mark is on slide A as in steps 4 and 5; however, now arrow is pointing in the S direction. Index reference mark is transferred from slide B to slide A.

STEP 7

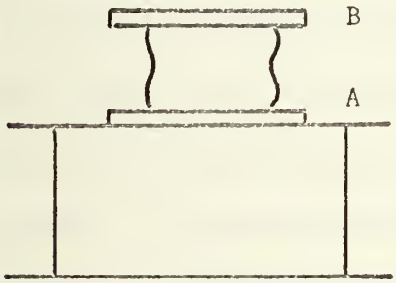

Slide is taken off of side B and a horizontal face is melted onto the crystal with the vertical planer. Another slide is then frozen onto new surface. Reference marks are unchanged.

STEP 8

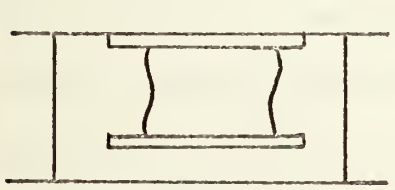

Crystal is turned over and suspended in the L.U.S. Side A is on top and in same relative position as in step 1. Crystal is ready for another observation with the microscope.

FIGURE D-3 (CONT'D).

however, now the arrow is pointing in the opposite direction. The index reference mark is transferred from slide B to slide A.

Step 7 -- The slide is taken off of side B and a horizontal face is melted onto the crystal with the vertical planer. Another slide is frozen onto the new surface on side B. Reference marks are unchanged.

Step 8 -- The crystal is turned over and suspended in the L.U.S. Side A is on top, in the same relative position as in step 1. The crystal is now ready for another observation with the microscope.

During the next observation, the optic axis figure should be close to the center of the field of view with the N-S and E-W gimbals positioned at lesser angles than those observed before the correction was applied; if a perfect correction was made, the N-S and E-W gimbals would be in their zero positions. If the optic axes is still far off the zero position (greater than 10°), it should be centered once again and steps 1 through 8 should be repeated.

When an optic axis can be seen close to the zero position, the inner ring of the L.U.S. should be rotated until the isogyre is parallel to one of the crosshairs in the ocular. Next, the N-S or E-W gimbal (the one used depends on the direction of the isogyre) is rotated so as to move the optic axis along the crosshair in the ocular which is parallel to the direction of the isogyre. As the optic axis is moved, the field of view will either become dark and the isogyre will broaden or the cross of the acute bisectrix figure and the other optic axis figure will be seen in sequence. (See Fig. 5 in Section 3.4.) If the former is observed, the gimbal must be rotated in the opposite direction to obtain the acute bisectrix figure. Once it is observed, the gimbals should be rotated until the cross coincides

with the crosshairs in the ocular. In this position the acute bisectrix, i.e., the b axis, is aligned parallel to the vertical axis of the microscope, but the N-S and E-W gimbals are at some angle with respect to the horizontal plane of the microscope; hence, the observed angles must be corrected for refraction, i.e., Snell's Law, to obtain the true angular relationship of the crystal with respect to the horizontal plane. Since the light is propagating close to the b-axis at this point, the index of refraction (1.64) corresponding to that direction is used.[73] (The observed angle must always be reduced to obtain the true angle.) After the corrections have been made, steps 1 through 8 are repeated except that now, in step 1, the acute bisectrix figure has been centered (and corrected for refraction) rather than the optic axis figure. The procedure of observing, correcting, and preparing new surfaces (steps 1-8) is repeated as often as is necessary to bring the b-axis coincident with the vertical axis of the microscope with the N-S and E-W gimbals in their zero positions. If the N-S reference marks are in the same direction after each sequence, each succeeding observation will require rotation of the N-S and E-W gimbals in the same direction as in the previous observation but the amount of correction required will be less each time. If the angles become greater, the "corrections" have been applied in the wrong direction. If one carries the procedure out carefully, an orientation to within ±2° can be obtained.

A practical difficulty in these steps arose because the cold box was not large enough to accommodate both the microscope and the planer surface simultaneously; hence, each piece of apparatus had to be alternately taken out and put into the box to accomplish the required procedures. A larger work area would have been desirable.

If the b-axis is the axis to be oriented, the orientation is maintained with the glass slide which has been frozen onto the final surface. To orient the a or c axis the appropriate isogyre is aligned with the E-W crosshair in the ocular. The crystal is then set on top of the innermost ring and the index reference mark, which was previously put onto the upper slide, is transferred to the lower slide with the two marks agreeing as closely as possible. The L.U.S. is returned to the microscope stage and the alignment is checked with the 3x objective lens. The pattern seen with the 3x objective is much more diffuse than the corresponding pattern seen with the 30x objective; consequently, it takes some practice to correlate the two patterns correctly. By alternately viewing the crystal in the suspended position with the 30x objective and in the "on top" position with the 3x objective, it was found that if the procedure is carried out carefully, a correction of a degree or two in the horizontal plane was all that was necessary to compensate for the movement.

Once the crystal is oriented in the "on top" position, the L.U.S. is transferred to the planing apparatus shown in Fig. D-4. The L.U.S. is fastened onto the platform of the planer in the same relative position as it had when it was on the microscope stage. Thus, the E-W position on the platform coincides with the axis aligned on the microscope stage and the face of the heated planer is exactly perpendicular to the axis. Consequently, a face can be melted onto the crystal which is perpendicular to the desired axis. The final surface is sealed with a glass slide.

The orientation of the a or c axis can be checked again with the L.U.S. and the 30x objective lens. The directions of the a and c axes correspond to the obtuse bisectrix and to the optic normal of the indicatrix,

respectively. Each of these directions also has a characteristic interference pattern associated with it (described by Wahlstrom[74]). However, the resolving power of the 30x objective lens is not great enough to obtain as well defined patterns as seen along the acute bisectrix. Consequently, these patterns were used only as a secondary check on the alignment. The resolving power of the 30x objective also limited the amount of the acute bisectrix pattern which could be seen in the field of view. Usually the optic axes would be at the extreme edge of, or just outside, the field of view. Therefore, to determine which isogyre corresponds to the a axis, the crystal has to be rotated back and forth on the N-S and E-W gimbals to see the optic axes. After the a axis has been identifed, the cross can be centered in the field. It would be desirable to use a 40x or 50x objective lens with the L.U.S., to obtain a greater resolving power which, in turn, would yield sharper interference patterns.

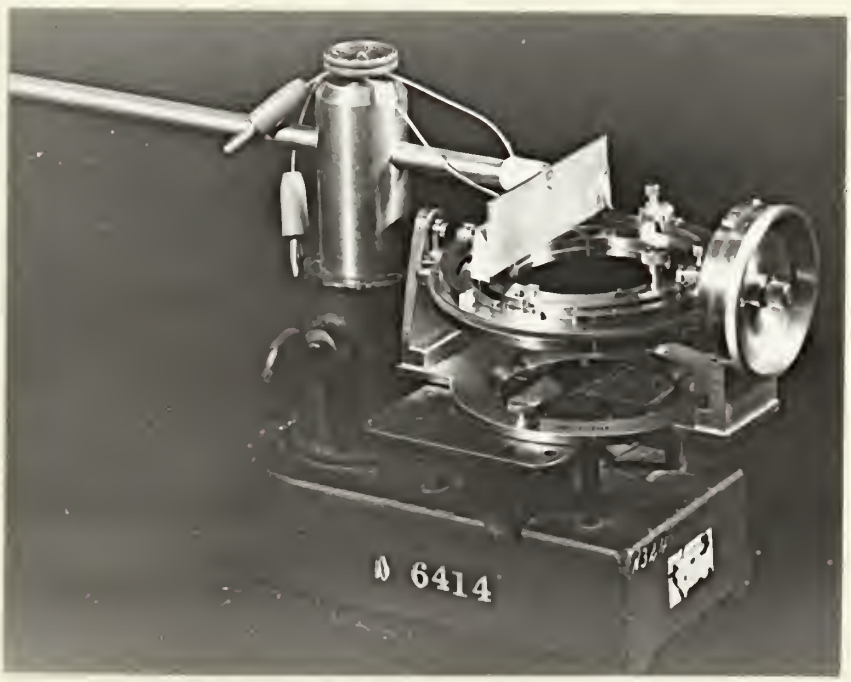

Fig. D-4. Planing apparatus used for preparing surfaces perpendicular to the a or c axis.

Appendix E

Sample Cutting and Polishing Procedure

To cut a sample on the apparatus described in Sec. 3.5, the apparatus is used in the vertical position as shown in Fig. 6b. The cavity is removed from the sample holder housing and a small glass plate (3 x 3 inches) is set on top of the upper face of the housing. A piece of oriented crystal is frozen onto the glass plate with a few drops of benzene, using the microscope slide which was attached during the orientation procedure as a base. Hence, the oriented axis is perpendicular to the glass plate and parallel to the axis of the cutter. The sample is cut by bringing the heated cutter down onto the sample for 4-5 second intervals. The cutter cannot be kept on the sample continuously because the sample will be melted into the shape of a truncated cone by the heat inside the cutting cylinder. Therefore, the cutter is raised off the sample after each cutting interval to ensure that the sample will be cylindrical and also to reheat the tip of the cutting tool. Thus, the cutter is alternately raised and lowered until a sample is cut out. It was found that the use of two cutting tools with diameters of 7/8-inch and 3/4-inch, respectively, produced a more cylindrical sample than obtained with making only one cut with a 3/4-inch diameter tool. After each cut is complete, the excess crystal is trimmed away with a sharp razor blade. The result is a sample which is approximately 3/4-in. ($\sim$ 1.9 cm) in diameter and one inch long; the glass slide is still frozen onto one face of the sample to preserve orientation.

With the sample resting on the microscope slide, a brass spacer plate that has a 2 in. O.D., is 1/8-in. thick, and has a 3/4-in. diameter hole in the center is slipped over the sample so that one face of the plate rests

on the slide. The sample holder is set on top of the spacer plate and the sample is frozen to the holder by inserting a few drops of liquid benzene into the small space between the sample and the holder. The oriented crystal axis is now parallel to the sample holder axis. In order to be able to prepare flat, parallel faces on the sample, approximately 1/8-in. of benzene must protrude beyond each side of the sample holder. The spacer plate provides the necessary excess on one side whereas the amount of excess on the opposite side is determined by the length of the piece of crystal being prepared. Thus, the length of the oriented piece of crystal must be at least 1/4-in. greater than the thickness of the sample holder.

The sample holder and spacer plate along with the enclosed sample and the attached microscope slide are mounted on the planing apparatus shown in Fig. 6a. The holder is held flush against the cavity in the sample holder housing by two long screws which pass through the housing and the cavity and thenscrew into the holder. Hence, the face of the planer and the side of the sample holder are exactly parallel. The glass slide and the spacer plate are removed and the heated planer is used to melt a flat face onto the sample. The sample is then turned around, secured once again to the cavity, and a face is melted onto the opposite side of the sample. The temperature of the planer surface is maintained about 2-3°C above the freezing point of benzene during the facing operations. The sample faces are melted to the point where approximately 1/16 of an inch of benzene still protrudes beyond the sides of the sample holder. The excess benzene is rubbed off during the final polishing procedure.

Many different types of abrasives and polishing cloths were tried in efforts to make the final surfaces of the sample smooth and flat. Because

benzene is relatively soft, it was found that even the finest grit abrasive papers left scratches on the crystal surfaces. A velveteen polishing cloth was finally used to obtain the requisite surfaces. (The velveteen was procured from the J. J. Morris Company, Southbridge, Mass.) The velveteen cloth has an adhesive backing; consequently, a polishing surface was made by attaching it to a flat glass plate. To obtain the final surfaces on the crystal, the sample holder is set onto the plate and the excess benzene rubbed off by pushing the sample holder across the velveteen surface in one direction with short, positive strokes. At the end of every third or fourth stroke, the sample holder is turned 90°. This procedure is repeated until the benzene is flush with the flat side of the sample holder. The parallelism of the sample is determined by the degree of parallelism to which the sample holder could be machined. For this case, the sides of the sample holder are parallel to within 0.0005 in.

After the final surfaces of the sample have been prepared, one face is covered with a piece of 1/4-mil clear mylar which has been cut into a 1.25-in. diameter disc. The edges of the disc are sealed onto the sample holder with a few drops of a glycerine-water solution (to be described later); then the mylar is covered with a teflon plate which is screwed onto the sample holder. The mylar-teflon seal prevents sublimation of the prepared surface. The opposite sample face is covered with a transducer mylar seal which is described in Appendix F.

Appendix F

Bonding Procedure

The bonding procedure is initiated by cutting a piece of 1/4-mil aluminum coated mylar into a 1.25-in. diameter disc and removing the oxide layer from the aluminum by immersing the disc in concentrated nitric acid and then rinsing with distilled water. The transducer is bonded onto the mylar at room temperature with Nonaq stopcock grease. Prior to making the bond, a small amount of Nonaq is heated on a glass slide to boil off any absorbed water vapor. After the Nonaq is allowed to cool, a drop is put onto the mylar and the transducer is bonded by twisting it back and forth on the mylar with considerable thumb pressure until all the excess grease is squeezed out of the bond. It is important to note that the transducer-mylar bond must be made at room temperature in order to obtain a thin, strong bond. If the procedure is carried out at - 10°C, a poor bond will result, especially when utilizing thick transducers. (During the course of the experiment, a peculiar property of the Nonaq stopcock grease was observed. It was found that Nonaq which had been allowed to set and absorb water vapor from the air, and subsequently heated to boil off the water vapor, yielded a much stronger bond than Nonaq from a freshly opened bottle. The "old" Nonaq had a milky, opaque appearance and a smooth consistency whereas the "new" Nonaq appeared to be translucent and had a grainy consistency. There was a considerable difference in the bonding properties of the two types.)

Once the transducer-mylar bond was made, the combination is cooled down in the cold box and, immediately after one face of the prepared sample is sealed with the teflon-mylar combination, the transducer-mylar combination

is bonded onto the opposite face with a glycerine-water solution. It was found that if pure glycerine was used, the glycerine would freeze onto the benzene before a thin bond could be made, which resulted in a very poor ultrasonic echo pattern. After a great deal of experimentation, it was determined that a solution of 90% glycerine and 10% distilled water by weight exhibited the best bonding characteristics. The bond would remain fluid at - 10°C and would freeze at approximately - 20°C.

To bond the transducer-mylar combination onto the benzene, a small drop of glycerine solution is put onto the center of the sample face and the transducer-mylar combination is set on top. The ends of two Q-tip sticks are used to twist the transducer-mylar combination back and forth gently until the glycerine is spread evenly across the sample face and the excess is squeezed out. The aluminized mylar seals the sample and provides the ground connection for the transducer.

The experimental limitations of the bond are discussed in Section 3.6. An estimate of bond losses and how they were obtained is given in Section 4.2.

Appendix G

Apparent Sound Absorption Due to Transducer Thickness

The results of Sylwestrowicz's[67] experiments in determining the sound absorption due to differences in transducer thicknesses were briefly presented in Section 4.2. Although Sylwestrowicz offered no explanation for the thickness effect, one possible cause of the effect could be the change in the quality factor (Q) of a transducer when it is operated above its fundamental frequency. The Q of a transducer depends on the specific acoustic impedences of the transducer material and that of the substance on which the transducer is bonded. For an air-backed transducer the Q is defined by[75]

$$Q = n \frac{\pi}{2} \frac{(\rho s)_t}{(\rho s)_m} \tag{G.1}$$

Here n is the number of the harmonic at which the transducer is being excited and $(\rho s)_t$ and $(\rho s)_m$ are the specific acoustic impedences of the transducer and of the solid, respectively. Equation G.1 shows that the Q of the transducer depends on the loading conditions imposed by the sample. In general, the presence of the bonding agent will cause the Q to be lower than predicted by Eq. G.1.

For a given loading condition the Q of the transducer can be defined in terms of its bond width characteristic as

$$Q = \frac{\nu_r}{\Delta\nu} \quad . \tag{G.2}$$

$\Delta\nu$ is the bandwidth of the device at the resonant frequency ν_r and is defined by the points at which the acoustic power is 3 db (50%) below the peak power of the acoustic pulse at the fundamental resonant frequency.

Hence, if $\frac{\Delta\nu}{\nu} = 10\%$ at the fundamental frequency, the bandwidth is 500 KHz for a 5 MHz transucer whereas it is 1500 KHz for a 15 MHz transducer. The value of $\Delta\nu$ is a characteristic of a given device; consequently, does not change with the harmonic at which the transducer is operated. Therefore, for a 5 MHz transducer operating at 15 MHz the Q is three times that of a 15 MHz transducer operating at its fundamental.[76]

A relationship between Q and the energy transmitted into the detection system can be obtained by first considering the spectral distribution of the voltage response $V(\nu)$ of the transducer. For a voltage which contains components in the frequency range $\nu_r \pm \nu$, the total voltage seen by the detection system is proportional to the area defined by the curve which describes the spectral distribution on a voltage vs. frequency plot and the two vertical lines drawn through the points $\pm\nu$ on the frequency axis. If a Gaussian curve is assumed, the area can be expressed in terms of the Gaussian distribution function, which can be written in the form

$$\text{Area} = \frac{2}{\sqrt{2\pi}} \int_{\nu_r}^{\nu} e^{-\frac{1}{2}(\nu_r - \nu)^2} d\nu$$

$$= \frac{2\nu_r}{\sqrt{2\pi}} \int_{o}^{1/Q} e^{-(1/Q)^2} d(1/Q)$$

$$= \frac{\nu_r}{\sqrt{2}} \text{ erf } (\frac{1}{Q}) \qquad \text{(G.3)}$$

Since the error function (erf) decreases with decreasing values of its argument, Eq. G.3 shows that the area is smaller for the system with the higher Q. The transmitted energy is proportional to the square of the

voltage--hence, proportional to $(\text{Area})^2$. Hence, for a pulse of acoustic power which has a given frequency spectrum, the device with the lower Q will pass more of the frequency components into the detection system which, in turn, yields a lower apparent attenuation.

If Eq. G.3 is used to calculate the area for two different values of Q that have a ratio of 3:1, it is found that the system with the higher Q transmits 81.5% less energy than the system with the lower Q. Sylwestrowicz made sound absorption measurements on three different materials at 15 MHz with transducers which had fundamental frequencies of 5 MHz and 15 MHz. The apparent attenuation obtained with the 5 MHz transducer was 73%, 88%, and 25% greater for the three substances, respectively, than that obtained with the 15 MHz transducer. Hence, there is a qualitative agreement between the predicted and observed effect of Q on the apparent attenuation in two of the three cases.

The procedure described by Sylwestrowicz was used to obtain an estimate of the apparent attenuation due to the thickness effect for this experiment. Transducers with fundamental frequencies of 2.0, 2.5, and 5.0 MHz were successively bonded onto the same sample (oriented along the c-axis) and absorption measurements were taken at 250°K. The results obtained with each transducer is shown in Fig. G-1. The several measurements exhibit the same frequency dependence but are displaced with respect to each other in magnitude. Next, the absorption values at a particular frequency, e.g., 5, 6, 7.5 MHz etc., are taken from each curve and are replotted as a function of transducer thickness. This generates another family of curves (Fig. G-2) on an absorption versus transducer-thickness plot, which are parametric in frequency. It is assumed that the absorption associated with transducer

thickness vanishes at zero thickness. Hence, the curves of absorption versus transducer thickness are extrapolated to zero thickness and the difference between α at the intercept and the value of a particular transducer thickness represents the energy loss related to the transducer at the frequencies of interest. By applying the corrections obtained from Fig. G-2 to each experimental point obtained with the three transducers, the three curves collapse into the single corrected curve shown in Fig. G-1. A comparison of the measured and corrected absorption values is made in Table G-1. It can be seen that the corrections for the 5 MHz transducer are much less than for the thicker 2.0 and 2.5 MHz transducers.

The experiment did show the existence of an apparent attenuation due to transducer thickness; however, further experimentation would be necessary to be able to make corrections to all the data obtained. Transducers with 10 and 20 MHz fundamentals should be used to obtain more points on the absorption versus transducer-thickness plot which, in turn, would make the extrapolation to zero thickness more accurate. Also, values should be obtained as a function of temperature for each transducer to determine the temperature dependence of the effect. Such an experiment would be a formidable task and was not carried out in this work due to the difficulties associated with the sample preparation. It would be feasible, however, to perform the experiment with a "hard" solid with moderate intrinsic attenuation.

Table G-1

Correction of α Due to Transducer Thickness Effect

ν (MHz)	α_{exp} ** (cm^{-1})	correction *** (cm^{-1})	α_{corr} ** (cm^{-1})	% correction
5	0.156	0.023	0.133	14.7
6	0.235	0.075	0.160	31.8
7.5	0.294	0.081	0.213	27.5
10	0.433	0.118	0.315	27.2
12.5	0.523	0.123	0.400	23.5
14	0.807	0.367	0.440	45.5
15	0.604	0.124	0.480	20.5
17.5	0.905	0.305	0.600	33.8

*All measurements taken on the same sample

(Single crystal benzene c-axis 250°K)

**See Fig. G-1.

***See Fig. G-2.

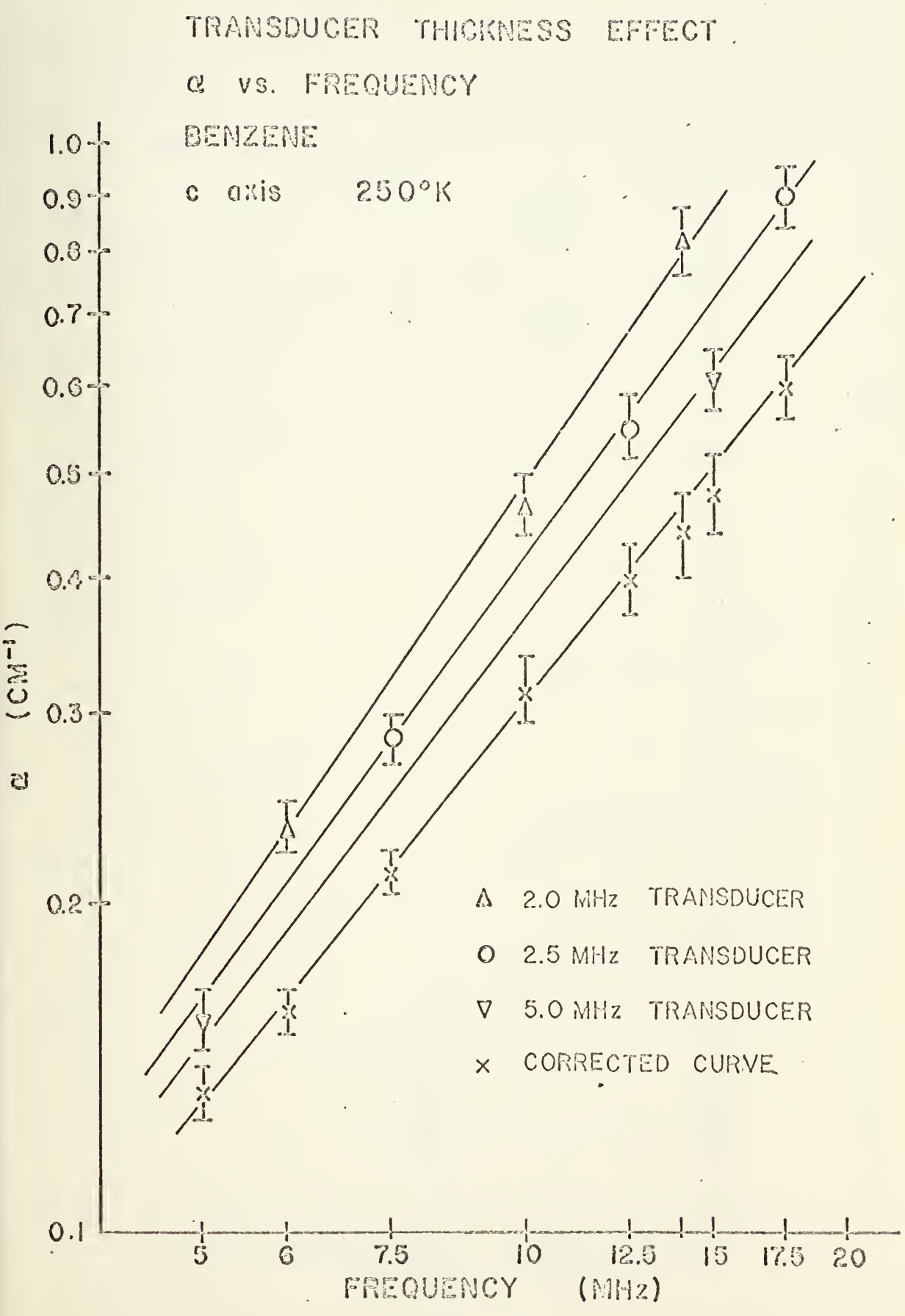
TRANSDUCER THICKNESS EFFECT
α vs. FREQUENCY
BENZENE
c axis 250°K
1.0
0.9
0.8
0.7
0.6
0.5
0.4
0.3
0.2
0.1
α (CM⁻¹)
5
6
7.5
10
12.5
15
17.5
20
FREQUENCY (MHz)
Δ 2.0 MHz TRANSDUCER
O 2.5 MHz TRANSDUCER
∇ 5.0 MHz TRANSDUCER
× CORRECTED CURVE

Figure G-1

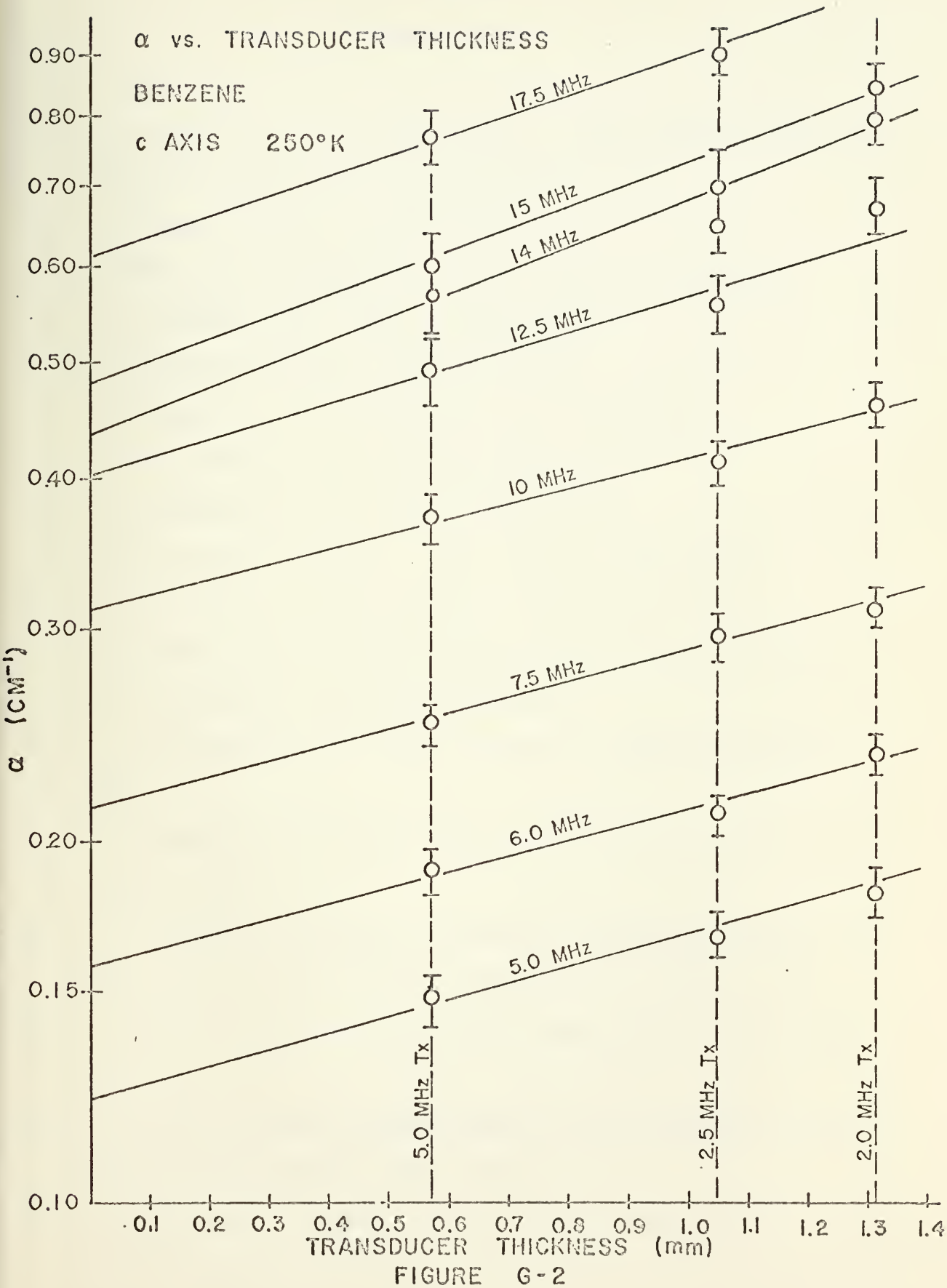
α vs. TRANSDUCER THICKNESS
BENZENE
c AXIS 250°K
17.5 MHz
15 MHz
14 MHz
12.5 MHz
10 MHz
7.5 MHz
6.0 MHz
5.0 MHz
5.0 MHz Tx
2.5 MHz Tx
2.0 MHz Tx
α (CM⁻¹)
0.90
0.80
0.70
0.60
0.50
0.40
0.30
0.20
0.15
0.10
0.1 0.2 0.3 0.4 0.5 0.6 0.7 0.8 0.9 1.0 1.1 1.2 1.3 1.4
TRANSDUCER THICKNESS (mm)

FIGURE G-2

BIBLIOGRAPHY

1. E. B. Wilson, Jr., J. C. Decius and P. C. Cross, Molecular Vibrations, (McGraw-Hill Book Company, New York, 1955), p. 2.
2. A. Frühling, Ann. Phys. 6, 401 (1951).
3. I. Harada and T. Shimanouchi, J. Chem. Phys. 41, 2016 (1966).
4. D. F. Hornig, J. Chem. Phys. 16, 1063 (1948).
5. L. Liebermann, Phys. Rev. 113, 1052 (1959).
6. L. Liebermann, J. Acoust. Soc. Amer. 31, 1073 (1959).
7. R. A. Rasmussen, J. Chem. Phys. 36, 1821 (1962).
8. R. A. Rasmussen, J. Chem. Phys. 46, 211 (1967).
9. S. S. Yun and R. T. Beyer, J. Chem. Phys. 40, 2538 (1964).
10. S. S. Yun and R. T. Beyer, J. Chem. Phys. 41, 4004 (1964).
11. J. D. Wilson and S. S. Yun, J. Acoust. Soc. Amer. 50, 164 (1971).
12. H. G. Danielmeyer, Acustica 17, 102 (1966).
13. H. G. Danielmeyer, Ph.D. Thesis, Technische Hochschule Stuttgart, 1965.
14. J. C. Heseltine, D. W. Elliot, and O. B. Wilson, Jr., J. Chem. Phys. 40, 2584 (1964).
15. L. N. Liebermann, "Resonance Absorption" in Physical Acoustics (W. P. Mason, ed.) Vol. IV A (Academic Press, New York, 1966), p. 183.
16. J. J. Markham, R. T. Beyer, and R. B. Lindsay, Rev. Mod. Phys. 23, 353 (1951).
17. M. Born and K. Huang, Dynamical Theory of Crystal Lattices (Oxford University Press, London, 1954), first ed., p. 8.
18. R. D. Mair and D. F. Hornig, J. Chem. Phys. 17, 1236 (1949).

19. R. C. Lord, Jr., J. E. Ahlberg, and D. H. Andrews, J. Chem. Phys. 5, 649 (1937).

20. Reference 17, p. 40.

21. L. Brillouin, Wave Propagation in Periodic Substances (Dover Publications, Inc., New York), chap. 7.

22. D. E. Williams, J. Chem. Phys. 45, 3370 (1966).

23. E. R. Bernstein, J. Chem. Phys. 52, 4701 (1970).

24. A. O. Williams, Jr., Brown University, Providence, R.I., private communication.

25. Reference 21, p. 52.

26. F. Erickson, "A Criticism of the Pesonance Theory of Acoustic Absorption in Soft Organic Crystals," Sc.B. Thesis, Brown University, 1965.

27. G. Liebfried and W. Ludwig, "Theory of Anharmonic Effects in Crystals," in Solid State Physics-Advances in Pesearch and Applications (F. Sietz and D. Turnbull, ed.) Vol. 12 (Academic Press, New York, 1961), p. 275.

28. K. F. Herzfeld and F. O. Rice, Phys. Rev. 31, 691 (1928).

29. J. M. Ziman, Electrons and Phonons (Oxford University Press, London, 1960) first ed., p. 145.

30. A discussion of this point is given for the gas and liquid case by H. O. Kneser and J. Lamb, Physical Acoustics (W. P. Mason, ed.) Vol. II A (Academic Press, New York, 1965), p. 145 and p. 258, respectively.

31. R. Truell, C. Elbaum, and B. B. Chick, Ultrasonic Methods in Solid State Physics (Academic Press, New York, 1969), Appendix J, p. 413.

32. A full discussion of the transformations involved here is given in Reference 31, Appendix J, p. 413.

33. Reference 31, p. 414.

34. Reference 29, p. 154.

35. R. T. Beyer and S. V. Letcher, Physical Ultrasonics (Academic Press, New York, 1969), first ed., p. 249.

36. Reference 31, p. 8.

37. Ibid, p. 3.

38. For detailed discussion of the relationships between different relaxation times see H. J. Bauer, Physical Acoustics (W. P. Mason, ed.) Vol. II A (Academic Press, New York, 1965), p. 47.

39. See for example, R. T. Beyer and S. V. Letcher, Physical Ultrasonics (Academic Press, New York, 1969), p. 102.

40. K. F. Herzfeld and T. A. Litovitz, Absorption and Dispersion of Ultrasonic Waves (Academic Press, New York, 1949), p. 406.

41. E. L. Heasell and J. Lamb, Proc. Phys. Soc. (London) B69, 869 (1956).

42. J. L. Hunter and H. D. Dardy, J. Acoust. Soc. Amer. 36, 1914 (1964).

43. T. O. Woodruff and H. Ehrenreich, Phys. Rev. 123, 1553 (1961).

44. Reference 29, p. 296.

45. N. I. Sax, Dangerous Properties of Industrial Materials (Reinhold Publishing Corporation, New York, 1966) second ed., p. 488.

46. R. S. Tipson, "Sublimation" in Technique of Organic Chemistry (A. Weissberger, ed.) Vol. IV (Interscience Publishers, Inc., New York, 1951), p. 603.

47. "A Compendium of the Properties of Materials at Low Temperatures (Phase I); Part I, Properties of Fluids," U. S. Department of Commerce Publication, PB 171 618, p. 303.

48. T. E. Jordon, Vapor Pressure of Organic Compounds (Interscience Publishers, Inc., New York, 1954), plate I.

49. G. S. Zhdanov, Crystal Physics (Academic Press, New York, 1965), p. 371.

50. J. C. Brice, The Growth of Crystals From the Melt (North-Holland Publishing Company, Amsterdam, 1965), p. 52.

51. F. Cuomo, University of Rhode Island, Kingston, R.I., private communication.

52. J. S. Blinick, Brown University, Providence, R.I., private communication.

53. W. D. Scott, "Liquid Temperature Controller," in Electronics World, November 1964.

54. R. A. Rasmussen, "Resonance Absorption in Solid Cyclohexane," SIO Reference 61-6, Scripps Institution of Oceanography, San Diego, Calif., 1961, p. 33.

55. F. A. Mullens, "Use of An Optical Means to Orient Benzene Crystals," Sc.M. Thesis, U. S. Naval Postgraduate School, 1961.

56. A. F. Hallimond, The Polarizing Microscope, Vickers Ltd., York, England, 1970) third ed., p. 6.

57. E. E. Wahlstrom, Optical Crystallography (J. Wiley and Sons, Inc., New York, 1969) fourth ed., p. 341.

58. N. H. Hartshorne and A. Stuart, Crystals and the Polarizing Microscope, (Edward Arnold [Publishers] Ltd., London, 1960) third ed., p. 168.

59. J. C. Heseltine and D. W. Elliot, "Determination of the Elastic Constants of Benzene," Sc.M. Thesis, U. S. Naval Postgraduate School, 1962.

60. E. G. Cox, D. W. J. Cruickshank, and J. A. Smith, Proc. Roy. Soc. (London), 247A, 1 (1958).

61. B. Chick, G. Anderson, and R. Truell, J. Acoust. Soc. Amer. 32, 186 (1960).

62. Reference 31, Chapter II.

63. H. Seki, A. Granato, and R. Truell, J. Acoust. Soc. Amer. 28, 230 (1956).

64. E. P. Papadakis, J. Acoust. Soc. Amer. 31, 150 (1959).

65. L. E. Kinsler and A. R. Frey, Fundamentals of Acoustics (J. Wiley and Sons, Inc., 1962) second ed., p. 136.

66. Reference 31, p. 113.

67. W. D. Sylwestrowicz, IEEE Trans. on Sonics and Ultrasonics, SU-11-1, 50 (1964).

68. R. Bass and J. Lamb, Proc. Roy. Soc., A243, 94 (1958).

69. J. H. Andreae, Proc. Phys. Soc. (London), B70, 71 (1957).

70. Reference 1, Chapter X.

71. A. G. Gee and G. W. Robinson, J. Chem. Phys. 46, 4847 (1967).

72. J. L. Hollenberg and D. A. Dows, J. Chem. Phys. 37, 1300 (1962).

73. Reference 58, p. 151.

74. Reference 57, p. 338.

75. T. F. Hueter and R. H. Bolt, Sonics (J. Wiley and Sons, Inc., New York, 1955) first ed., p. 106.

76. The author is indebted to Mr. B. B. Chick for pointing out the effect that the transducer quality factor has on the apparent sound absorption.

Thesis
V649

131440

Victor
Ultrasonic absorption along the principal axes of single crystalline benzine.